

A VASCULAR GRAFT ON-A-CHIP PLATFORM  
FOR ASSESSING THROMBOGENICITY WITH  
TUNEABLE FLOW AND SURFACE  
CONDITIONS

A VASCULAR GRAFT ON-A-CHIP PLATFORM FOR  
ASSESSING THROMBOGENICITY WITH TUNEABLE FLOW  
AND SURFACE CONDITIONS

BY  
VERONICA A. BOT, B. Sc.

A Thesis Submitted to the School of Graduate Studies in Partial Fulfilment of the  
Requirements for the Degree Master of Applied Science

McMaster University © Copyright by Veronica A. Bot, April 2022  
All Rights Reserved

McMaster University MASTER OF APPLIED SCIENCE (2022): Hamilton, Ontario

**TITLE:** A vascular graft on a chip platform for assessing thrombogenicity with tuneable flow and surface conditions

**AUTHOR:** Veronica A. Bot  
B.Sc. (Medical Physics)  
McMaster University, Hamilton, Ontario

**SUPERVISOR:** Dr. Tohid Didar

**NUMBER OF PAGES:** *xviii*, 110

## Lay Abstract

The goal of this thesis was to investigate the thrombogenicity of lubricant infused surface (LIS) coated ePTFE vascular grafts in the presence of blood flow *in vitro*. This was achieved by first generating a microfluidic testing platform (“vascular graft on-a-chip”) that enables thrombogenic testing of coated expanded polytetrafluoroethylene (ePTFE) grafts under vascular wall shear stress (WSS) conditions. We then introduced lubricant infused (LIS) coatings into the device and investigated clot formation on these surfaces using fluorescent detection markers with and without the presence of endothelial cells. We show that LIS coatings perform well under flow and may have translational potential for *in vivo* vascular graft applications.



## Abstract

The failure of vascular grafts due to thrombosis is an ongoing problem in cardiovascular disease (CVD) management. This issue has motivated the development of novel antithrombogenic strategies capable of attenuating clot formation on the graft surface. The biocompatible lubricant infused surface (LIS) coating has emerged as a promising strategy that has rendered expanded polytetrafluoroethylene (ePTFE) vascular grafts antithrombogenic under static *in vitro* testing conditions. Although compelling, these surfaces have not been tested in the presence of blood flow, and their thrombogenicity remains poorly understood. In this work, we develop a method for robustly binding ePTFE into a microfluidic device using medical-grade pressure sensitive adhesive (PSA) tape (delamination shear stress of 519 dyne per cm<sup>2</sup>). We then functionalize ePTFE surfaces on-chip and introduce coated surfaces in a parallel array of channels.

Leveraging the small scale and visibility of the graft on-a-chip platform, we then compared the thrombogenic performance of coated test surfaces in real time in the presence of vascular wall shear stress (WSS). This was achieved using fluorescein fibrin(ogen) and fluorogenic Boc-Val-Pro-Arg-AMC (7-amino-4-methylcoumarin (AMC)) as markers for clot formation and thrombin activity, respectively. In our study, for the first time, we show that LIS ePTFE surfaces are thromboresistant under flow and outperform standard ePTFE in a dynamic *in vitro* testing environment. We also show that graft surfaces can be endothelialized and that CD34 antibody LIS may confer dual thromboresistance in the presence of endothelial cells.

This work illuminates the translational potential of LIS as an antithrombogenic strategy for *in vivo* grafting applications. It moreover reveals that the vascular graft on-a-chip platform could be a valuable tool for testing the thrombogenicity of novel coatings and or vascular grafts and aid the translation of novel prostheses in general.

## Acknowledgements

I would like to thank my supervisor Dr. Tohid Didar for his guidance and for entrusting me with this challenging project. I appreciated having the freedom to explore science independently and develop my interests in the field. My experience during this degree has made me a more confident and courageous scientist as a result. Thank you for providing opportunities to present my work at the 2022 MicroTas Conference and the Bioengineering and Biotechnology Conference – those were invaluable experiences that have shaped my career tremendously.

The Thrombosis and Atherosclerosis Research Institute (TAaRI) has played an integral role in the development of this project. I would like to thank Dr. Jeffrey Weitz for his invitation to learn at TAaRI and for sharing his extensive knowledge on thrombosis. His mentorship has been instrumental in my development, and I thank him for his encouragement throughout this experience. Extended thank-you to Dr. Jim Fredenburg for supporting me throughout my master's journey and for providing advice on experimental protocols. Dr. Iqbal Jaffer, Rida Malik- thank you for your insights on the clinical aspects of vascular prosthesis and for your assistance preparing reagents. TAaRI became a second home for me- and I am eternally grateful for that.

I extend my sincerest thank-you to my peers in the School of Biomedical Engineering who have provided their insights about this project. In particular: Dr. Maryam Badv, Dr. Amid Shakeri, Tamaghna Gupta, and Martin Villegas - who tolerated my bizarre questions and did their best to answer them. Their assistance enabled me to perform CFD simulations, cell culture, surface functionalization, and helped me gain a broader understanding of biomedical engineering in general. I would also like to thank the faculty at McMaster; in particular, Marcia Reid for her assistance with scanning electron microscopy (SEM), Dr. Mark Inman for his valuable insights on the scientific method, and Dr. Ravi Selvaganapathy for his advice on microfluidic fabrication.

Finally, to my parents Mitzi and David- I could not have gotten this far without you. I am grateful for your kindness and support throughout life. To my partner Jae-Min; thank-you for being by my side for the past 5 years. I look forward to embarking on the next chapter of life together

## Table of Contents

Lay Abstract .....	iv
Abstract .....	v
Acknowledgements .....	vi
Table of Contents .....	vii
List of Figures .....	xi
List of Tables .....	xv
Declaration of Academic Achievement .....	xviii
Chapter 1: Literature Review .....	1
1.0 Foreword .....	1
1.1 Cardiovascular Disease and the Role of Vascular Grafts .....	1
1.1.1 Vascular System .....	1
1.1.2 Blood .....	3
1.1.3 Cardiovascular Disease .....	5
1.2 Vascular Graft .....	6
1.2.1 Vascular Graft Materials .....	6
1.3 Vascular Graft Thrombosis .....	8
1.3.1 Vascular Graft Performance .....	8
1.3.2 Thrombosis .....	9
1.3.3 Conclusion .....	13
1.4 Coatings .....	14
1.4.1 Properties of the Graft Surface .....	14
1.4.2 Antithrombogenic Coating Strategies .....	16
1.5 Testing and Translation of Novel Antithrombogenic Coatings .....	22
1.5.1 Outlook .....	22
1.5.2 Translational Pathway .....	22

1.5.3 Static In Vitro Testing Platforms .....	26
1.6 The Importance of Flow.....	27
1.6.1 Virchow’s Triad .....	27
1.6.2 Hemodynamics.....	29
1.6.2.1 Wall Shear Stress .....	30
1.6.2.2 Hemodynamics and Thrombosis.....	30
1.7 Dynamic In Vitro Testing Platforms.....	33
1.7.1 Shear Flow Models .....	34
1.7.2 Other Testing Approaches.....	39
1.8 Microfluidics .....	40
1.8.2 Advantages .....	42
1.8.3 Organ On-a-Chip.....	47
1.9 Vascular Graft On-a-Chip.....	50
1.9.1 Rationales.....	50
1.8.2 Objectives.....	52
Chapter 2: A vascular graft on a chip platform for assessing thrombogenicity with tuneable flow and surface conditions.....	53
2.1 Abstract .....	54
2.2 Introduction.....	54
2.3 Results .....	56
2.3.1 Principle, Fabrication, and Functionalization of the Vascular Graft On-a-Chip Device .....	56
2.3.2 Assessing the Thrombogenicity of Lubricant Infused (LIS) and Uncoated ePTFE Vascular Graft Surfaces Without Endothelial Cells.....	60
2.3.3 Assessing the Thrombogenicity of Endothelialized LIS, anti-CD34 LIS ePTFE Graft Surfaces With Endothelial Cells.....	63
2.4 Discussion .....	69
2.5 Conclusion .....	71

2.6 Materials and Methods.....	71
2.6.1 Materials.....	71
2.6.2 Chip Fabrication.....	72
2.6.3 Blocking Polymethylmethacrylate (PMMA) with PLL-g-PEG Copolymer.....	73
2.6.4 Shear Tolerance and Perfusion Tests.....	73
2.6.5 Channel Geometry and Wall Shear Stress.....	74
2.6.6 Perfusion.....	74
2.6.7 Surface Coating Procedures.....	75
2.6.8 HUVEC Cell Culture.....	75
2.6.9 VE-Cadherin, F-Actin, and Nuclear Staining.....	76
2.6.9 Scanning Electron Microscopy.....	76
2.7 Statistical Analysis.....	77
2.8 Acknowledgements.....	77
2.9 Disclosures.....	77
Chapter 3: Closing Remarks and Future Directions.....	78
3.1 Findings.....	78
3.2 Contribution to the Field.....	78
3.3 Future Directions and Closing Remarks.....	79
3.4 Challenges.....	80
Chapter 4: Supplementary Information and Methods Elaboration.....	82
4.1 Chip Fabrication.....	82
4.1.1 Development of the Platform.....	82
4.2 Coating Protocols.....	84
4.2.1 Stability of Lubricant Infused Surface (LIS) Under Shear Flow Conditions.....	84
4.2.2 Verifying the Presence of anti-CD34 On Anti-CD34 LIS Surfaces.....	85
4.3 Channel Fabrication.....	86
4.3.1 Optimization of Laser Settings.....	86
4.4 Perfusion and Clot Formation.....	86
4.4.1 Experimental Set-Up.....	86

4.5 Channel Dimensions and Flow Parameters .....	88
Appendix .....	90
A.1 Fluorescent Protein Labeling Protocol.....	90
References .....	92

## List of Figures

<b>Figure 1:</b> Anatomy of artery, vein, and capillary. Reprinted from Gomes De Almeida, V., 2013. (dissertation).....	4
<b>Figure 2:</b> The coagulation cascade. Reprinted from Kuchinka J., in New. Front. Art. Org. Eng. 2021 (8). Copyright <i>Elsevier</i> .....	12
<b>Figure 3:</b> Key structural and functional properties of the material surface. Reprinted from Rahmati M., in Chem. Soc. Rev. 2020 (49), 5178-5224, Copyright <i>Royal Society of Chemistry</i> .	15
<b>Figure 4:</b> Lubricant infused surface (LIS) with nanostructured substrate, HUVEC adhesion on uncoated and ECM/anti-CD34 coated ePTFE grafts, TLP and uncoated polycarbonate cannulas and patency after 8-hour perfusion, ePTFE vascular grafts functionalized with poly(1,8-octanediol-co-citrate) (POC) heparin layer. Reprinted from Li J., in Adv. Fun. Matl. 2018 (4) Copyright <i>Wiley-VCH</i> ; Leslie D., in Nat. Biotech., 2014 (32) Copyright <i>Springer Nature</i> ; Chen L., in Tiss. Eng. Regen. Med., 2017 (14) Copyright <i>Springer Nature</i> ; Smith, R., in Sci. Trans. Med., 2012 (4), 803-811, Copyright <i>Science</i> .....	20
<b>Figure 5:</b> Quantifying thrombogenicity in vitro: Blood clot formation anti-CD34 conjugated ePTFE surfaces with and without perfluorinated lubricant. Fluorogenic thrombin substrate Boc-Val-Pro-Arg-AMC which generates blue fluorescent 7-amino-4-methylcoumarin (AMC) product upon cleavage of the amide bond by thrombin. SEM of adhered activated platelets with dendritic-like structure. Adhesion of fluorescent fibrinogen and fluorescently labeled platelets on APTES/TPFS coated and uncoated surfaces. Reprinted from Varju I., 2018. Sci. Reports, (8) Copyright <i>Springer</i> ; Badv M., 2019. ACS Biomater. Sci. Eng. (5), 6485-6496, Copyright <i>ACS</i> ; Badv M., 2018. ACS Nano, (12), 10890-10902, Copyright <i>ACS</i> .....	24
<b>Figure 6:</b> Virchow's Triad for vascular prosthesis thrombosis, with shear-dependent behaviour of platelets and von Willebrand Factor, and thrombus formation on explanted arterial and venous polyurethane grafts in vivo sheep model. Reprinted from Dangas J., et al. J. Am. Coll. Cardiol. 2016 (24), 2670-2690, Copyright <i>Elsevier</i> ; Hong J., et al. Biomater. Sci., 2020 (8), 5824-5845, Copyright <i>Royal Society of Chemistry</i> ; and Fleser P., et al. J. Vasc. Surg., 2004 (4), 803-811, Copyright <i>Elsevier</i> .....	28

<b>Figure 7:</b> Reynold’s Number, Laminar Flow, and Turbulent Flow. Reprinted from Westerhof N., 2010. Snapshots of Hemodynamics, pp. 23-25, Copyright <i>Springer</i> .....	29
<b>Figure 8:</b> Chandler Loop, peristaltic pump, parallel plate, and well plate in vitro thrombogenicity testing platforms. Reprinted from Hong J., et al. <i>Biomater. Sci.</i> , 2020, 8, 5824-5845, Copyright <i>Royal Society of Chemistry</i> ; and Albadawi H., et al. <i>Adv. Sci.</i> , 2021, 8, 2003327 Copyright <i>Wiley-VCH</i> .....	36
<b>Figure 9:</b> Microfluidic chip and related uses modeling vascular flow and physiology. Reprinted from Tran R., et al. <i>J. Cell. Mol. Med.</i> 2013, (5), 597-596, Copyright <i>Wiley-VCH</i> ; Zhou J., et al. <i>Microsystems &amp; Nanoengineering</i> . 2019, (5) Copyright <i>Springer Nature</i> .....	41
<b>Figure 10:</b> Pressure sensitive adhesive (PSA) assisted fabrication of a microfluidic device. Reprinted from Sen A, et al. <i>Sci. Reports</i> . 2021, (11) Copyright <i>Springer</i> .....	44
<b>Figure 11:</b> Parallel plate flow condition with parabolic velocity profile. Reprint from Westerhof N., 2010. Snapshots of Hemodynamics, pp. 23-25. Copyright <i>Springer</i> .....	45
<b>Figure 12:</b> Conceptual sketch of the graft on-a-chip platform, fabrication, and functionalization, with <b>(a)</b> graft on-a-chip platform with blood perfusion. <b>(b)</b> expanded diagram of the platform with component layers, including: PMMA, channels (PSA biocompatible tape sheet), ePTFE, and 3D printed inlets. <b>(c)</b> shear tolerance of the graft-chip device when bonded to 6 clinically relevant materials: poly (methyl methacrylate) (PMMA), polyethylene (PE), ePTFE, polyvinyl chloride, nylon, silicone used in catheters, stents, grafts, hemofilters, and heart valves respectively. Delamination of ePTFE bonded PSA adhesive is illustrated in the left panel with dyed water. <b>(d)</b> common grafting sites with corresponding wall shear stresses and recapitulation of in vivo grafting conditions in vitro on the graft-chip device <b>(e)</b> illustration of graft thrombosis, antithrombogenic graft surfaces, and functionalization of those surfaces in the graft on-a-chip device. Uncoated surface exhibiting non-specific adhesion and thrombosis, CD34 antibody LIS exhibiting endothelial proliferation and attenuated thrombosis, LIS showing <b>(f)</b> 4-step fabrication protocol requiring: substrate selection, cutting PSA channels, functionalization, and perfusion...59	59
<b>Figure 13:</b> Application of graft on-a-chip platform for probing the thrombogenicity of ePTFE and LIS ePTFE graft surfaces under arterial WSS. <b>(a)</b> illustration of the device cross section with associated testing surfaces and channel geometry with physiological WSS inspiration (lower extremity bypass). <b>(b)</b> perfusion set-up consisting of syringe pump, reservoir, and fluorescent	



microscope. **(c)** qualitative assessment of thrombogenicity at 3 time points: 0min (left), 8 min (middle), 20min (right). Fluorescent labels include: fibrin(ogen) (AlexaFluor488 in green  $\lambda_{488nm}$ ), thrombin activity with Boc-Val-Pro-Arg-AMC (blue  $\lambda_{350nm}$ ). **(d)** appearance of occluded channel(s) both with and without fluorescence. **(e)** in **(i)** quantification of adherent fibrin(ogen) post-occlusion, after gently washing the channel with HEPES buffer and in **(ii)** Boc-Val fluorescent intensity as a function of time during the course of perfusion. **(f)** SEM images of surfaces post-perfusion with the presence of activated platelet (PLT), red blood cells (RBC), and white blood cells (WBC). Data are shown with Mean $\pm$ SD error bars with significance  $p < 0.05$ , area under the curve (AUC) was tabulated in **(e-ii)**. .....62

**Figure 14:** **(a)** endothelialized channel surfaces prior to thrombogenicity testing with: top row- Anti-CD34 lubricant infused (LIS) ePTFE, middle row- ePTFE, bottom row- lubricant infused (LIS) ePTFE. Immunofluorescence labels include: endothelial cells (RFP HUVEC in orange  $\lambda_{544nm}$ ), nuclei (Hoescht 33342 in blue  $\lambda_{350nm}$ ), VE-Cadherin CD-144 (AlexaFluor 647 in red  $\lambda_{647nm}$ ), and F-actin (AlexaFluor 488 in green  $\lambda_{488nm}$ ). **(b)** distinct graft-chip testing channels and surfaces during blood perfusion with human hand for size comparison. **(c)** cell density on the 3 test surfaces. **(d)** Brightfield images of each surface at 20X. ....65

**Figure 15:** Application of graft on-a-chip platform for probing the thrombogenicity of endothelialized ePTFE, LIS ePTFE and Anti-CD34 LIS ePTFE grafts in parallel. **(a)** illustration of the device cross section with associated testing surfaces and channel geometry, with physiological WSS inspiration (arterial anastomosis) **(b)** qualitative assessment of thrombogenicity at 3 time points: 0min (left), 8 min (middle), 20min (right). Fluorescent labels include fibrin(ogen) (AlexaFluor488 in green  $\lambda_{488nm}$ ), thrombin activity with Boc-Val-Pro-Arg-AMC (blue  $\lambda_{350nm}$ ), endothelial cells (RFP HUVEC in orange  $\lambda_{544nm}$ ). **(c)** representative image of channels at occlusion. **(d-i)** quantification of adherent fibrin(ogen) post-occlusion after gently washing the channel with HEPES buffer and **(d-ii)** Boc-Val fluorescent intensity as a function of time during perfusion. **(e)** SEM images of surfaces post perfusion with the presence of red blood cells, fibrin, activated platelets (top-bottom). Data are shown with Mean $\pm$ SD error bars with significance  $p < 0.05$ , area under the curve (AUC) was tabulated in **(d-ii)**. .....69

**Figure 16: Microfluidic Chip Design-** (A-C) early iterations of the platform involving PDMS casting, embedding of the ePTFE graft. Inlet integration was at an undesired 90-degree angle and the device performed poorly. (D-F) Later iterations of the platform involving pressure sensitive

adhesive spacer tape was the bonding agent. Device exhibited robust attachment to ePTFE, PVC, PMMA, nylon, silicone, polyethylene. 3D printed inlets were produced in a parallel configuration and attached using spacer tape. (G) Inspecting channel leakage on various clinically relevant substrates after sustained flow (30 minutes) under low shear stress conditions (5 dyne/cm<sup>2</sup>).. .....83

**Figure 17:** Surface Functionalization and Coating Stability (A-D) To verify the presence lubricant on LIS coated ePTFE surfaces, optical transmittance and sliding angle were measured. Increased transmittance and lowered sliding angle were suggestive of lubricant infiltration on the surface. Stability was tested under a physiological range of wall shear stresses and changes in transmittance were quantified. ....85

**Figure 18:** Verifying the presence anti-CD34 Alexa Fluor 488 conjugated primary antibody on EDC-NHS and CO<sub>2</sub> plasma treated ePTFE substrates for testing the CD34-LIS ePTFE surface condition. (A) ePTFE control, and (B) anti-CD34 ePTFE. Images were taken prior to lubricating the surface, immediately following incubation with EDC-NHS anti-CD34 solution and gently washing with PBS. FITC 4x fluorescence microscopy was used.. .....86

**Figure 19:** Channel Fabrication (A) quality of laser cut as function of power and speed ratio, with (B) representative images of cut performance with varying power/speed parameters. (C) Illustration of channel edges under 20x magnification. ....86

**Figure 20:** Perfusion Set-Up and Channel Occlusion (A-B) perfusion set up with chip placement on the microscope stage. (D-C) Representative image of clot formation in the perfusion channel(s) with 20X fluorescent image of fluorescein fibrin(ogen). (E) A facile fabrication protocol was developed as shown with time estimates in the bottom panel: preparing PMMA, PSA channels, bonding, functionalization, and perfusion.....87

List of Tables

**Table 1:** Synthetic Vascular Grafts and Applications .....6

**Table 2:** In Vitro Dynamic Thrombogenicity Testing Platforms .....38

**Table 3:** Microfluidic Vascular Thrombosis Models and Applications .....49

**Table 4:** Channel Parameters and Flow Calculations.....89

## List of Abbreviations

ADP:	Adenosine Diphosphate
AFM:	Atomic Force Microscopy
AMC:	7-Amino-4-Methylcoumarin
AT:	Antithrombin
CA:	Contact Angle
CPV:	Cone and Plate Viscometer
CTI:	Corn Trypsin Inhibitor
CVD:	Cardiovascular Disease
CVD*:	Chemical Vapor Deposition
EC:	Endothelial Cell
ECM:	Extracellular Matrix
EDC:	N-(3-dimethylaminopropyl)-N'-ethylcarbodiimide
EDTA:	Ethylenediaminetetraacetic acid
ELISA:	Enzyme Linked Immunoassay
EPCs:	Endothelial Progenitor Cells
ePTFE:	Expanded Polytetrafluoroethylene
ET-1:	Endothelin-1
GPIb:	Platelet Glycoprotein Ib
HSA:	Human Serum Albumin
HEPES:	4-(2-Hydroxyethyl)piperazine-1-ethanesulfonic acid
HePTFE:	Small-Caliber Heparin-Bonded Vascular Graft
HMWK:	High Molecular Weight Kininogen
LIS:	Lubricant Infused Surface
LVD:	Liquid Vapor Deposition
MES:	2-(N-morpholino)ethanesulfonic acid
MHV:	Mechanical Heart Valve
MTT:	3-(4,5-dimethylthiazol-2-yl)-2,5-diphenyl-2H-tetrazolium bromide
NHS:	N-Hydroxysuccinimide

NO:	Nitrous Oxide
OOC:	Organ On-a-Chip
PCB:	Prosthetic Carotid Bypass
PEG:	Polyethylene Glycol
PEO:	Polyethylene Oxide
PET:	Polyethylene Terephthalate
PFPP:	Perfluoroperhydrophenanthrene
PGI <sub>2</sub> :	Prostacyclin
PK:	Prekallikrein
PMMA:	Polymethylmethacrylate
PPACK:	Trifluoroacetate salt
PSA:	Pressure Sensitive Adhesive
PU:	Polyurethane
PVC:	Polyvinyl Chloride
RFP:	Red Fluorescent Protein
TEVG:	Tissue-Engineered Vascular Graft
TF:	Tissue Factor
TFPI:	Tissue Factor Pathway Inhibitor
TLP:	Tethered Liquid Fluorocarbon
TPFS:	Trichloro (1H, 1H, 2H, 2H-perfluorooctyl) silane
VEGF:	Vascular Endothelial Growth Factor
vWF:	Von Willebrand Factor
WSS:	Wall Shear Stress
XPS:	X-Ray Spectroscopy
αIIbβ <sub>3</sub> :	Platelet Integrin αIIbβ <sub>3</sub>

## Declaration of Academic Achievement

- Chapter 1, “Literature Review” was drafted by Veronica A. Bot and reviewed to the final version by Dr. Tohid F. Didar.
- Chapter 2, “A Vascular Graft On-a-Chip Platform for Assessing Thrombogenicity with Tuneable Flow and Surface Conditions” was drafted by Veronica A. Bot under the supervision of Dr. Tohid F. Didar. Veronica A. Bot performed the experiments with the assistance of Dr. Amid Shakeri (endothelialization protocol). The manuscript was reviewed by Dr. Amid Shakeri, Dr. Jeffrey I. Weitz, and Dr. Tohid F. Didar.
- Chapter 3, “Conclusions and Future Directions” was drafted by Veronica A. Bot and reviewed to the final version by Dr. Tohid F. Didar.
- Chapter 4 and Appendix, “Supplementary Information and Methods Elaboration” was drafted by Veronica A. Bot and reviewed to the final version by Dr. Tohid F. Didar.

## Chapter 1: Literature Review

### 1.0 Foreword

This thesis provides two major contributions. The first of these contributions is the generation of a microfluidic platform that incorporates expanded polytetrafluoroethylene (ePTFE) vascular graft(s), vascular-like wall shear stress (WSS) with tuneable flow and surface conditions. The second is the application of this platform for testing the thrombogenicity of novel lubricant infused surface (LIS) and anti-CD34 lubricant infused coated ePTFE surface(s) in the presence of blood flow *in vitro*. The overarching vision is that this device could help illuminate the translational potential of LIS coatings and or vascular prostheses in general. To capture the full scope of this project, the background has been comprehensively written.

Subchapters 1.1, 1.2 and 1.3 explore vascular graft performance and the cause(s) of graft thrombosis. An understanding the physiological context of vascular grafts is required and explained alongside the structure and function of the cardiovascular system in subchapter 1.1. In subchapter 1.4, coatings are introduced as a strategy for overcoming graft thrombosis *in vivo*. In subchapters 1.5 to 1.7, current types of *in vitro* testing models are examined and their shortcomings are investigated. Finally, in subchapter 1.8, microfluidics is presented as an emergent testing modality which harnesses tuneable flow and surface properties. The use of microfluidics for vascular modeling and thrombogenicity testing is described. In section 1.9, the rationales and experimental objectives for the project are outlined.

### 1.1 Cardiovascular Disease and the Role of Vascular Grafts

#### 1.1.1 Vascular System

The vascular system is a network of blood vessels and organ(s) that work together to move blood throughout the body. Blood vessels are classified as arteries, veins, or capillaries based on their characteristic structure and function. Arteries, such as the coronary artery and aorta, are thick muscular vessels that carry oxygenated blood from the heart to other parts of the body. Veins, such as the vena cavae, are thinner vessels that carry deoxygenated blood back to the heart (Tucker et al., 2021). Both arteries and veins are potent flow regulators and can constrict or dilate in response to cellular cues. Capillaries are microscale vessels that carry out gas and nutrient exchange in vascular networks

surrounding tissues and organs. Both arteries and veins have complex cellular architecture that is arranged into concentric layers that encompass the tunica externa (collagenous connective tissue), tunica media (elastic muscular tissue), and the tunica intima (interior endothelial surface). Capillaries have a simpler structure containing only a thin layer of endothelium and connective tissue (Tucker et al., 2021). The heart is a four-chambered muscular organ that serves as the pump which drives the movement of blood throughout blood vessels in the body.

The endothelial lining of blood vessels provides an important sensing interface that modulates vascular flow and physiology. Once thought of as a mere physical barrier between blood and vessel, the endothelium is now viewed as an active metabolic and endocrine organ (Galley & Webster, 2017). The endothelium is made up of endothelial cells (EC) and basal lamina containing type IV collagen(s), elastin, laminins, fibronectin, vitronectin, proteoglycans, perlecan, among other extracellular matrix (ECM) proteins (Krüger-Genge et al., 2019). ECs are thin, slightly elongated nucleated cells with an approximate length of 30-50 $\mu\text{m}$ , width of 10-30 $\mu\text{m}$ , and height of 0.1-10 $\mu\text{m}$  (Galley & Webster, 2017). These cells are polarized; meaning the apical (luminal) surface of the cells contacts blood flow and can interact with chemical and mechanical signals present in circulation (Krüger-Genge et al., 2019). This direct exposure to blood enables EC mechanosensing (e.g. deformation of ion channels, cytoskeletal tubules and filaments) and expression/secretion of regulatory solutes, macromolecules, proteins, and hormones (Fang et al., 2019; Krüger-Genge et al., 2019).

The intelligent structure of the vascular endothelium is reflected in its diversity of functions. The endothelium is involved with constriction and dilation of blood vessels, inflammation, hemostasis, and angiogenesis (Krüger-Genge et al., 2019). To regulate blood flow, ECs can sense wall shear stress (WSS) and respond via secretion and expression of vasodilating agents (e.g. nitric oxide (NO), thrombomodulin, prostacyclin (PGI<sub>2</sub>)) or contractile agents (e.g. endothelin-1 (ET-1)) (Krüger-Genge et al., 2019; Sandoo et al., 2010). ECs moreover modulate hemostasis and inflammation through direct interactions with plasma proteins, platelets, and leukocytes present in circulation (Krüger-Genge et al., 2019). In the event of bleeding or injury, ECs secrete procoagulant agents like platelet activating factor (PFA) and thromboxane A<sub>2</sub> to promote the formation of a blood clot (Sena et al., 2018). Conversely, when an unwanted blood clot is forming, ECs can slow the clotting process by upregulating inhibitors and releasing anticoagulant agents such as thrombomodulin (TM) and tissue plasminogen activator (tPA) (Housholder et al., 1991). Of lesser importance to this work, but of interest nonetheless is



angiogenesis. The sprouting of new blood vessels hinges on concurrent vasodilation, EC migration, and EC proliferation in blood vessels (Kruger-Genge et al., 2019). The expression of insulin-like growth factor and transforming growth factor is implicated in this process (Galley & Webster, 2017).

### 1.1.2 Blood

Blood is the fluid medium of the cardiovascular system and makes up the liquid portion of the blood-and-vessel interface. The main function of blood is to distribute oxygen and nutrients in the body. It is a red-colored colloidal suspension containing plasma and the formed elements (Sankar & Varacallo, 2021). Plasma is a straw-colored solution composed of electrolytes, immunoglobulins, plasma proteins, hormones, and coagulation factors which modulate blood osmolarity, immunity, and hemostasis in the body (Sankar & Varacallo, 2021). The formed elements consist of red blood cells (erythrocytes), white blood cells (leukocytes), and platelets (thrombocytes).

#### 1.1.2.1 Red Blood Cells

Red blood cells or “erythrocytes” are anuclear, flexible 6-8 $\mu$ m disk-like cells that make up over 95% of the total blood volume in humans (Sankar & Varacallo, 2021). The primary function of these cells is to transport oxygen from the lungs to other tissues in the body using iron-rich hemoglobin molecules (Klinken, 2002). The presence of hemoglobin gives blood its characteristic red color. In addition to serving as oxygen carriers, red blood cells express antigens (ABO phenotype) and contribute to the rheological properties of blood (Klinken, 2002).

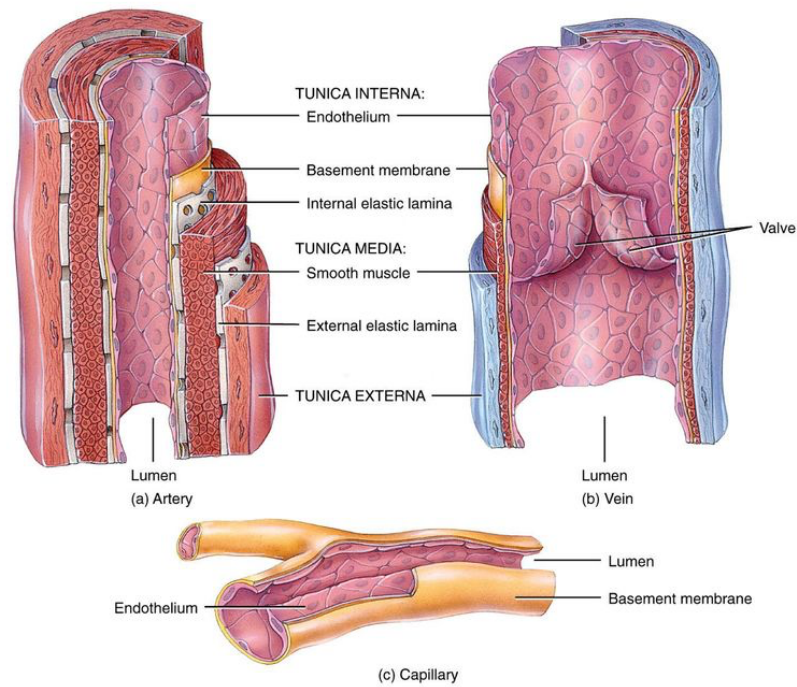
#### 1.1.2.2 White Blood Cells

White blood cells or “leukocytes” are larger 15  $\mu$ m cells that play an integral role in immunity and inflammatory response in the body. There are two types of white blood cells, generally classified as granulocytes or agranulocytes based on the appearance of “granular” cytoplasm and lobe-shaped nuclei. Neutrophils, eosinophils, basophils are granulocytes, whereas lymphocytes and monocytes are agranulocytes (Sankar & Varacallo, 2021). Lymphocytes are involved in adaptive and innate immunity with natural killer (NK), T-cells and B-cells (Gbyli et al., 2017). Monocytes and granulocytes are phagocytotic cells usually involved with innate immunity and compliment activation in response to

foreign materials (Gbyli et al., 2017). White blood cells are less abundant than red blood cells and make up only 1% of the total blood volume in humans.

### 1.1.2.3 Platelets

Unlike red and white blood cells, platelets are not complete cells, but rather, 1.5-3 $\mu$ m fragments of larger cells called megakaryocytes (Sankar & Varacallo, 2021). Like white blood cells, platelets make up only a small fraction of total blood volume at 1% or less. Platelets are responsible for hemostasis and the cessation of bleeding. They have membrane phospholipids and receptors that mediate this process. As will be explored in sub-chapter 1.3, blood plays an important role in mediating the adsorption of proteins, cells, and the formation of clots on vascular graft surface(s).



**Figure 1:** Anatomy of artery, vein, and capillary. Reprinted from Gomes De Almeida, V., 2013 ® (dissertation).

### 1.1.3 Cardiovascular Disease

When the vascular system does not function properly, a range of conditions can develop. One of the most prevalent conditions is cardiovascular disease (CVD). Cardiovascular disease is the leading cause of death and disability worldwide, contributing to an estimated 17 million deaths each year with over 500 million people affected (Sanchez et al., 2018; Kauffman, 2020). Although broadly defined, CVD usually refers to the build-up of fatty deposits (atherosclerosis) and clots on the interior of arteries and veins (Sanchez et al., 2018). Atherosclerosis is thought to be triggered by lifestyle factors such as obesity and smoking but has also been linked to genetics and age (Bahera et al., 2015). It is a progressive condition that begins with the appearance of fatty streaks on the innermost layer of small and medium sized arteries (Davies & Woolf, 1993). These deposits contain only lipid-laden macrophages termed “foam cells”, but in a progressed stage, may thicken to form fibrotic plaque with a lipid-filled core (Davies & Woolf, 1993). This resulting capsular structure causes reduced blood flow and thrombosis in the event of plaque rupture (Davies & Woolf, 1993).

The high prevalence of this condition incurred a financial burden of \$22.2 billion in 2020 in Canada alone; a figure which is expected to increase alongside changing demographics and aging population(s) (Smolderen et al., 2020). The profound cost and loss-of-life caused by CVD has urged the development of effective therapeutic strategies. Current strategies often involve the use of drugs such as statins, fibrinolytics, and blood thinners to attenuate blood cholesterol and the formation of blood clots without the need for surgery (Bergheanu et al., 2017). Although effective, drugs alone are insufficient in complex cases and surgical procedures involving vascular prosthetics (e.g. grafts, stent, MHVs) are required. In surgical procedures, the development of antithrombogenic prosthesis is required for sustained success of treatment and to prevent recurrent disease in affected blood vessel(s) (Bergheanu et al., 2017).

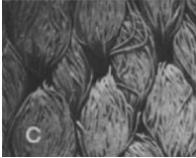
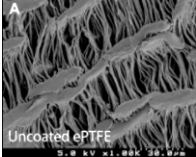
Surgical procedures involving vascular grafts are a mainstay clinical practice. The use of shunts, stents, and grafts as operative tools and *in vivo* implants are essential for treating CVD (Bittl, 1996). Vascular bypass grafting in lower extremity arteries and the aorta has proven instrumental in bolstering long term survival outcomes (Bittl, 1996; Lau & Cheng, 2000). The use of these devices alongside atherectomy and angioplasty has moreover been implicated as a potent “double line of defence” for recurrent CVD (Bittl, 1996). The use of grafts helps alleviate limb-loss, ischemia, and death that would otherwise occur in individuals suffering from advanced CVD (Kinlay, 2007). Their role as an essential healthcare strategy is undisputed.

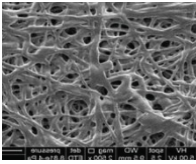
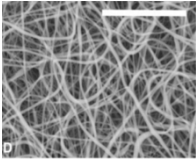
## 1.2 Vascular Graft

### 1.2.1 Vascular Graft Materials

Vascular grafts encompass a range of materials and applications *in vivo*. Since the inception of the first “homograft” by DuBost in 1952, numerous biological (autologous), synthetic, and tissue engineered vascular grafts (TEVGs) have been developed (Callow, 1986). These devices have since been used in coronary, femoral and aortic bypass as well as less common applications in carotid or renal arteries (Khoffi et al., 2014; Camiade et al., 2003). Autologous grafts, such as the mammary artery or saphenous vein, remain the gold standard. However, up to one-third of CVD sufferers do not have access to these vessels due to recurrent disease or repeat surgeries (Carraba & Madedu, 2018). As a result, synthetic substitutes are required. Some of the earliest forms of synthetic grafts were made of Vinyon-N (polyvinyl chloride) and nylon (Callow, 1986). Dacron and expanded polytetrafluoroethylene (ePTFE) have since emerged as a preferred choice due to their porosity, tuneable surface structure, and tensile resilience (Desai & Hamilton, 2011; Callow, 1986). Polyurethane is another popular material, but it is typically used for haemodialysis access rather than vascular bypass (Desai & Hamilton, 2011). Although vastly differing in material properties, Dacron, ePTFE, and polyurethane are all inert, biocompatible, with generally good thromboresistance (Desai & Hamilton, 2011). The table below presents a list of relevant synthetic graft materials, their defining properties, applications, and surface architecture.

**Table 1:** Synthetic Vascular Grafts and Applications

Vascular Graft (Trade Name)	Property	Application	Surface Topography
Knitted Dacron DeBakey®, Meadox®, Cooley Veri-Soft®, Gelseal®, Braun Uni- Graft®	Woven, crimped polyester (C <sub>10</sub> H <sub>8</sub> O <sub>4</sub> ) <sub>n</sub> , microporous, low thrombogenicity	Femoropopliteal <sup>[1]</sup> , aortoiliac, thoracic aorta <sup>[2]</sup> , ascending aorta <sup>[2]</sup>	
ePTFE GoreTex®, Bard®, Boston Exxcel Soft®, Vascutek Maxiflow®	Smooth, porous polytetrafluoroethylene (C <sub>2</sub> F <sub>4</sub> ) <sub>n</sub> , low thrombogenicity	Femoral-popliteal <sup>[3]</sup> , prosthetic carotid bypass (PCB) <sup>[4]</sup> , aorta, liver outflow reconstruction venoplasty (LDLT) <sup>[5]</sup>	

<p>Polyurethane electrospun Tecoflex (EG-80A) and Pellethane (2363-80A)</p>	<p>More elastic than ePTFE and Dacron, <math>C_3H_8N_2O</math><sup>[7]</sup>, low thrombogenicity</p>	<p>Arteriovenous graft <sup>[6]</sup>, artificial heart valves</p>	
<p>Polycarbonate polyurethane/ segmented aliphatic polyurethane/polyurethane polydimethylsiloxane</p>	<p>Elastic, nanofibrous <sup>[9]</sup>, <math>C_3H_8N_2O</math>-(X) spongy, low thrombogenicity</p>	<p>Arteriovenous graft <sup>[6]</sup> coronary artery bypass (postulated) <sup>[8]</sup></p>	

[1] Chester, J. in *Ann. Coll. Surg.* 2008 (4); [2] Takami, Y. in *Int. Cardio. Thor. Surg.* 2012 (5); [3] McCollum, C. in *Eur. J. Vasc. Surg.* 1991 (4); [4] Camadie in *J. Vasc. Surg.* 2003 (5); [5] Arikan, T. in *Transpl. Proc.* 2019 (7); [6] Kakisis, J. in *J. Vasc. Surg.* 2017 (6); [7] Akduman, C. in *Asp. Poly.* 2017; [8] Okoshi, T. in *J. Thor. Cardio. Surg.* 1993 (5). [9] Qiu, X in *Acta. Biomat.* 2017 (51).

In addition to synthetic and autologous grafts, efforts have been made to develop hybrid materials using biological and tissue engineering techniques (TEVGs). Although beyond the scope of this review, noteworthy examples include the use of degradable polymeric and biopolymer graft materials. Biocompatible degrading polymers such as polyglycolic acid (PGA), poly(D,L-lactide/glycolide copolymer), PLLA and poly-lactic acid (PLA) have been shown to promote EC integration and attenuate thrombogenicity *in vivo* animal studies (Mallis et al., 2020; Strohbach & Busch, 2021). Biopolymers such as hyaluronan and silk have been deployed in Sprague-Dawley rat and rabbit models and yielded desirable mechanical properties after sustained use (Mallis et al., 2020; Gupta et al., 2021). Xenografts are somewhat controversial but have also explored and shown satisfactory outcomes *in vivo* in preliminary studies (e.g. bovine xenograft for hemodialysis access) (Pineda et al., 2017). Ideally, vascular grafts should be biocompatible, thromboresistant, with mechanical and surface properties like that of native vasculature. The use of hybrid materials is an exciting frontier in materials science that could provide grafts with the required properties to ensure long term success *in vivo*.

### 1.3 Vascular Graft Thrombosis

#### 1.3.1 Vascular Graft Performance

Despite their importance for treating CVD, synthetic vascular grafts do not always perform well *in vivo*. The formation of blood clots – or thrombi- on the graft surface is one of the most prevalent issues. Thrombi arise from interactions between the graft surface and blood flow in local vascular microenvironment(s) (to be described in more detail in sub-chapter 1.6). Other less common causes of failure include *Staphylococcus aureus* and *Candida* infection in both the early and late post-operative stage (Lairmore & Audisio, 2006). Structural degeneration and progression of disease at the material and vessel interface have moreover been cited as complications that can arise on vascular grafts (Hoffman et al., 2004). Compliance mismatch and dilation of the graft over time causing leakage has been cited as a cause of hemorrhage and even death in rare cases (Duvnjak, 2014). Proliferation of smooth muscle cells onto grafts has been reported as a cause of intimal hyperplasia and restenosis leading to graft failure (Bush, 1989; Hoffman et al, 2004). Abnormal hemodynamics and graft kinking have moreover been cited as contributors to this process *in vivo* (Chester, 2008).

Expanded polytetrafluoroethylene (ePTFE) vascular grafts are one of the most popular synthetic grafts used worldwide today (Gourlay & Black, 2010). ePTFE is a linear thermoplastic polymer consisting of tightly packed carbon and fluorine bonds. It becomes “expanded” through stretching and extrusion during the manufacturing process (Gourlay & Black, 2010). Its low surface energy, porosity, and thermal/chemical stability make it a near-ideal prosthetic material for blood contacting applications. Although performing generally well compared to other graft materials, ePTFE vascular grafts continue to fail in small diameter (<6mm), low flow scenarios *in vivo*. A reported 50% of ePTFE grafts fail within 10 years of use; with poor performance(s) and 39% (5-year) and 14% (45 months) patency rates in the lower extremity and coronary arteries (Sanchez et al., 2018). The necessity of synthetic alternatives and poor performance of ePTFE grafts has prompted the development of improved antithrombogenic strategies. In addition to systemic drug administration, coatings are a promising method of enhancing the thrombogenic performance of ePTFE grafts (lubricant infused surfaces- LIS are an example of this). The use of coatings as an antithrombogenic strategy will be comprehensively addressed in chapter 1.4.

### 1.3.2 Thrombosis

#### 1.3.2.1 Protein Adsorption

When a vascular graft contacts blood, a number of interactions occur. The nature of this interaction(s) depends on the properties of the graft surface and those of interacting proteins, cells, and neighboring blood flow. These interactions are part of an interconnected “web” of events that take place within the vascular environment(s) *in vivo*. One of the first events that occurs when blood encounters the vascular graft is the adsorption of proteins onto the material surface. Blood contains over 300 proteins of varying shape, size, and concentration (Jaffer et al., 2016). These proteins are made of amino acids that assemble into primary, secondary, tertiary, and quaternary structure(s) (Latour, 2008). Proteins possess unique structural properties that contribute to their roles as enzymes, receptors, transport proteins, and or inhibitors/cofactors in the body. The adsorption of proteins onto blood-contacting surfaces results in the formation of a protein layer that mediates cellular adhesion and thrombosis. Although involving many different proteins of varying shapes and size(s); fibrinogen, albumin, and immunoglobulins (IgG) are cited as the main contributors to the formation of the adsorbed layer (Brash et al., 2019). Uncontrolled adsorption of proteins and cells onto the surface is termed non-specific adhesion (Brash et al., 2019).

Protein adsorption is a complex process. The dynamics of protein adsorption are thought to be governed by kinetic (e.g. diffusion and convection) and thermodynamic (e.g. Gibb’s Free Energy) principles as described by Sask. The hydrophobicity, topography, electrostatic charge, and chemical reactivity of the graft surface moreover modulate the kinetic/dynamic aspects of this blood-material interaction. For reference, a comprehensive review of surface and protein interactions is provided by Schmidt et al. Fibrinogen is usually one of the first plasma proteins to adsorb onto the surface. It is a rod-shaped 350 kDa protein with an estimated concentration of 3-5% in human blood. It plays an important role in the formation of thrombi through its polymerization to fibrin and role in tethering blood cells onto the material surface. Other proteins, such as von Willebrand Factor (vWF), fibronectin, factor XII, high molecular weight kininogen (HMWK), and prekallikrein (PK) adsorb afterwards and mediate platelet adhesion and compliment activation (Jaffer et al., 2015). These proteins are present in lower concentrations *in vivo*, usually of the order 70µg/mL or less- but exhibit higher affinity and can displace other proteins attached to the surface (the so-called “Vroman Effect”) (Leeman et al., 2018).

Factor XII (factor-12) is a particularly important protein that is responsible for the production of thrombin via the intrinsic “contact pathway” of the coagulation cascade. Factor XII is especially prone to adsorbing on negatively charged surfaces where it becomes autoactivated to form factor XIIa (Jaffer et al., 2015). This autoactivation is thought to occur due to a conformational change(s) in the protein upon contacting the material surface (Jaffer et al., 2015). According to recent studies, it is also possible that activation of factor XII is linked to procoagulant platelets in plasma, wherein activated platelets promote coagulation in a factor XII dependent manner (Bauer et al., 2017).

#### 1.3.2.2 Blood Cell Adhesion

Following the formation of a protein layer on the graft surface, platelets, leukocytes, and red blood cells deposit onto the blood-graft interface. Platelet adhesion usually occurs through interaction with fibrinogen via platelet integrin  $\alpha\text{IIb}\beta_3$  and by vWF-mediated binding to glycoprotein GPIb (Sask, 2012). Fibronectin and von Willebrand Factor (vWF) are also believed to play a role in tethering platelets material surfaces via receptor-mediated interactions to a lesser extent (Sask, 2012). Once adhered, platelets become activated, change shape, and secrete thromboxane  $A_2$ , adenosine diphosphate (ADP), platelet factor 4 (PF4), and other prothrombotic factors from dense and  $\alpha$ -granules into the surrounding blood (Sask, 2012). The secretion of these substances promotes further adhesion, activation, and aggregation of platelets onto the material surface. Leukocytes adhere to material surface(s) via interaction with fibrin through cell receptor CD11b/ CD18 (Jaffer et al., 2015). Platelets are also believed to mediate leukocyte adhesion via P-selectin and glycoprotein ligand-1 (Jaffer et al., 2015). Adhered leukocytes (compliment) are thought to promote thrombosis through the secretion of platelet activating factor (PAF) from degranulating vesicles (Jaffer et al., 2015). In contrast to both leukocytes and platelets, red blood cell adhesion does not depend on receptor-mediated interactions. Rather, red blood cells passively adsorb based on fluidic shear stress and electrostatic attraction. The presence of adsorbed proteins, activated platelets, leukocytes, and red blood cells “primes” the surface for thrombosis and activation of the coagulation cascade.

#### 1.3.2.3 Coagulation Cascade

Thrombosis can be thought of as a cascade of events involving coordinated activity of proteins and cells to form a clot- or thrombus. The coagulation cascade involves 12 distinct clotting factors and 2 cofactors (factor VIII and V) and that are arranged into a series of proteolytic reactions (Palta et al., 2014). Clotting



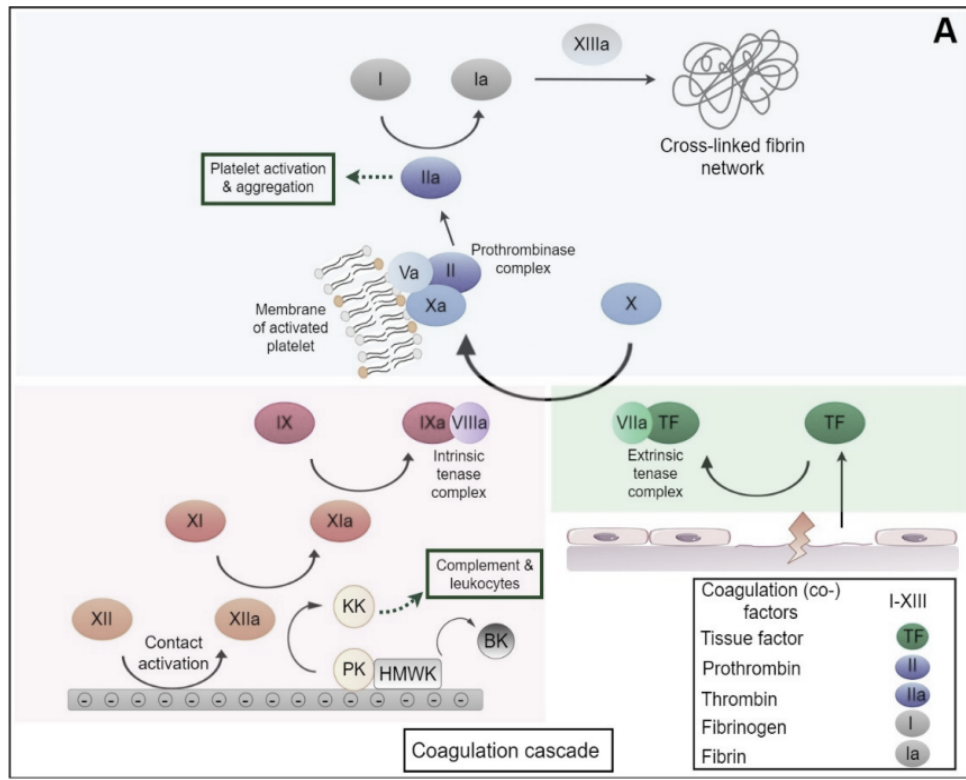
factors are usually produced in the liver and exist in low concentrations in human blood, typically on the order of 30 mg/L or less (Leeman et al., 2018). The coagulation cascade is generally viewed as having three pathways, the intrinsic or “contact pathway”, and the extrinsic or “tissue factor pathway”, and the common pathway (Sask, 2012). In the event of vascular injury, the extrinsic pathway is triggered by exposure of tissue factor (TF) in the vascular sub-endothelium (Smith et al., 2012). This sets off the binding of TF to factor VIIa and calcium to promote conversion of factor X to Xa (Smith et al., 2012).

The intrinsic contact pathway is a parallel and distinct mechanism of thrombus formation. Unlike the extrinsic pathway, the contact pathway is initiated by the adsorption of factor XII to the material surface, and its conversion to activated factor XIIa. The activated factor XIIa then converts prekallikrein to kallikrein and factor XI upon binding to high molecular weight kininogen cofactor (HMWK) (Sask, 2012). Concurrently, factor XIa converts factor IX to factor IXa, which associates with cofactor VIIIa, calcium and phospholipid to generate factor Xa. The common pathway begins with the conversion of prothrombin to thrombin in the presence of factor Xa (from either the intrinsic or extrinsic pathway), factor Va, phospholipid, and calcium. The complex containing factor Xa, factor Va, and phospholipid makes up the prothrombinase complex. The intrinsic pathway is slower than the extrinsic pathway (1-6 minutes versus 15 seconds) but is an equally robust mechanism of generating a clot (Leeman et al., 2018).

The blood-graft interaction is complex and does not depend on coagulation alone. There is crosstalk between the coagulation cascade and complement activation that results in engagement of an inflammatory response *in vivo*. In the contact pathway, complement activation begins with factor XII and a conformational shift in complement protein C3 of the C3/C5 alternative pathway. C3 is the central protein of the complement system and is involved with opsonization, cell lysis, chemotaxis, and the release of anaphylatoxins in response to foreign materials and pathogens (Gbyli et al., 2017). Interaction between C3 and factor XII triggers the production of C3a and C5a and promotes adhesion of leukocytes and monocytes onto the blood contacting surface (Gbyli et al., 2017).

Although beyond the scope of this review, negative feedback and inhibition are aspects of thrombosis and will be briefly discussed to illustrate the importance of hemostatic regulation *in vivo*. Several anticoagulation mechanisms exist to prevent over-coagulation. One such example is the conversion of plasminogen to plasmin (tPA) and production of antithrombin (AT) (Shimada et al., 1991). In this process, plasmin degrades fibrin clot(s) and AT decreases the production of thrombin and factor Xa.

Secretion of thrombomodulin, heparans, and tissue factor pathway inhibitor (TFPI) from endothelial cells can moreover disrupt coagulation through inhibition of thrombin and factor Xa (Shimada et al., 1991). Anticoagulation can also be achieved by assembly of protein C and S on cell surfaces with inactivation of factor Va and factor VIIIa (Esmon et al., 1987). A number of antithrombotic strategies have been inspired by the inhibitory mechanism(s) of these proteins. Direct thrombin inhibitor hirudin and vitamin K antagonists are two such examples.



**Figure 2:** The coagulation cascade. Kuchinka J., in New. Front. Art. Org. Eng. 2021 (8). Elsevier ®

#### 1.3.2.4 Thrombin and Clot Formation

Thrombin (factor IIa) is a 36 kDa enzyme that is responsible for driving the conversion of fibrinogen to fibrin in the final step of the coagulation cascade (common pathway). It circulates in an inactivated form, prothrombin, and becomes activated upon interacting with factor Xa. In addition to its role in generating fibrin, thrombin is also a potent platelet agonist that promotes activation and participates in inflammatory (compliment) response through the C3/C5 pathway (Jaffer et al., 2015). In its cleaved form, fibrin is a soluble protein that polymerizes to form a web-like structure (Weisel et al., 2007). This web-like architecture helps stabilize the fibrin clot and enmeshes platelets, red blood cells and white blood cells within the thrombus. It is this physical aggregate of proteins and cells that fouls material surfaces and produces blood clots on vascular grafts *in vivo*.

#### 1.3.2.5 Anticoagulants and Antiplatelet Drugs

The predominant method of attenuating thrombosis for *in vivo* vascular grafts is the use of antithrombotic drugs. Common types of antithrombotic drugs involve either endogenous or synthetic agents that inhibit platelets, obstruct the coagulation cascade, and/or deactivate thrombin through binding of its active site(s). Anticoagulants such as dabigatran, heparin, and warfarin have been extensively reported in literature as suitable agents for combating thrombosis of synthetic vascular grafts (Keneko & Aranki, 2013). Antiplatelets such as aspirin and clopidogrel have reportedly been used to prevent clot formation on stents in particular (Jaffer et al., 2015). Even though usage of these drugs has been linked to lower incidence of graft (or device) thrombosis, antithrombotic drugs are known to cause bleeding complications (Gambir & Weerasekera, 2017). Antithrombotic drugs have also been implicated with adverse drug interactions. One example is the interaction of direct oral anticoagulants (DOACs) with azoles in particular (Lowe et al., 2010). The magnitude of this problem was well described in a 2012 report by Shepherd et al, which cites systemic anticoagulation as leading cause of clinical-type drug related deaths in the United States (Lowe et al., 2010).

#### 1.3.3 Conclusion

Recognizing the limitations of antithrombotic drug therapy, efforts have been made to develop materials that can overcome material thrombogenicity using alternative approaches. In addition to bulk modification of the graft material, coating remains an attractive option for modulating blood- and-

material surface interaction *in vivo*. The relatively low cost and low risk of surface coatings has enabled the development of a breadth of technologies. At present, coatings have been deployed on small-caliber heparin-bonded (HePTFE) vascular grafts and pyrolytic carbon coated mechanical heart valves (MHV), among other clinical devices. Antithrombogenic coatings strategies have since diversified into other forms involving biomimetic, repellent and/or drug containing agents. These strategies and the principles of coating design are discussed at length in section 1.4, below.

## 1.4 Coatings

The application of coatings onto vascular grafts aims to alter the properties of the blood contacting surface. Compared to antithrombotic drugs, coatings have a low bleeding risk and allow direct application of the antithrombogenic agent onto the material surface (rather than by systemic administration). When considering coatings, it is important to understand the properties of the material surface to which they are applied. The surface charge, topography, hydrophobicity, and chemical reactivity of the graft surface govern its thrombogenic performance and optimal coating strategy.

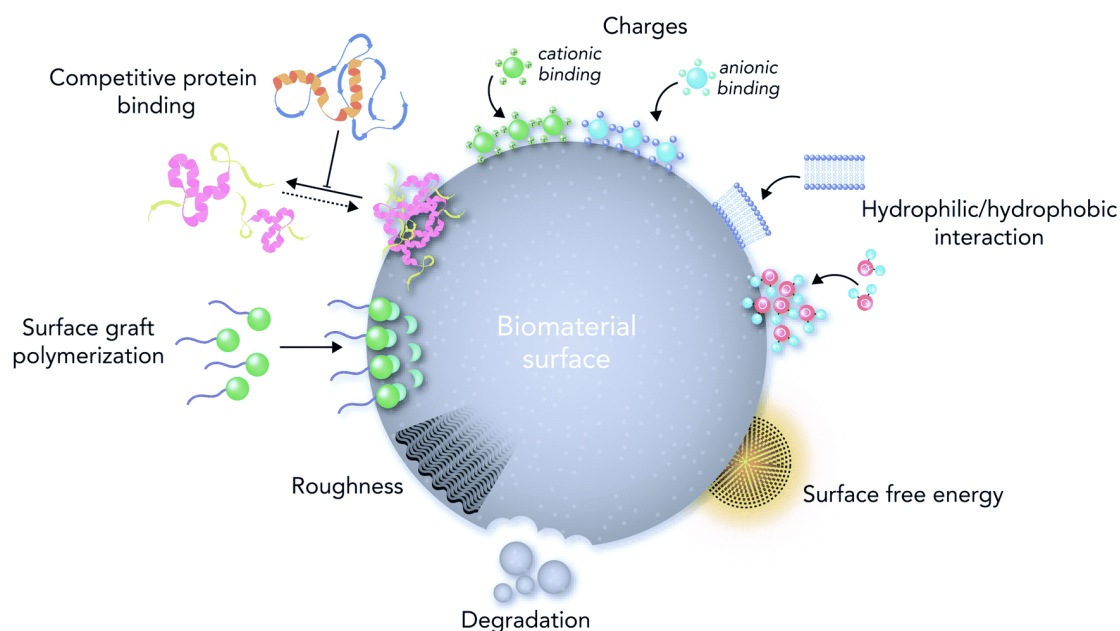
### 1.4.1 Properties of the Graft Surface

#### 1.4.1.1 Hydrophobicity/Hydrophilicity

Hydrophobicity, or the water repellent property of surface(s), describes how well a material can resist wetting. A hydrophobic surface is characterized by contact angles (CA) of 90 degrees or larger and low surface energy of the order  $50 \text{ mJm}^{-2}$  or less (Law, 2014). Hydrophobic surfaces generally exhibit high blood protein adsorptability compared to hydrophilic (CA < 90 degrees) surfaces (Latour, 2005). This is thought to be due to interactions between the surface and hydrophobic domains of the protein(s) causing entropy driven displacement of water from the surface by the so-called “hydrophobic effect” (Hlady & Buijs, 2012; Kuchinka et al., 2021; Agrawal et al., 2017). Compared to CA > 90 degree surfaces, superhydrophobic surfaces (>150 degrees CA) show reduced protein adsorption and lesser blood-material interfacial contact (Mitra et al, 2022). Hydrophilic surfaces demonstrate a high affinity for water, have high surface energy ( $200 \text{ mJm}^{-2}$  or greater), and show generally reduced blood protein adsorptability (Manivasagam et al., 2021). Omniphobicity is a phenomenon describing the tendency of a surface to repel multiple fluids at once- including blood, water, and oil.

### 1.4.1.2 Topography

Topography refers to the architecture or “texture” of material surfaces. This encompasses wrinkles, wells, pillars, and or other structural formations. Some features, such as wrinkles, are known to modulate cellular and protein adhesion and attenuate thrombosis (Pocivavsek et al., 2019). Although the exact mechanism is not fully understood, this is thought to occur due to variations in surface area and the presence of trapped air in microscale grooves (Kuchinka et al., 2021). The presence of roughness on hydrophobic surfaces is known to enhance water repellency due to free energy phenomena described by the Wenzel and Cassie-Baxter models (Yang et al., 2006). Textured superhydrophobic materials are a common occurrence in nature (e.g. rose petals and lotus leaves) and exhibit robust surface repellency.



**Figure 3:** Key structural and functional properties of material surface(s). Rahmati M., in Chem. Soc. Rev. 2020 (49), 5178-5224. The Royal Society of Chemistry ®.

#### 1.4.1.3 Surface Charge and Chemical Reactivity

Surface charge plays an integral role in blood-material interaction in a similar fashion to hydrophobic and or hydrophilic surfaces (e.g. attraction between protein domain(s) and the material surface) (Kuchinka et al., 2021). Chemical reactivity may also alter hemocompatibility via the interaction of surface groups and blood species at the blood-and-material interface. According to Nie et al, some chemical structures, like sulfonic groups, can reduce protein adsorption and contact activation with blood; whereas others, like carboxyl groups, tend to heighten platelet activation and thrombin antithrombin complex (TAT) generation (Nie et al., 2014).

In most cases, material thrombosis occurs due to the combined effects of hydrophobicity/hydrophilicity, surface texture, surface charge, and the chemical composition of the material surface. The complexity of this issue presents a major obstacle for developing antithrombogenic surfaces. Fortunately, a variety of coatings strategies exist and can be used to confer thromboresistance.

#### 1.4.2 Antithrombogenic Coating Strategies

Coating strategies usually involve the use of bioinert polymers, synthetic/endogenous antithrombogenic agents, direct alteration of surface charge, topography, hydrophilicity using liquid vapor deposition (LVD), or etching with laser/plasma irradiation (Badv et al., 2020; Assadian et al., 2005). In most instances, a combination of these strategies is deployed. In addition to the above strategies, “biomimetic” agents such as antibodies and growth factors and/ or lubricant infused surfaces (LIS) have been applied to materials to promote hemocompatibility and endothelial integration *in vivo*. This is conventionally achieved using techniques involving self-assembled monolayers, layer-by-layer deposition, spin coating, chemical vapor deposition (CVD), electrostatic or hydrophobic deposition, polymer grafting, or plasma irradiated polymerization (Yu, 2018). Below is a review of current antithrombogenic coatings that have been applied to blood-contacting materials.

##### 1.4.2.1 Antiplatelet, Anticoagulant, and Drug Eluting Coatings

To overcome the issue of systemic drug administration, anticoagulant and antiplatelet agents have been deployed directly onto blood-contacting surfaces. This is usually achieved by covalent attachment, physical adsorption, and or layer-by-layer deposition of synthetic and or endogenous anticoagulant agents onto the material surface (Badv et al., 2020). Heparin is one of the most well-known anticoagulant

surface coatings, although corn trypsin inhibitor (CTI), nitrous oxide (NO), and direct (synthetic) thrombin inhibitors such as hirudin, bivalirudin, and argatroban have also been described (Jaffer et al., 2015). Strategies involving hirudin modification on polyester, polyurethane, PTFE, and polyethylene have shown good hemocompatibility within *in vitro* testing models (Kuchinka et al., 2021). Moreover, at present, several heparinized grafts are available in the market. Gore® and Gentige® are two such examples that have been used for small and large diameter grafting applications with ePTFE and Dacron, respectively (Badv et al., 2020). Drug eluting devices containing everolimus and zotarolimus have also been developed (Cutlip & Abbot, 2021). Contrary to regular coatings, eluting coatings are designed to slowly release bioactive substances (often drugs) into the bloodstream. Although effective to some extent, drug elution has proven unsustainable over long periods of time; a point at which device failure becomes imminent (Cutlip & Abbot, 2021).

Endogenous anticoagulant agents have also been explored for use in anticoagulant coatings. Vasilets et al demonstrated immobilization of endothelial-derived thrombomodulin (TM) onto ePTFE surfaces, observing attenuated clot formation with reduced platelet activation and adhesion compared to unmodified controls (Jordan & Chaikof, 2007). Other anticoagulant proteins such as tissue factor pathway inhibitor (TFPI) and protein C have been immobilized onto vascular stents/grafts and shown thromboresistance within *in vitro* studies (Kuchinka et al., 2021). Antithrombin (AT)-heparin complex has moreover been coated on polycarbonate urethane (Corethane ®) grafts and revealed lower clot weight *in vivo* rabbit model compared to hirudin-coated and uncoated controls (Klement et al., 2002). Although performing generally well, antithrombogenic drug coatings provide only a “single line of defence” that renders thrombosis a persistent problem if the coating is depleted.

#### 1.4.2.2 Bioinert Polymer Coatings

Bioinert agents bolster hemocompatibility and attenuate thrombosis through blocking the adsorption of proteins and cells on the blood contacting surface (Badv et al., 2020). This is usually achieved by coating the surfaces with a hydrophilic polymer through passivation or by covalent grafting. Polyethylene oxide (PEO)- also termed polyethylene glycol (PEG)- is a common type of polymer which exploits hydrophilicity to generate a hydrated layer that can repel proteins and cells from the surface (Sask, 2012). This mechanism is present in other hydrophilic polymers like dextran and tetraethylene glycol dimethyl ether (tetraglyme) (Sask, 2012). Zwitterionic polymers containing phosphorylcholine and sulfobetaine have been also explored for use on vascular prosthetic devices. They are believed to behave

like cellular membrane(s) containing phospholipid zwitterion head groups (Badv et al., 2020). While showing promising performance in animal models, the efficacy of phosphorylcholine-coated surfaces in humans remains uncertain (Jaffer et al., 2015). More recent work has explored the use of poly(acrylamide)s, poly(2-alkyl-2-oxaline)s (PAOXAs), and poly(2-alkyl-2-oxazine)s (PAOZIs) for non-fouling applications on sensors and medical devices (Yan et al., 2019; Traschel et al., 2020). These coatings exploit brush-like architecture and steric repulsion to repel and lock-in a lubricous interface (Yan et al., 2019). Early results have shown that these coatings may outperform PEO and PEG in blood contacting applications.

While an effective means of attenuating thrombosis, the functionality of bioinert surfaces is limited. As a result, endothelialization is rarely achieved and undesired proliferation of smooth muscle cells (intimal hyperplasia) may occur (Traschel et al., 2020). It has moreover been reported that bioinert coatings can foul over extended periods of time and render materials thrombogenic in the long term (Traschel et al., 2020). For this reason, more sophisticated coating strategies involving “smart surfaces” and biological agents have been developed.

#### 1.4.2.3 Bioactive Coatings

Given the antithrombogenic properties of the vascular endothelium, efforts have been made to apply biologically derived agents to mimic native vascular surfaces. Most prominently, direct application of endothelial cells onto materials through seeding has been explored (Badv et al., 2020). Although improving the patency of vascular grafts; harvesting and attaching endothelial cells (EC) can be time consuming and difficult. To combat this issue, *in situ* endothelialization with covalently attached EC antibodies and ligands has been proposed as an alternative method of generating cellularized graft interfaces (Badv et al., 2020). Covalent immobilization of EC antibodies, growth factors, and peptides is commonly achieved through plasma-induced functionalization of hydroxyl and carboxyl groups on blood contacting surfaces (Kyziol et al., 2017). Leveraging this technique, Crombez et al demonstrated “wet” chemical immobilization of vascular endothelial growth factor (VEGF) and human serum albumin (HSA) on ePTFE using plasma treatment and glutaric anhydride (Crombez et al., 2005). Even though thrombogenicity was not tested, VEGF-HSA ePTFE surfaces showed robust endothelial adhesion and proliferation *in vitro* (Crombez et al., 2005).

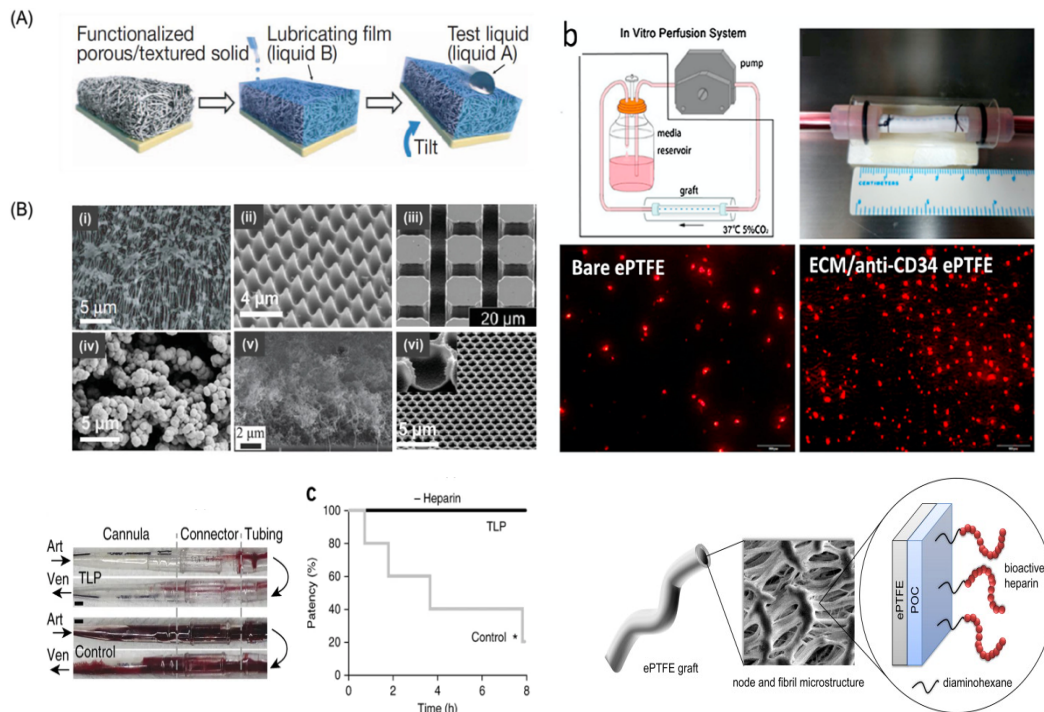


Endothelial antibodies have also been exploited as a plausible mechanism of generating antithrombogenic EC interfaces *in vivo*. Antibody coated surfaces are capable of recruiting ECs from circulation (endothelial progenitor cells, EPCs) and/or through transmural migration (Sanchez et al., 2018). Using carbodiimide crosslinking chemistry with EDC and NHS, anti-CD34 and anti-CD144 have been successfully deployed onto blood contacting surfaces (Jordan & Chaikof, 2007). Although promising, the long-term efficacy of these coatings *in vivo* has not been investigated and their translatability remains poorly understood (Badv et al., 2020). Short peptide sequences mimicking components of the extracellular matrix (ECM) have been developed and applied to blood contacting devices. One such example is the use of RGD, a fibronectin tripeptide sequence (Arg-Gly-Asp) that facilitates EC mediated cell-peptide interaction(s) (Sivkova et al., 2020). Leveraging the thromboresistance of the ECM; fibronectin, vitronectin, and perlecan have been immobilized onto various synthetic materials and shown reduced clot formation *in vitro* and *in vivo* (Sivkova et al., 2020; Clauder et al., 2020). Elastin-inspired polymers have also emerged as promising coating strategy. The mechanism of action is thought to arise from the thromboresistant properties of elastin in blood vessels (Jaffer et al., 2015). These coatings have been applied onto synthetic vascular grafts and shown reduced thrombogenicity in live baboon arterio-venous shunt model(s) (Jaffer et al., 2015).

#### 1.4.2.4 Micro-Nano Structure

Micro-nano structure surface patterning has also been explored as a means of modulating the thrombogenicity of surfaces *in vitro*. The biological response(s) to surface architecture is not fully understood, but it is believed that the scale and orientation of features on the surfaces confer repellency and specific adhesion properties. This is thought to depend on the presence of (i) varying surface area (surface energy), and (ii) anchoring sites for proteins and cells (Kyziol et al., 2017). Chong et al report novel microgrooved and nanopit patterned polymer films for polycarbonate urea urethane (POSS-PCU) vascular graft material(s). They observed heightened endothelial proliferation and adhesion on nanostructured surfaces compared to planar controls (Chong et al., 2015). This finding was supported by Pareta et al, who similarly reported improved EC adhesion on nanostructured ePTFE, PET, and polyurethane (PU) surfaces after ionic plasma deposition and nitrogen ion plasma deposition (NIIPD), respectively (Pareta et al., 2009). Even though compelling, the thrombogenicity of the above surfaces has not been investigated and their translatability remains poorly understood.

The concept of micro-nano structuring for thromboresistance has been explored through protein adsorption and thrombogenicity assays *in vitro*. A novel biomimetic “shark skin” thermoplastic polyurethane (TPU) surface by May et al. was presented as a promising venous catheter construct, wherein platelet adhesion was reduced up to 80% compared to planar controls (May et al., 2015). This finding was supported by Nath et al, who demonstrated reduced platelet adhesion on wrinkled silicone graft conduits compared to unmodified controls (Nath et al., 2020). Hoshian et al demonstrated flexible and repellent polydimethylsiloxane “tubes” with suppressed platelet adhesion (Hoshian et al., 2017). Moreover, work by Hyltegren et al suggests that nanostructured silica surfaces can attenuate fibrinogen adsorption under static conditions (Hyltegren et al., 2020). Although a promising approach, the efficacy of micropatterned vascular devices has not been fully explored *in vivo*, and the mechanism of protein and cell adhesion on these surfaces remains unclear (although attempts have been made to define theory of surface texture and cellular adhesion- see review by Assender et al for a reflection on this subject).



**Figure 4:** Clockwise from Left- lubricant infused surface (LIS) with nanostructured substrate, HUVEC adhesion on uncoated and ECM/anti-CD34 coated ePTFE grafts, TLP and uncoated polycarbonate cannulas and patency after 8-hour perfusion, ePTFE vascular grafts functionalized with poly(1,8-

octanediol-co-citrate) (POC) heparin layer. From Li J., in *Adv. Fun. Matl.* 2018 (4) Wiley-VCH ®; Leslie D., in *Nat. Biotech.*, 2014 (32) Springer Nature ®; Chen L., in *Tiss. Eng. Regen. Med.*, 2017 (14) Springer Nature ®; Smith, R., in *Sci. Trans. Med.*, 2012 (4), 803-811 Science ®.

#### 1.4.2.5 Lubricant Infused Surface (LIS)

The above review reveals a subset of ideal coating properties. When reflecting on antithrombogenic drug and/or drug-eluting coatings- it is clear that a surface with a second “line of defence” against thrombosis would be ideal. Likewise, bioinert coatings perform generally well, but do not impart any biofunctionality. This renders endothelialization a challenge *in vivo*. Nanostructured and textured surfaces provide an antithrombogenic backbone but fail to integrate finer regulation of thrombosis on the material surface. Moreover, bioactive coatings with antibodies, endothelial proteins and cells perform well- but would perhaps be useful as a building block for multifunctional coatings.

Recognizing the advantages and limitations of coatings thus far, it is fitting to introduce the lubricant infused surface (LIS). This surface technology presents a highly versatile coating which is often used in combination with prior described approaches. Inspired by the *Nepenthes* pitcher plant, LIS robustly “locks in” perfluorinated lubricants on material surfaces to generate a repellent and slippery interface. These surfaces have been used for the prevention of fouling, bacterial adhesion, and thrombosis in both industrial and healthcare applications (Badv et al., 2020). LIS have shown compatible with a variety of medical grade materials; including polyurethane (PU), ePTFE, PET, PMMA, as well as metals such as titanium and stainless steel (Badv et al., 2020). Lubricant infusion is usually achieved through direct infiltration of porous materials with biocompatible perfluorinated lubricants or through silanization (Badv et al., 2020). Although more complex than simple infiltration, silanization is a relatively straightforward procedure involving liquid phase deposition (LPD) or chemical vapor deposition (CVD) as reported by Badv et al. Krytox-100, Krytox-103, perfluoroperhydrophenanthrene (PFPP), perfluorodecalin (PFD), perfluorohexane (PFH), and perfluorooctane (PFO) lubricants have all been used for generating lubricant infused surfaces (LIS) (Villegas, 2018).

One such example of a lubricant infused coating on a blood contacting surface was described by Badv et al. In their study, the authors demonstrated facile integration of LIS on PTFE catheters via generation of self-assembled monolayers of trichloro (1H, 1H, 2H, 2H-perfluorooctyl) silane (TFPS). The resulting surfaces were reported as antithrombogenic; with attenuated clotting time (s) and reduced thrombi adhesion (SEM) (Badv et al, 2019). Latter work explored the use of endothelial-specific CD34 antibody

and lubricant infused coatings on medical-grade ePTFE grafts. This dual functionality proved effective for increasing EC proliferation and thromboresistance in a static testing model (Badv et al., 2018). Leslie et al moreover reported application of tethered liquid perfluorocarbon (TLP) LIS onto medical-grade tubing and catheters and achieved reduced fibrin and platelet adhesion *in vitro*. Their study validated those findings in an *in vivo* arteriovenous shunt porcine model (Leslie et al., 2014). Given the persistent concern of lubricant stability under shear conditions- alternative surfaces involving LIS with nanostructured surfaces have been explored. Combining LIS with an antithrombogenic backbone provides a “second line of defence” wherein in the absence of lubricant, a surface still retains its thromboresistant property. One such study involved the use of lubricant-infused nanostructured wrinkled PDMS material for reduced fibrin(*ogen*) and bacterial deposition under static and dynamic conditions (Khan et al., 2022).

## 1.5 Testing and Translation of Novel Antithrombogenic Coatings

### 1.5.1 Outlook

The failure of vascular grafts and fouling of blood contacting medical devices has spurred efforts to develop well-performing antithrombogenic coatings. From 2008 to 2016, a total of \$36,946,764 USD was awarded in grants to 213 research proposals focused on overcoming material-induced coagulation (Gbyli et al., 2017). Novel coating strategies were thought to comprise a large share of these funds (Gbyli et al., 2017). Even though promising, many of these coatings are solely tested *in vitro* in the absence of physiological conditions. As a result, their translatability *in vivo* remains poorly understood and the role of blood flow is overlooked. In this chapter, the translation of novel antithrombogenic coatings will be discussed. The importance of dynamic testing systems for probing thrombogenicity will be moreover described in subchapter 1.6. Methods of measuring thrombogenicity on surfaces using both direct (surface) and indirect (solution) assays will be addressed in turn.

### 1.5.2 Translational Pathway

The translation of new antithrombogenic coatings and or materials is a long and convoluted process. Translation usually begins with robust synthesis of the coating and or material(s) in a reproducible manner. This is followed by a characterization phase; where the tensile properties, chemical and thermal resistance, and surface architecture of the coating/material are analyzed with specialized instruments.

The use of x-ray spectroscopy (XPS), atomic force microscopy (AFM), contact angle analysis (CA), 3D profilometry, and universal testing machine(s) (UTM) have been described for testing the elemental composition, surface hydrophobicity/hydrophilicity, roughness, and material integrity of blood contacting surfaces/coated materials respectively (Peltonen et al., 2012).

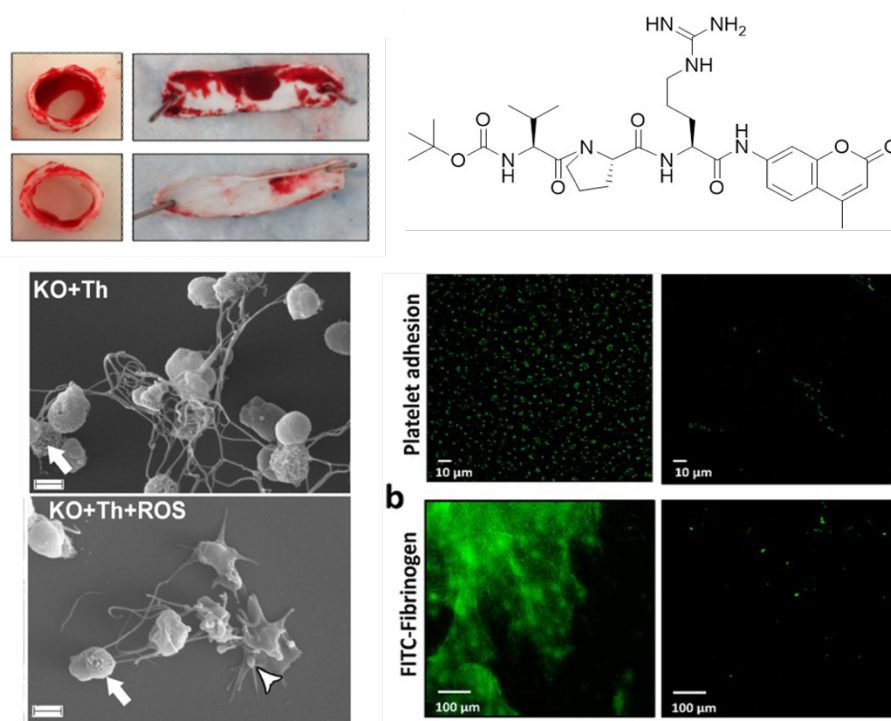
Once coatings/materials have been characterized, it becomes of interest to test their biological interaction(s) with proteins, cells, and blood. In the case of blood contacting devices/coatings, the International Organization for Standardization (ISO 10993-4) outlines essential testing criteria that are required for translation (Weber et al., 2018). The criteria encompass thrombosis, coagulation, platelets, and inflammation. In early stages, the thrombogenicity of blood-contacting devices/coatings is usually the primary interest (Weber et al., 2018). Thrombogenicity tests are first carried out *in vitro* using well plates and tubular reservoirs where visibility and risk can be precisely controlled. Once benchtop testing is completed, and if the coating/material performs well and is safe for use *in vivo*, animal models are usually deployed. The use of *in vitro* devices with blood flow fulfils an important role as an intermediate step between static *in vitro* and complex *in vivo* testing platforms (Braune et al., 2019). The importance of *in vitro* flow models is discussed at length in sub-chapters 1.6 and 1.7.

#### 1.5.2.1 Methods of Measuring Thrombogenicity In Vitro

Measuring the thrombogenic performance of coated surfaces is not an easy task. Due to the complexity of the blood material interaction, there are various proteins and/or cells that could be assessed to gain insight into thrombogenicity. Platelets and proteins are popular markers due to their role in the formation of thrombi (Weber et al., 2018). Alternatively, measuring reaction products such as platelet factor 4 (PF4) or ADP can offer insights into the magnitude and progression of the thrombogenic response. To accommodate these diverse approaches, several techniques have been developed. Direct quantification of surface fouling through measurement of platelets and proteins has been well described (Weber et al., 2018). Indirect (solution) assays of the surrounding blood have moreover been implemented. Below is a list of methods that have been implemented for measuring the thrombogenicity of blood contacting surfaces (with or without coatings) *in vitro*.

##### 1.5.2.1.1 Surface Analyses

- I. *Platelets*: Quantification of adhesion and or activation via cell counting or visualization with radiolabelling (Indium-111, Iodine-125), scanning electron microscopy (SEM), Western Blot, DiO6-labeled platelets, quinacrine dihydrochloride-labeled platelets, CD41, CD61, CD62P-antibody labeled platelets (Brockman, 2015; Resmi et al., 2004; Mathias & Welch, 1984; Weber et al., 2018; Cihova et al., 2021)
- II. *Proteins*: Analysis of adsorbed protein layer via mass spectrometry, X-ray photoelectron spectroscopy (XPS), fluorescein fibrin(ogen), anti-fibrin clone 59d8 labeled fibrin, secondary ion mass spectroscopy (SIMS), iodine-125/131 radiolabelling, atomic force microscopy (AFM), western blot (Braune et al., 2018; Castner, 2017, Weber et al., 2018; Nechipurenko et al., 2019)
- III. *Bulk Clot Formation*: Clot mass, turbidity, blood viscoelasticity (Weber et al., 2018)



**Figure 5:** Clockwise from Left – Bulk blood clot formation anti-CD34 conjugated ePTFE surfaces with and without perfluorinated lubricant. Chemical structure of fluorogenic thrombin substrate Boc-Val-Pro-Arg-AMC which generates blue fluorescent 7-amino-4-methylcoumarin (AMC) product upon proteolytic cleavage by thrombin (amide bond is cleaved). Adhesion of fluorescein fibrinogen and AlexaFluor-488 labeled platelets on APTES/TPFS coated and uncoated substrates. SEM of adherent

activated platelets on collagen-coated glass in the presence of 25nM thrombin and reactive oxygen species ROS (scale bar 1 $\mu$ m). Varju I., 2018. Sci. Reports, (8) Springer ®; Badv M., 2019. ACS Biomater. Sci. Eng. (5), 6485-6496 ACS ®; Badv M., 2018. ACS Nano, (12), 10890-10902 ACS ®.

#### 1.5.2.1.2 Solution Analyses

- I. *Platelets*: Platelet Factor 4 (PF4) from degranulating platelets, platelet activation by enzyme immunoassay (EIA) using monoclonal antibody binding to P-selectin, thromboxane B2,  $\beta$ -thromboglobulin flow cytometry, enzyme-linked immunoassay (ELISA), ADP, colorimetric lactate dehydrogenase assay (LDH) for platelet adhesion (Braune et al., 2019; Brockman, 2015; Wu et al., 2007; Nalezinkova et al., 2020)
- II. *Intrinsic (contact) pathway and common*: partial thromboplastin time (PTT), C1-esterase inhibitor factor XIIa, alpha-2-macroglobulin (F- $\alpha_2$ M) (Nalezinkova, 2020)
- III. *Extrinsic (tissue factor) pathway and common*: prothrombin time (PT)
- IV. *Thrombin*: Thrombin Generation Assay (TGA) with Boc-VPR-AFC, Boc-Val-Pro-Arg-7-AMC, chromogenic Boc-Val-Pro-Arg-pNA, Thrombin Time (TT), Thrombin Anti-Thrombin complex (TAT), prothrombin fragment F1+2, fibrinopeptide A, D-dimer, with ELISA, chromogenic assays (Weber et al, 2018; Braune et al., 2019)

#### 1.5.2.1.3 Blood Preparation

The thrombogenic testing of materials usually involves fresh human whole blood. In some cases, platelet rich plasma and platelet poor plasma are preferred. Blood is typically collected with sodium citrate or heparin, although other reagents are sometimes used. Inhibitory reagents like sodium citrate and heparin deactivate different parts of the coagulation cascade and enable controlled blood handling prior to and or during thrombogenic testing. The choice of reagent depends about investigation. Blood has a limited shelf life and must be used within 4-6 hours of extraction to preserve cellular function(s) (Weber et al., 2018). Prolonged storage (> 4 hours) can impair platelet and leukocyte function and/or contribute to red blood cell hemolysis (Weber et al., 2018). A list of blood preparations for various *in vitro* thrombogenicity assays is provided below for reference (Colace et al., 2013; Weber et al., 2018):

- I. *Ethylenediaminetetraacetic acid (EDTA) or citrate*: These reagents transiently inhibit clot formation through chelation of Ca<sup>2+</sup> (EDTA and citrate), Mg<sup>2+</sup> (citrate) and

Zn<sup>2+</sup> (citrate) ions which are required for the coagulation cascade. Recalcification of blood (10-20mM) can reverse the effect of EDTA and restore coagulation (Mg<sup>2+</sup> and Zn<sup>2+</sup> are not restored). Of note, production of factor XIIa may occur even if these reagents are present. Both EDTA and citrate are commonly used for studying bulk clot formation *in vitro*.

- II. *Corn trypsin inhibitor (CTI)*: A 12.5 kDa protein derived from corn kernels that specifically inhibits FXIIa (Yau et al, 2012). it provides about 40–60 min of inhibition of the contact pathway without interfering with TF-mediated (extrinsic pathway) clotting. Other less commonly used routes of controlling *in vitro* contact pathway activation include antibodies against XIIa and XIa (Colace, 2013). CTI is usually used to study extrinsic coagulation but can also aid the study of contact activation on materials *in vitro* (Colace et al., 2013).
- III. *Trifluoroacetate salt (PPACK) or heparin*: PPACK and heparin provide strong inhibition of thrombin. This approach is useful for the study of platelet activation, adhesion, and or aggregation in the absence of thrombin and fibrin (Colace et al., 2013).

An important consideration for developing *in vitro* testing methods is determining what markers to use for evaluating thrombogenicity. In some cases, visualizing bulk thrombus formation or measuring adherent thrombus weight is sufficient for addressing the thrombogenicity of the material. However, if the goal is to optimize a specific performance feature (e.g. attenuate contact activation), more sensitive markers and specific blood preparations may be required.

### 1.5.3 Static In Vitro Testing Platforms

Static *in vitro* models provide a relatively simple and controlled method of assessing material thrombogenicity at the benchtop (Weber et al., 2018). Common set ups involving well-plates use low volumes of blood, small material samples, and have good visibility and control (Weber et al, 2018). These testing platforms usually focus on incubating whole blood or platelet rich plasma and assaying for thrombin generation or platelet/protein adhesion on the surface (Weber et al., 2018). Despite their ease-of-use, static models with open well plate(s) present challenges due to cell sedimentation and



blood-air interfaces that can cause undesired platelet aggregation and platelet activation (Nalezinkova et al., 2020). These platforms also neglect the role of blood flow as a determinant of graft performance.

To combat this issue, several hybrid static-flow platforms have been developed. Agitating testing platforms in open or closed configurations have been used to reduce sedimentation and simulate blood flow *in vitro* (Nalezinkova et al., 2020). The “Bowry Chamber” is one such example that “shakes” blood-material incubation chamber(s) for desired periods of time (Weber et al, 2018; Nalezinkova et al., 2020). The use of an agitating platform with thromboelastography has moreover been described and used to quantify clot formation (e.g. blood viscoelasticity) on PTFE and polyurethane surfaces (Shankarraman et al., 2011). Agitating platforms offer improvements in *in vitro* testing but have non-uniform flow patterns that undermine their physiological representativeness (Jamiolkowski et al., 2015).

## 1.6 The Importance of Flow

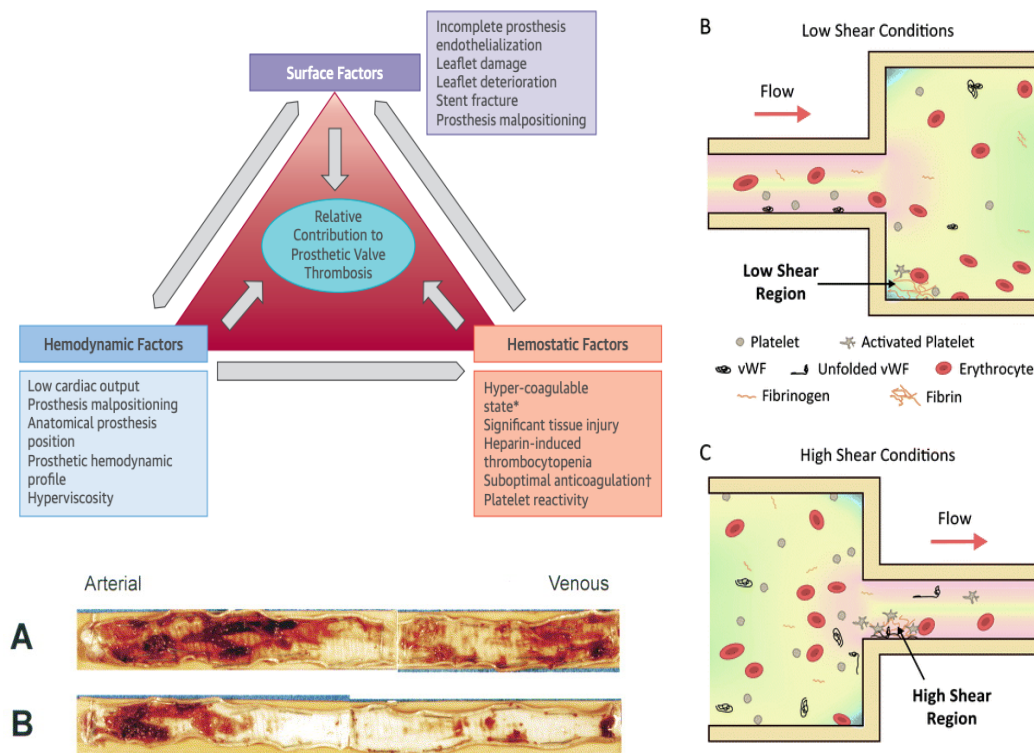
The development of antithrombogenic coatings is intensely focused on the surface. As such, thrombogenicity *in vitro* is usually viewed through a narrow lens that fails to capture the full scope of thrombogenicity *in vivo* (Hong et al, 2020; Braune et al., 2019). This oversight leads three major concerns (Hong et al., 2020, Braune et al., 2019):

1. The absence of flow alters thrombogenicity and may give an unrealistic impression of performance *in vitro*.
2. The absence of flow hinders our ability to understand how novel antithrombogenic coatings/materials will perform *in vivo*.
3. Mismatched *in vitro/in vivo* performance outcomes can undermine (or slow) the translation of novel antithrombogenic coatings/materials.

### 1.6.1 Virchow’s Triad

Thrombosis on vascular grafts *in vivo* is complex and depends on both flow and surface interactions on the blood contacting surface. This principle was eloquently captured by 19<sup>th</sup> century scientist Rudolph Virchow in “Virchow’s Triad”, which has since been used to explain the role of blood flow in the thrombogenicity of prosthetic vascular devices (Labarrere et al., 2020). According to Virchow’s Triad,

“altered vascular surface” (e.g. the vascular graft), “blood flow” (e.g. hemodynamics) and “abnormal blood coagulability” (e.g. hypercoagulability) work in concert to achieve clotting *in vivo* (Ogawa et al., 2012; Topaz, 2018; Bush, 1989). For “altered vascular surface”, the absence of endothelium and presence of a prosthetic graft material is inherently thrombogenic, as described in section 1.3 on material thrombosis and the coagulation cascade. “Altered blood coagulability” refers to heightened activation of the clotting system in vicinity of the graft caused by congenital (e.g. Factor V Leiden – activated protein C resistance), acquired (e.g. anemia, obesity), local injury (e.g. vascular trauma), and or drug-related factors (Dangas et al., 2016). The role of “blood flow” depends on the *in vivo* hemodynamics of the person and the vascular prosthesis/graft (Dangas et al., 2016). Blood flow alters the conformation, concentration, and location of clotting precursors nearby the blood-contacting surface (Hathcock, 2006). This collection of factors causing thrombosis is referred to as the etiology of thrombosis.



**Figure 6:** Clockwise from Left - Virchow’s Triad for vascular prosthesis thrombosis, with shear-dependent behaviour of platelets and von Willebrand Factor in the presence of blood flow, and thrombus formation on explanted NO-secreting arterial and venous polyurethane grafts harvested from an *in vivo* sheep model. Copied from Dangas J., et al. J. Am. Coll. Cardiol. 2016 (24), 2670-2690 from Elsevier

©; Hong J., et al. *Biomater. Sci.*, 2020 (8), 5824-5845, from Royal Society of Chemistry ©; and Fleser P., et al. *J. Vasc. Surg.*, 2004 (4), 803-811 from Elsevier ©.

### 1.6.2 Hemodynamics

Hemodynamics refers to behaviour of blood flow in the presence of blood vessels *in vivo*. It is a broad term that encompasses the rheological properties of blood, as well as its interactions with surrounding vascular environment(s). Blood is a heterogenous mixture of cells and plasma which exhibits dynamic fluid properties (Sochi, 2014). The viscosity, viscoelasticity, yield stress, and shear thinning properties of blood change when force is applied (it is a non-Newtonian Fluid) (Sochi, 2014). The viscosity of blood at a particular time depends on the viscosity of plasma, hematocrit level, blood cell distribution, and mechanical properties of blood cells (Sochi, 2014). It also varies due to deformation and shear forces that are applied when blood interacts with rigid structures like vessels or grafts. Under normal conditions, blood flows in smooth concentric layers in what is called laminar flow (Sochi, 2014). This type of flow is described by a Reynold's Numbers (Re) of magnitude 2300 or less. When flow is disturbed due to structural changes on the flow surface (or changes in the velocity field), these smooth layers become disorganized and the flow becomes turbulent (Re > 2300). Although both types of flow occur *in vivo*, the vascular system is almost entirely comprised of laminar blood flow.

Reynold's Number: 
$$Re = \frac{\rho UL}{\mu} \quad (\text{Eq 1})$$



With fluid density  $\rho$ , flow velocity  $U$ , characteristic length  $L$ , and dynamic viscosity  $\mu$ .

**Figure 7:** Reynold's Number, Laminar Flow, and Turbulent Flow. Copied from Westerhof N., 2010. *Snapshots of Hemodynamics*, pp. 23-25. In Springer ©

### 1.6.2.1 Wall Shear Stress

Blood flowing through the body is engaged in a balanced interaction of forces. These forces help propel circulation, constrict/dilate vessels, modulate thrombosis, and stabilize vessels *in vivo* (Secomb, 2016). Hydrostatic pressure and wall shear stress are two important forces which facilitate this activity. Pressure is a measure of pressure per area (Pa or pascal) that arises from stress at the blood and vessel interface (Secomb, 2016). Conversely, wall shear stress (WSS) is the tangential force per unit area (dyne per cm<sup>2</sup>) that is exerted by flowing fluid on the surface of a blood vessel or graft (Kasiridis et al., 2007). The magnitude of wall shear stress depends on the magnitude of velocity gradient on the interior of the blood vessel (Kasiridis et al., 2007). This velocity gradient produced by flowing blood is referred to as the shear rate ( $\gamma s^{-1}$ ) (Kasiridis et al., 2007). In general, the magnitude of wall shear stress is high in small-diameter arteries (on the order of 10 dyne per cm<sup>2</sup> or more) and low in veins (10 dyne per cm<sup>2</sup> or less) (Papaioannou & Stefanadis, 2005). The normal range of WSS in humans is 10 to 70 dyne per cm<sup>2</sup>, although values of 1000 dyne per cm<sup>2</sup> or higher are sometimes reported (Paszowski & Dardik, 2003). Wall shear stress is involved with shear activation of platelets, von Willebrand factor (vWF), endothelial cells, and is a potent modulator of thrombogenicity (Hathcock, 2006). Wall shear stress can be quantified using the Navier-Stokes equation as will be demonstrated in subchapter 1.8 (Secomb, 2016).

### 1.6.2.2 Hemodynamics and Thrombosis

Hemodynamics play an important role in thrombosis *in vivo*. This is thought to occur for two reasons. The first reason is the shear dependent (WSS) activation of blood cells, proteins, and endothelial cells in the presence of blood flow. The second reason is the flow dependent transport of pro-coagulant proteins and cells to thrombogenic sites. (Hong et al., 2020; Hathcock et al, 2006).

#### 1.6.2.2.1 Shear-Induced Activation of Blood Cells and Proteins

In the presence of flow, red blood cells, platelets, endothelial cells, and coagulation proteins exhibit shear dependent activity. Shear dependent activation can promote clot formation through heightened association and the production of pro-coagulant complexes (Brockman, 2015). Shear-dependent activity may also occur through the unfolding, cleavage, and or degranulation of cells and proteins under flow conditions (Hathcock, 2006; Rana et al, 2019). Recent studies have shown that platelets have heightened activation and increased expression of receptor GP IIb/IIIa in the presence of high wall shear stress ~315

dyne per  $\text{cm}^2$  (Holme et al., 1997). Rapid and dramatic changes in blood flow have been implicated as a driver of this process. It has also been revealed that platelets marginate along the vessel wall in high flow high shear conditions and are prone to forming platelet-rich thrombi (Hong et al., 2018; Sarode & Roy, 2019). Studies have also shown that 140 kDa cell adhesion molecule (CAM) P-selectin is involved in shear-induced platelet aggregation and has heightened expression in the presence of pulsatile arterial flow (10 to 200 dyne per  $\text{cm}^2$ ) (Merten et al., 2000; Yin et al., 2011).

Besides platelets, Von Willebrand factor (vWF) is an example of a protein with shear-dependent conformation. vWF is a large plasma protein containing 5 distinct functional domains (Hassan et al., 2012). Under low shear rates, vWF is “folded up” due to monomeric self-association (Rana et al., 2019). At shear rates of  $\gamma$  3,000-5,000 $\text{s}^{-1}$ , however, the protein elongates, and its A1 active site becomes exposed and promotes clotting through the binding of platelet receptor GPIb (Rana et al., 2019). Association between the vWF Arg-Gly-Asp (RGD) C1 domain and platelet integrin  $\alpha\text{IIb}\beta_3$  is also thought to depend on wall shear stress (Rana et al., 2019). Under low wall shear stress, the association between the vWF RGD C1 domain and  $\alpha\text{IIb}\beta_3$  is dominated by platelet integrin  $\alpha\text{IIb}\beta_3$ , whereas under high shear rates ( $\gamma > 1,000 \text{ s}^{-1}$ ), platelet integrin  $\alpha\text{IIb}\beta_3$  and receptor GPIb are thought to play a shared role in platelet aggregation (Rana et al., 2019). vWF also exhibits shear-dependent cleavage by proteolytic enzyme ADAMTS 13 in its A2 domain (10-30 dyne per  $\text{cm}^2$ ) (Shim et al., 2008). ADAMTS 13 breaks down vWF multimers (“ultra large” 500 to 20,000 kDa vWF) into monomers (360 kDa) and modulates its thrombogenic activity (Hassan et al., 2012).

Red blood cells also exhibit shear dependent properties on a bulk scale (Hathcock, 2006). Regions with low shear stress and rapid flow deceleration are known to cause red blood cell (RBC) Rouleaux formation (Hathcock, 2006). This results in coin-like stacks of RBCs which aggregate and increase blood viscosity, causing pro-coagulant conditions (Hathcock, 2006). Low shear conditions are thought to favor other cell-cell interactions involving platelets, leukocytes, and red blood cells (Hathcock, 2006). Leukocyte and red blood cell interactions also reportedly occur under low shear conditions (Hathcock, 2006). In addition, red blood cells show shear-dependent secretion of ADP and are thought to promote platelet activation in the presence of high shear conditions (Hathcock, 2006). Endothelial cells are other, exceptionally shear-sensitive modulators of thrombogenicity *in vivo*. In the presence laminar flow and WSS of 10 to 30 dyne per  $\text{cm}^2$ , endothelial cells elongate in the direction of flow and have an antithrombogenic phenotype. Under these flow conditions, ECs secrete and/or express nitrous oxide

(NO), thrombomodulin (TM), and prostacyclin (PGI<sub>2</sub>) (Traub & Berk, 1998). Conversely, under very low shear conditions (< 5 dyne per cm<sup>2</sup>), the cells exhibit a pro-coagulant phenotype with “cobblestone” appearance and heightened expression of nuclear factor  $\kappa$ B-regulated genes (Hathcock, 2006).

#### 1.6.2.2.2 Flow Transport Properties

The transport of cells and coagulation proteins under flow conditions is another important aspect of clot formation *in vivo* (Hathcock, 2006). The spatial and temporal progression of thrombosis depends on the rate of delivery, removal, and accumulation of pro-coagulant factors on the blood contacting surface (Hathcock, 2006). Compared to stationary blood, flowing blood serves as a mobile reservoir of platelets, coagulation proteins, and blood cells. Studies have shown that convective-diffusive delivery of factor X to exposed subendothelial surfaces *in vivo* is affected by blood flow (Hathcock, 2006). It has also been shown that accumulation of reaction products in low flow environments can overcome inhibition and promote coagulation (Hathcock, 2006). Low flow, low shear “stasis” is moreover thought to promote the formation of fibrin-rich thrombi due to prolonged presence of fibrin(*ogen*) on the blood contacting surface (Brockman, 2015). These findings suggest that blood flow not only impacts the dynamics of thrombosis, but also the composition of formed thrombi (Hathcock, 2006). In fact, the porosity and permeability of formed thrombi are known to depend on the local shear stresses (Xu et al., 2017). Low-shear, porous clots are usually unstable and prone to propagating into circulation (Xu et al., 2017).

Turbulence is a unique flow condition that is associated with heightened thrombogenicity *in vivo*. Unlike laminar flow, turbulent blood flow is chaotic and introduces rapid shifts in shear stress (Chiu et al., 2011). Cell-cell and cell-wall collisions among platelets, red blood cells and endothelial cells are thought to increase (Chiu et al., 2011). Flow fields in bifurcating, curved, and valvular vessels/prostheses have moreover been characterized and shown prone to thrombosis *in vivo* (Williams et al., 2021). For example, recirculation and stasis on mechanical heart valves (MHV) and bioprosthetic heart valves (BHV) is thought to be responsible for coagulation and platelet adhesion on the blood contacting surface (Dangas et al., 2016). Reduced washout of activated clotting factors and limited inflow of inhibitors can also promote clot formation in these areas (Freudenberger et al., 2007).

#### 1.6.2.2.3 Flow and Vascular Prosthesis Thrombosis In Vivo

The *in vivo* impacts of flow on blood contacting surfaces are especially evident with prosthetic heart valves (Bluestein et al., 2017). These devices suffer from thrombosis arising from irregular (turbulent) flow patterns and regions of high/low wall shear stress (Bluestein et al., 2017; Nygaard et al., 1994). For example, to understand the high incidence of thrombosis in the hinge region of mechanical heart valves (MHV), Herbertson et al used Doppler velocimetry to map out wall shear stress. Their findings indicated that thrombosis in the hinge region of MHVs were likely to form in areas with high shear stress and flow recirculation (Herbertson et al., 2011). As a result, design modifications of the hinge region were explored to reduce thrombogenicity. Studies by Vahidkhah et al showed that flow disturbances and stasis on aortic valve leaflets act as a precursor to leaflet thrombosis (Vahidkhah et al., 2017). Work by Williams et al moreover revealed differing thrombogenic outcomes in regions of stasis and high flow within vascular grafts (Williams et al., 2021). Investigations into flow has enabled researchers to develop geometries and surfaces with improved antithrombogenic properties (Dangas et al., 2016).

These studies show that thrombogenicity does not depend on the surface alone- but rather, the interaction of blood flow and surface in a dynamic context. It is evident that blood flow can impair the clinical performance of vascular prostheses *in vivo*. For this reason, blood flow is an important consideration for the design and testing of novel antithrombogenic materials/coatings for vascular applications.

#### 1.7 Dynamic In Vitro Testing Platforms

At present, the role of flow in *in vitro* thrombogenicity testing is often overlooked. It is an important pillar of Virchow's Triad that alters thrombosis on both the small (e.g. shear dependent activation of pro-coagulant proteins and cells) and large scale (e.g. thrombogenic failure of devices *in vivo*). Recognizing the importance of blood flow in thrombosis and the necessity of *in vitro* testing models, efforts have been made to develop dynamic *in vitro* testing platforms. Chantler Loops "Haemobile", cone-and-plate viscometers, closed-loop roller-pump, and flat-plate flow chambers have since been deployed to fulfil this need (Hong et al., 2020; Weber et al., 2018; Ku et al., 2018).

## 1.7.1 Shear Flow Models

### 1.7.1.1 Tubular and Cone-and-Plate Viscometer

The Chandler Loop consists of a tubing circuit that is lined with the test material, filled with whole blood, and rotated to simulate blood circulation (Weber et al., 2018). In this set-up, the test material is rolled into a tube and inserted into the perfusion loop. This apparatus has been used to assess the thrombogenicity of stent and graft materials *in vitro*. Using a 120-minute flow duration with whole blood, Sinn et al demonstrated differential platelet and leukocyte (compliment) activation on copper-coated, parylene, and bare metallic stent materials (Sinn et al., 2011). In contrast to the Chandler Loop, cone and plate viscometers (CPV) generate flow in planar configuration (Rhodes et al., 1999). The device consists of a layered assembly containing a rotating cone and flat bottom plate (test substrate). Blood circulates in the middle region between the cone and plate partitions. The substrate is in a planar “sheet” in the lower part of the device. CPV does not require a pump to generate flow, which precludes the risk of damaging red blood cells and generating unwanted platelet activation (Topaz, 2018).

Rhodes et al reported the use of CPV for assessing the thrombogenicity of polymethylmethacrylate (PMMA), PEO-coated PMMA, and stainless steel at low ( $\gamma$  500s<sup>-1</sup>) and high ( $\gamma$  4000s<sup>-1</sup>) shear rates (Rhodes et al., 1999). They quantified platelet adhesion post-perfusion by incubating CD41 antibody (for platelet integrin  $\alpha$ IIb $\beta$ 3) and inspecting the size of aggregates on the surface (Rhodes et al, 1999). They revealed shear rate as a cause of differential platelet adhesion and assert the antithrombogenic property of PEO coatings in the presence of blood flow (Rhodes et al., 1999). Although more representative than static testing models, tubular flow devices have limitations. Most prominently, none of these devices have demonstrated integration of endothelial cells. Tubular and CPV devices also use large volumes of blood and offer testing with reduced throughput and visibility (Weber et al., 2018).

### 1.7.1.2 Parallel Plate Flow Chambers

Unlike the tubular substrate geometry present in Chandler Loops, parallel plate chambers introduce a flat test substrate into a rectangular flow duct. Comprised of a unidirectional flow circuit and a clamped gasket assembly, parallel plate platforms are easily assembled and allow whole blood perfusion under well-defined shear stress (WSS) conditions. Due to their planar configuration, real-time observation of test substrates is achievable. Jamilokowski et al report real-time observation of deposition of quinacrine



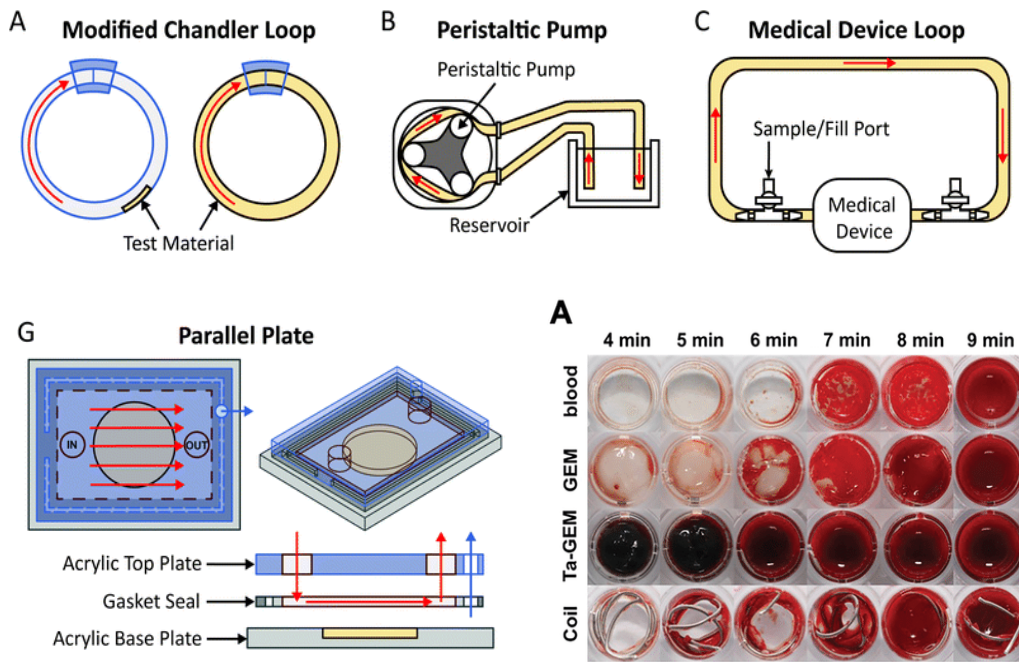
dihydrochloride-labeled platelets at  $\gamma$  400 s<sup>-1</sup> onto titanium alloy (Ti<sub>6</sub>Al<sub>4</sub>V), silicon carbide, and 2-methacryloyloxyethyl phosphorylcholine polymer coated Ti<sub>6</sub>Al<sub>4</sub>V surfaces using a silicon-aluminum parallel plate flow chamber (Jamilokowski et al., 2015). Their study revealed enhanced thrombogenic performance on coated Ti<sub>6</sub>Al<sub>4</sub>V compared to uncoated controls (Jamilokowski et al., 2015). In a follow up study, the authors modified the surface of Ti<sub>6</sub>Al<sub>4</sub>V with grooves (50-150 $\mu$ m) to explore the interaction between flow recirculation sites and thrombosis *in vitro*. They report increased deposition of quinacrine dihydrochloride-labelled platelets on irregular flow surfaces (53-90 $\mu$ m divots) at low shear rates- and helped illuminate the importance of surface texture as a determinant of thrombosis (Jamilokowski et al., 2016). Real-time observation of platelet adhesion, activation, and aggregation have also been quantified in these testing systems using epifluorescence/ radiolabeling, particle counting and/or enzyme-linked immunoassay (ELISA) of the outflow (Topaz, 2018; Sukavaneshar et al., 2017). The controllability of the flow circuit also enables pressure measurements in real-time and can offer insight into occlusion and the build-up of thrombi (Topaz, 2018).

### 1.7.1.3 Miniaturized Parallel Plate Flow Chamber

Miniaturized parallel plate flow platforms are smaller parallel-plate chambers with channel dimension(s) greater than 1mm (usually on the order of 3cm or greater). These devices are like regular parallel plate chambers but consume less reagent volume and have more easily tuned shear stress (Hong et al., 2020). Due to their convenience and versatility, these platforms have been used to model platelet adhesion on various polymers and metals under flow with defined shear stress (Hong et al., 2020). Yang et al report a custom-made, single pass, 4mm (channel width) by 0.05mm (channel height) parafilm and clamp sealed parallel plate perfusion chamber for testing the thrombogenicity of monoethylene glycol coated metal stent(s). Leveraging the imaging capabilities and the small scale of the device, shear rates of  $\gamma$  100-900s<sup>-1</sup> were applied and the adhesion of DiO6-labeled platelets on test surface(s) was monitored in real time (Yang et al., 2021). Their *in vitro* investigation revealed lesser platelet adhesion and improved thrombogenic performance on monoethylene glycol coated stents compared to uncoated controls; suggesting that their novel coating may confer antithrombogenic properties under *in vivo* flow conditions (Yang et al., 2021).

Han et al similarly report the use of a 1mm height by 4mm wide (channel) parallel-plate perfusion chamber for testing the thrombogenicity of Dacron, PTFE, ceramic, silicone, polyvinyl chloride (PVC) and stainless steel under shear rates  $\gamma$  150-5000s<sup>-1</sup>. Unlike prior described model(s), their flow chamber

was assembled from 3D printed acrylic, high-pressure vacuum grease, and silicone sealant (Han et al, 2021). Although small-scale, the perfusion circuit used 500 mL of blood, thus rendering the assay inefficient. Moreover, real-time parameters were omitted, and only endpoint occlusion and surface area coverage on test materials were quantified (Han et al., 2021). With their small scale and low reagent volumes, these platforms are generally well suited for testing thrombogenicity in the presence of sensitive reagents/blood samples (Hong et al., 2020). Although promising, miniaturized parallel plates are usually limited to a single test condition and their small-scale properties have not been fully exploited (Hong et al., 2020). The use of microfluidic (<1mm channels) chambers has subsequently been explored as an alternative testing approach. Microfluidics will be extensively addressed in chapter 1.8.



**Figure 8:** Clockwise from Left - Chandler Loop, closed-loop peristaltic and medical device circuits, parallel plate, and well-plate *in vitro* thrombogenicity testing platforms. Reprinted from Hong J., et al. *Biomater. Sci.*, 2020, 8, 5824-5845, from Royal Society of Chemistry ®; and Albadawi H., et al. *Adv. Sci.*, 2021, 8, 2003327 from Wiley-VCH ®.

#### 1.7.1.4 Microfluidic Flow Chamber

Despite their small scale, control, and good visibility, the use of microfluidic testing models (on the scale of 1mm or less) for testing the thrombogenicity of vascular prosthesis/antithrombogenic coatings

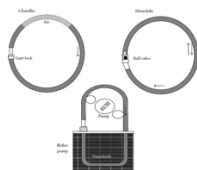
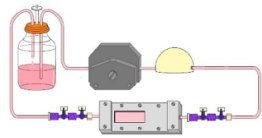
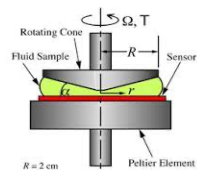
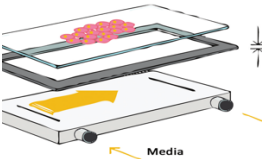
has been poorly described. One approach was a loop perfusion system mimicking coronary artery stent hemodynamics by Vlatin et al. In this study, the authors describe a modular *in vitro* flow platform containing an array of 250 $\mu\text{m}$  microfluidic perfusion channels for analyzing blood and surface interactions under physiological-like flow conditions. They moreover achieved a microfluidic testing scenario with parallel channels and coronary stent like WSS (12-22 dyne per  $\text{cm}^2$ ) (Vlatin et al., 2021). The device was used to test platelet adhesion (fluorescent DiOC6), compliment activation (C5a with ELISA), leukocyte activation (eluent flow cytometry CD11b) on glass, Teflon, and polyurethane (PU) substrates (Vlatin et al., 2021). Although more capably modeling thrombogenicity *in vitro*, this device failed to integrate endothelial cells and only tested a single surface condition. The study moreover failed to demonstrate incorporation of coatings for thrombogenic testing applications.

In contrast to the model proposed by Vlatin et al, Zhang & Horbett describe the use of a shear flow chamber with tailored shear stress conditions to assess the performance of tetraglyme coating(s) on polystyrene surfaces. In their study, fibrinogen, von Willebrand Factor (vWF), and platelets were radiolabeled with  $\text{I}^{125}$  and perfused at  $\gamma$  50-500 $\text{s}^{-1}$  to quantify flow dependent adhesion on coated and uncoated polystyrene surfaces (Zhang & Horbett, 2009). After perfusion, the substrates were cut into segments and the retained radioactivity was quantified using an Auto-Gamma counting system. They reported improved surface performance and less adhesion on tetraglyme coated surfaces versus unmodified controls- thereby suggesting the coating confers antithrombogenic properties under *in vitro* flow conditions (Zhang & Horbett, 2009). While promising, this platform failed to incorporate clinically relevant prosthetic materials and only used a single perfusion channel (Zhang & Horbett, 2009). Leslie et al report a similar study with novel liquid fluorocarbon (TLP) coated PDMS surfaces. Using a series of 200 $\mu\text{m}$  by 75 $\mu\text{m}$  microchannels, the authors perfused whole blood at 50 dyne per  $\text{cm}^2$  (high arterial wall shear stress) on TLP and control surfaces. They then monitored thrombus formation in real time using a pressure sensor (Leslie et al., 2014). The authors reported reduced occlusion in TLP coated channels compared to uncoated controls, suggesting that TLP conferred thromboresistance under flow.

A different approach was described by Lau et al. In their study, the authors generated an *in vitro* thrombogenicity test system with a cyclic olefin copolymer (COC) perfusion chamber. The chamber was comprised of COC microchannels that were bonded to glass. This system was presented as a tool for testing the thrombogenicity of novel drugs and vaccines (Lau et al., 2021). The device enabled real-time observation of endothelial cell proliferation and platelet adhesion inside the flow chamber under a

shear rate of  $\gamma 1100s^{-1}$  (Lau et al., 2021). Although integrating vascular flow and visibility, it is not clear whether different substrates could be tested in the flow circuit. It is also not clear if this system could be adapted for testing the thrombogenicity of vascular prosthesis or coatings. While promising, the above studies fail to incorporate prosthetic vascular materials. Moreover, despite their small scale, the above testing platforms did not integrate distinct testing conditions in parallel. It is therefore apparent that the small-scale properties of the device have not been fully exploited for efficient, high-throughput testing of materials and/or coatings under physiological-like conditions.

**Table 2:** *In Vitro* Dynamic Thrombogenicity Testing Platforms

Platform	Application	Advantages	Disadvantages	Image
“Haemobile”, Chandler Loop, tubular models [10,11]	$\gamma 50-428s^{-1}$ , 3-20mL blood, metal stent, ePTFE, platelet adhesion/ELISA	<ul style="list-style-type: none"> <li>·whole blood</li> <li>·simple low-cost</li> <li>·material embedded inside tube(s)</li> </ul>	<ul style="list-style-type: none"> <li>·narrow shear testing range</li> <li>·recirculation</li> <li>·end-point assay</li> <li>·poor visibility</li> </ul>	
Parallel Plate [12-14]	$\gamma 10-10,000s^{-1}$ , <1mL to 500mL, metal stent, ceramic, PTFE, Dacron, occlusion, platelet adhesion	<ul style="list-style-type: none"> <li>·whole blood</li> <li>·range of shear rates</li> <li>·changeable material</li> <li>·good visibility</li> </ul>	<ul style="list-style-type: none"> <li>·only the bottom surface contains test material</li> <li>·non-physiologic flow geometry (rectangular)</li> </ul>	
Cone-and-Plate Viscometer [15]	$\gamma 0.1-10,000s^{-1}$ , <1mL blood, PU, PMMA with PEO coating, PTFE	<ul style="list-style-type: none"> <li>·whole blood</li> <li>·range of shear rates</li> <li>·changable material</li> <li>·some visibility</li> </ul>	<ul style="list-style-type: none"> <li>·complicated flow regime</li> <li>·fluid evaporation</li> </ul>	
Miniaturized Parallel-Plate/Microfluidic [16,17]	$\gamma 50-1000s^{-1}$ , <1mL blood, PU, metal stents, PTFE, polystyrene, platelet adhesion, fibrinogen	<ul style="list-style-type: none"> <li>·whole blood</li> <li>·low cost</li> <li>·range of shear rates</li> <li>·changeable material</li> <li>·low blood volume</li> <li>·good visibility</li> </ul>	<ul style="list-style-type: none"> <li>·impact of viscosity is greater</li> <li>·hard to replicate turbulence</li> <li>·only the bottom surface contains test material</li> </ul>	

\*PTFE (polytetrafluoroethylene), PU (polyurethane), ELISA (enzyme-linked immunoassay), PEO (polyethylene oxide), PMMA (polymethylmethacrylate)

[10] Weber, M. in *Front. Bioeng. Biotec.* 2018 (6); [11] Hong, J. in *Biomater. Sci.* 2020 (21); [12] Jamilokowski, M. in *Biomater.* 2016 (96); [13] Han, Q. in *Artif. Org.* 2021; [14] Yang, T. in *Mater.* 2021 (9); [15] Rhodes, N. in *Mat. Med.* 1999 (9); [16] Valtin, J. in *Curr. Dir. Biomed. Eng.* 2021 (2). [17] Qui, X in *Acta. Biomater.* 2017 (51).

## 1.7.2 Other Testing Approaches

The testing of novel materials and antithrombogenic coatings may also involve *in vivo* or *in silico* testing platforms. These strategies differ from *in vitro* approaches and depend on animals or computational algorithms to predict thrombogenic performance. Although beyond the scope of this review, these methods will be described to illustrate the breadth of testing approaches presently available.

### 1.7.2.1 In Vivo

Animal models simulate many aspects of the human vascular system and can be a preferred method of testing the thrombogenicity of vascular prosthesis/coatings. Both small and large animals are sometimes used, with large animals possessing more similarity to humans (Kokozidou et al., 2019). Popular animal models such as mouse, rabbit, goat, and pig have been developed and standardized for thrombogenicity testing. For example, work by Baek et al demonstrated the use of mature *Landrace* pigs to investigate patency outcomes of sirolimus-eluting and paclitaxel coated ePTFE vascular grafts. Similarly, small animal studies involving rabbits have been used to model PLGA- polyurethane urea elastomer (PUU) graft endothelialization (Zhu et al., 2021). The use of rat models less common but well-reported for small-diameter (1-2mm) grafts in aortic and femoral arteries (Kokozidou et al., 2019).

Despite the desirable properties of animal models, their testing outcomes do not always accurately predict thrombogenicity in humans. For example, some of the animal studies conducted on the HeartMate II left ventricular assist device (LVAD) and the HeartWare ventricular assist device (HVAD) reported little pump thrombosis (Jamiolkowski et al., 2021). However, a substantial number of thrombosis related events were reported during human clinical use (Jamiolkowski et al., 2021). Moreover, significant differences in platelet adhesion among humans, pigs, and sheep on synthetic materials has been reported (Jamiolkowski et al., 2021). Studies have also shown that there are rheological differences between human blood and rat blood in particular (Panteleev et al., 2020). For example, mouse platelets are known to support platelet attachment through integrins at much higher

wall shear rates than human platelets (Pantelev et al., 2020). Correspondingly, the role of hemodynamics and blood flow in Virchow's triad are sometimes altered in animal models.

### 1.7.2.2 In Silico

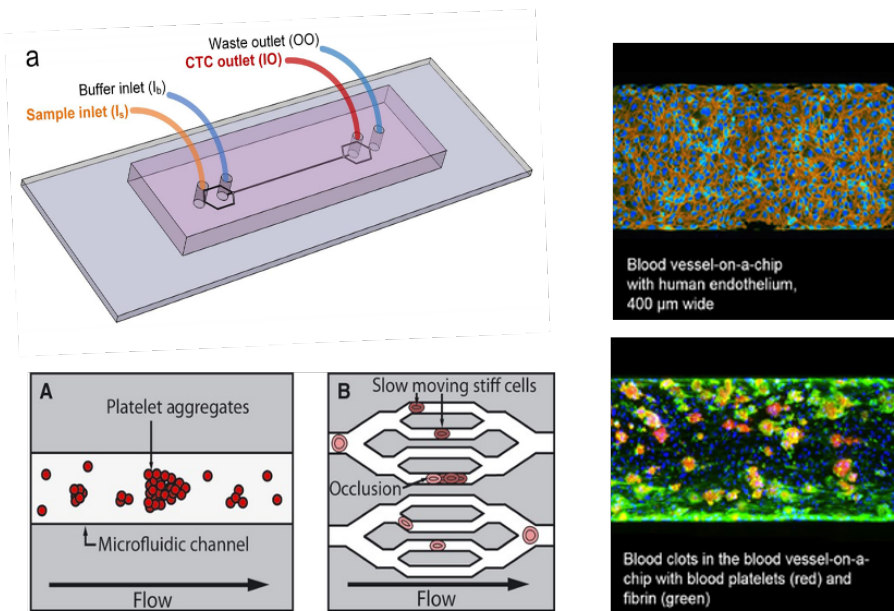
Computational modeling of blood flow has the potential to improve the design and evaluation of novel materials and or coatings. The hemodynamic properties of vascular stents, valves, and grafts have been modeled with computational software. Bluestein et al performed numerical simulations of the HeartMate II ventricular assist devices (VADs) implanted in various configurations and showed that the thrombogenic potential may be improved by optimizing device geometry and implant configuration (Bluestein et al., 2017). Using computational fluid dynamics (CFD), Zhang et al investigated the positioning of a left ventricular assist device (LVAD) cannula in the aorta and showed that the placement significantly affects thrombus distribution due to altered aortic flow. This finding correlated with clinically observed instances of device failure (Zhang et al., 2016). Moreover, flow changes caused by catheters, stents, MHVs have been quantified and corrected using CFD (Hong et al., 2020). Mathematical algorithms modeling thrombus growth, platelet activation, platelet aggregation on smooth and textured surfaces has also been described (Hong et al., 2020). Although promising, *in silico* models can be challenging to develop and require experimental validation to be used as a translational tool.

## 1.8 Microfluidics

As we have seen in the previous chapter, the translation of new materials and coatings is long and complex. We have noted the inefficiency of conventional *in vitro* testing platforms, the inaccuracy of static ones, and the challenges present in animal models. The goal of this subchapter is to explore microfluidics as an improved method of *in vitro* testing that integrates blood flow and test surfaces in an efficient format. We will first introduce the microfluidics concept and present a historical account of its inception. Following this introduction, the fabrication and flow properties of microfluidic devices will be described. Finally, we will explore the use of microfluidics for on-a-chip vascular models and present the vascular graft on-a-chip concept. An original manuscript will be attached in chapter 2.

### 1.8.1 Description and Origin

Microfluidics refers to the science and manipulation of small ( $\mu$ -scale) volumes of fluids in channels tens to hundreds of micrometers in dimension (Convery & Gadegaard, 2019). Since its inception in the 1990s, microfluidic devices have been employed in a range of settings such as healthcare, industry, and research (Convery & Gadegaard, 2019). Originally conceived as a miniaturized total analysis system ( $\mu$ TAS), microfluidics was developed to serve the need for rapid and high-throughput laboratory testing at the benchtop. The emergence of the microfluidic concept is attributed to the popularity of microelectronics (MEMS) in microprocessors and machines. It is also thought that the social climate at the time urged the development of deployable and accessible testing technologies which could serve government funded projects. One such project was DARPA's *Weapons Detection* program (1994), and another was the National Institute of Health's *Human Genome Project* (1990), both of which encouraged the microfluidics concept (Convery & Gadegaard, 2019). Moreover, the emergence of infectious disease epidemics in developing countries (e.g. HIV, malaria) necessitated portable and cheap diagnostic platforms (Convery & Gadegaard, 2019). Microfluidics have since generated publications and patents ranging from point-of-care diagnostics, bioreactors, and organ on-a-chip systems.



**Figure 9:** Clockwise from Left – A microfluidic chip, fluorescently labeled endothelium and clots on-chip, modeling vascular flow and (*patho*)physiology with tuneable flow conditions. Copied from Tran

R., et al. *J. Cell. Mol. Med.* 2013, (5), 597-596, from Wiley Open Access ®; Zhou J., et al. *Microsystems & Nanoengineering.* 2019, (5) from Springer Nature ®.

## 1.8.2 Advantages

Microfluidics offer a range of proven economic and technical advantages. Some of these advantages arise in the fabrication of microfluidic chips, while others are present in the application and use of the small-scale fluid flows. Whitesides et al succinctly summarize the advantages of microfluidics as follows: reduced consumption of samples and reagents, ability to carry out fluid manipulation with high resolution and sensitivity, short analysis times, portability/disposability (Duffy et al., 1998). Moreover, inherently small size of microfluidic channels generates a range of useful flow properties such as laminar flow, which have been used to sort, separate, and combine fluid elements on-chip (Duffy et al., 1998). The cost effectiveness of microfluidics has been furthered in recent years due to the introduction of inexpensive fabrication platforms (e.g. paper-based microfluidics) and integrated workflows that reduce the time and energy needed to process reagents (Nielson et al., 2019). One aspect of this was the development of rapid prototyping with soft lithography and xurography for polydimethylsiloxane (PDMS) and paper-based microfluidics (Nielson et al., 2019). These advantages present microfluidics as an excellent option when quick, controlled, efficient investigations into biological and chemical processes are required. The value of this technology is well reflected in its projected 2026 market value of \$58.8 billion dollars (Nielson et al., 2019).

### 1.8.2.1 Fabrication of Microfluidic Devices

One of the greatest advantages of microfluidics is the versatility of its fabrication protocols. This is reflected in the range of materials and methods that are used to make on-a-chip devices. Some of the earliest microfluidic devices were made with polydimethylsiloxane (PDMS) and glass (Gale et al., 2018). Since then, the range of materials has expanded to include thermoplastics, hydrogels, fluoropolymers, paper, among other elastomeric and polymeric materials (Gale et al., 2018; Convery & Gadegaard, 2019). Conventional fabrication methods involve the use of soft lithography, photolithography, and wet/dry etching (Nielson et al., 2019). While effective, many of these methods require the use of harsh chemicals and lengthy manufacturing processes. More recently, improved equipment has generated sophisticated fabrication techniques involving stereolithography, embossing, micromachining, injection molding, and laser ablation (Nielson et al., 2019).



### 1.8.2.2 Bonding of Microfluidic Devices

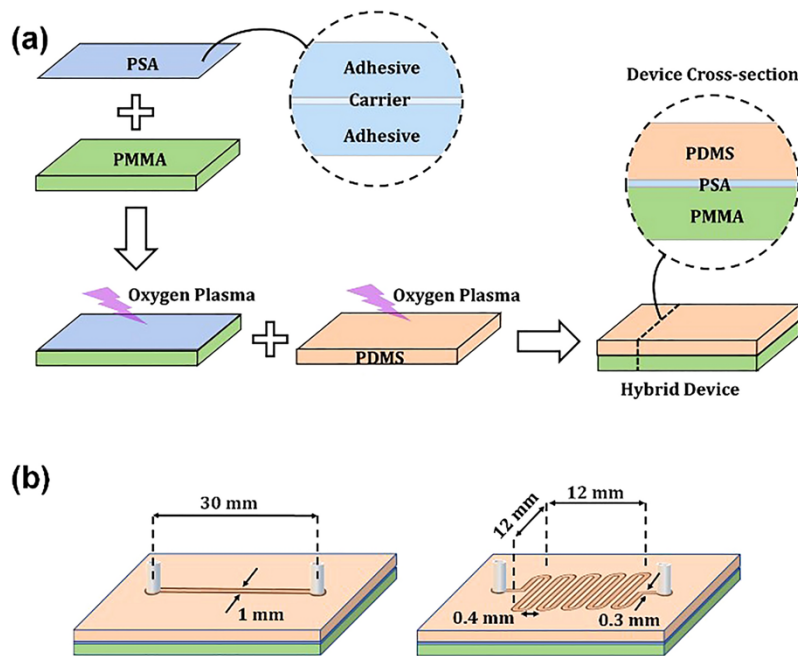
In addition to the fabrication strategies and materials available for on-a-chip technology, there are a variety of bonding strategies presently employed. In general, the choice of bonding reflects the materials involved and the performance requirements for the device. As a rule of thumb, the bonding process should preserve the integrity, geometry, and structure of the flow channels. Present bonding strategies generally fall under one of four distinct categories: plasma bonding, hot-press bonding, chemical assisted bonding, or adhesive bonding.

Plasma bonding is a popular choice for PDMS and glass devices. Plasma bonding uses siloxane bonds to create robust attachment on surface(s) without the need for adhesive agents. Briefly, this mode of bonding involves generating silanol (Si-OH) groups on the PDMS surface through gaseous plasma treatment (oxygen, argon, nitrogen) or corona discharge, and sandwiching the device to produce covalent siloxane linkages (Si-O-Si) (Nielson et al., 2019). Although a highly cited method in scientific literature, plasma bonding is typically limited to silicon-based materials such as glass and PDMS which are predisposed to forming siloxane linkages. Conversely, hot press bonding is preferable for thermoplastics like polymethylmethacrylate (PMMA) and cyclic-olefin-copolymer (COC) (Nielson et al., 2019). With this method, substrates are bonded using controlled heating. Chemically assisted bonding is another attractive option for microfluidic devices and involves the use of solvents or coupling agents to generate adhesive force(s). A range of chemical agents involving organosilanes and alcohols have been reported and used in literature.

#### 1.8.2.2.1 Adhesive Bonding

Adhesive bonding is a straightforward method which involves applying glues or tapes to seal substrates together. Bonding with adhesive “glues” depends on the balance of cohesive and adhesive forces on the adhesive and surface(s) (Mapari et al., 2020). UV curable acrylic adhesives and epoxy/silicone glues are a popular choice for thermoplastics in particular. The use of hot melt adhesives, electron beam curable adhesives, and pressure sensitive adhesives (PSA) has also been described (Mapari et al., 2020). Biocompatible double-sided PSA tapes made of acrylic and or silicone resins have been used for a range of applications including electrochemical sensors, lateral flow assays, and cell studies on-a-chip (Nielson et al., 2019). Adhesive tapes present in two forms. The first form, transfer tape, is entirely composed of adhesive material. The second form, double sided tape, consists of a carrier layer which is

coated with both sides with an adhesive. Acrylic adhesives containing acrylic acid and alkyl acrylate are transparent, colorless, and resistant to oxidation with good chemical and UV resistance (Mapari et al., 2020). Silicone adhesives are generally hydrophobic and exhibit strong bonding with low surface energy substrates such as polyimide, PTFE, polyester, and glass (Mapari et al., 2020). They are usually composed of silanol-terminated silicone polymer and siloxane resin in hydrocarbon solvent(s) such as toluene or xylene (Mapari et al., 2020). Pressure sensitive adhesion (PSA) has distinct mechanisms of bonding that depend on the substrate and chemistry of the adhesive. Adhesion between the substrate can occur through infiltration of adhesive “glue” into the pores of the substrate or through the direct formation of chemical bonds. Electrostatic forces or Van der Waal interactions between the substrate and adhesive may also be exploited for PSA bonding (Mapari et al., 2020).



**Figure 10:** Pressure sensitive adhesive (PSA) assisted fabrication of a microfluidic device. Copied from Sen A, et al. Sci. Reports. 2021, (11), from Springer ®.

### 1.8.2.3 Microfluidic Flow Properties

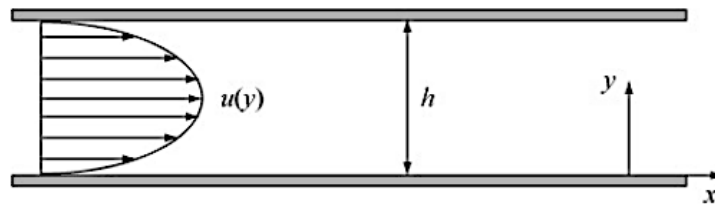
In addition to its desirable cost and fabrication features, microfluidics presents a third advantage: laminar flow. Due to their small scale and low Reynold’s Numbers, microfluidics almost always generate smooth orderly flow. This flow behaviour is present in blood vessels and therefore serves as an important link between microfluidic models and *in vivo* flow conditions. Laminar flow in microfluidic devices has been exploited to generate a range of flow conditions with physiological-like wall shear stress (WSS). We can derive WSS in microfluidic channels with the Navier-Stokes for an ideal incompressible Newtonian fluid (laminar flow assumption) between two infinite parallel plates as described below.

Most microfluidic systems are pressure-driven flows, and because of the dominance of viscous terms, the Navier-Stokes Equation simplifies from Equation 2 to Equation 3:

$$\rho (u \cdot \nabla u) = -\nabla P + \mu \nabla^2 u \quad (\text{Eq 2})$$

$$0 = -\nabla p + \mu \nabla^2 \vec{u} \quad (\text{Eq 3})$$

Where  $u$  is the velocity field and  $p$  is the pressure field. We can derive wall shear stress for a simplified parallel-plate microfluidic chamber; with flow velocity  $u(y)$  and plate separation distance,  $h$ . Flow is assumed to be pressure-driven between two infinite parallel plates.



**Figure 11:** Parallel plate flow condition with parabolic velocity profile. Copied from Westerhof N., 2010. Snapshots of Hemodynamics, pp. 23-25. In Springer ®

With a uniform and steady parabolic velocity profile  $u(y)$  along the length of the plate in the x-direction,

Equation 3 becomes:

$$0 = -\frac{dp}{dx} + \mu \frac{d^2u}{dy^2} \quad (\text{Eq 4})$$

Integration of Equation 4 yields parabolic velocity profile,  $u(y)$ :

$$u(y) = -\frac{1}{2\mu} \frac{dp}{dx} (hy - y^2), \quad (\text{Eq 5})$$

Where  $u(y)$  represents a parabolic velocity profile that satisfies no-slip condition at the walls and maximum velocity at the midplane between the plates,  $y=h/2$ . Since wall shear stress  $t_w$  is defined as:

$$\tau_w = \mu \frac{du}{dy}, \quad (\text{Eq 6})$$

With dynamic fluid viscosity,  $\mu$ .

The slope of the velocity profile from Equation 6 can be calculated to obtain  $t_w$  at the wall Equation 7

$$\tau_w = \mu \frac{du}{dy} = -\frac{h}{2} \frac{dp}{dx} \quad (\text{Eq 7})$$

For parallel-plate chamber with width  $w$ , the volumetric flow rate,  $Q$ , can be solved by integrating the velocity profile over the gap height  $h$

$$Q = w \times \int_0^h u(y) dy = -\frac{dp}{dx} \frac{wh^3}{12\mu} \quad (\text{Eq 8})$$

Combining Equation 8 and Equation 9 yields a simplified equation for wall shear stress ( $t_w$ ) in terms of volumetric flow rate, fluid viscosity and flow chamber dimensions

$$\tau_w = \frac{6\mu Q}{wh^2} \quad (\text{Eq 9})$$

Since Equation 9 is derived for an ideal case of infinite parallel plates which does not consider the presence of sidewalls, a minor revision must be made. The magnitude of this deviation depends on the cross-sectional aspect ratio,  $\alpha = h/w$ , where  $0 \leq \alpha \leq 1$ . Low  $\alpha$  ( $<1$ ) indicates wide plates and narrow separation resembling a two-dimensional model. Contrarily, a high  $\alpha$  ( $\geq 1$ ) indicates a square-like geometry which significantly alters the flow profile. An exact solution to the three-dimensional velocity profile in rectangular ducts can be derived from Fourier series expansion, which yields Equation 9 in algebraic form:

$$\tau_w = \frac{2\mu Q}{wh^2} \left( \frac{m+1}{m} \right) (n+1) \quad (\text{Eq 10})$$

Where  $m$  and  $n$  are empirical constants, with  $m = 1.7 + 0.5(h/w) \alpha^{-1.4}$  and  $n = 2$  for aspect ratios  $\alpha < 1/3$ .

The Reynold's Numbers in microfluidic systems are usually small ( $Re < 100$ ) (Bayraktar & Pidugu, 2006). In addition to its use for generating hemodynamic flow conditions *in vitro*, laminar flow has been exploited for controlled mixing and separation on-chip. Although beyond the scope of this review, it is of interest to acknowledge the capabilities of microscale flow systems as a launchpad for future work. Bayraktar & Pidugu provide a comprehensive review of microscale flow properties and their related applications for reference.

### 1.8.3 Organ On-a-Chip

The small scale, visibility, and laminar flow properties of microfluidic devices has contributed to the development of organ on-a-chip (OOC) technology. Organ on-a-chip devices are micro-scale *in vitro* systems that model *in vivo* conditions present in humans. Since its inception in the early 2000s, OOCs have been deployed as surrogates for *in vivo* drug testing and for modeling the (patho)physiology of disease (Ma et al., 2021). The vascular system has emerged as a highly translatable aspect of human physiology for *in vitro* modeling. Arterial and venous shear stress (WSS) have been recapitulated on these devices (Ma et al., 2021). Endothelialized microenvironments have moreover been achieved on-chip (Ma et al., 2021). The convergence of flow and surface on-chip has enabled realistic modeling of thrombosis *in vitro*. In contrast to existing *in vitro* thrombogenicity testing platforms, OOC can capture the entirety of Virchow's Triad with **(i)** vascular-like flow (WSS) conditions, and **(ii)** vascular-like

microenvironments (e.g. blood and endothelial cells) that are present *in vivo*. This is achieved with low (<1 mL) reagent consumption, high-throughput, and low visibility. It is plausible that these advantages could facilitate swifter translation of novel antithrombogenic coatings/devices.

### 1.8.3.1 Vascular Flow On-a-Chip

Microfluidic OOC devices generate *in vivo* vascular flow conditions using tailored flow channels and wall shear stress (WSS). One such example is provided by Jain et al, who report a “vein on-a-chip” model that incorporates endothelial cells, blood flow, and a WSS of 2 dyne per cm<sup>2</sup> (Jain et al., 2020). The platform was used to investigate the thrombogenic behaviour of venous valves in the presence of low shear stress conditions (Jain et al., 2020). Similarly, Al-Hilal et al report a novel “pulmonary artery hypertension (PAH) on-a-chip” model containing luminal, intimal, medial, and adventitial layers of the pulmonary artery and tailored WSS. Their model recapitulates WSS observed in normal and PAH-affected arteries at 1.9 dyne per cm<sup>2</sup> and 15 dyne per cm<sup>2</sup>, respectively (Al-Hilal et al., 2020). Models simulating arterial stenosis and occlusion have also been described (Luna et al., 2020; Costa et al., 2017). One such example was documented by Luna et al whom demonstrated a stenosed microfluidic model with mean arteriolar shear rate of  $\gamma$  1200s<sup>-1</sup> for assessing whole blood thrombosis *in vitro*. Even though conventionally used to model microvascular contexts, microfluidics have also been used to recapitulate larger-scale flow contexts such as the pulmonary artery model described above (vessel diameter 3cm).


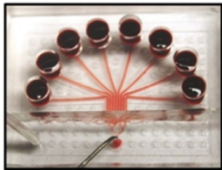
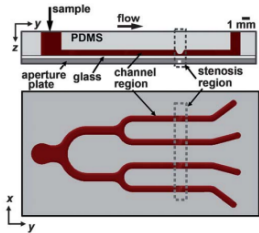
### 1.8.3.2 Thrombogenicity On-a-Chip

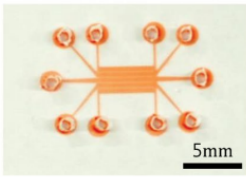
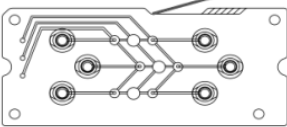
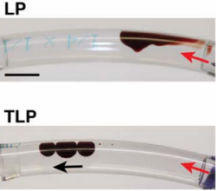
Given their ability to model vascular microenvironments, OOC have been deployed to realistically capture thrombosis *in vitro*. Microfluidic models of thrombosis usually center on the extrinsic (TF-mediated) coagulation pathway. Numerous studies have reported the use of TF, collagen, fibrinogen, and vWF coated surfaces in PDMS devices to study platelet adhesion, activation, and thrombogenicity *in vitro* (Colace et al., 2013). One such example was reported by Okorie et al, who induced platelet aggregation in microfluidic flow chamber(s) using microcontact printed collagen and TF surface(s). Similar methods were deployed by Berry et al, who report an occlusive thrombosis on-a-chip model with collagen and TF surface(s) under arteriolar shear stress. Ingber et al describe endothelial-covered microchannels for investigating whole blood thrombosis, platelet adhesion and fibrin formation *in vitro*. Of interest in this work, the contact pathway has also been explored using microfluidic models bonded to various biomaterials and polymers. Valtin et al describe a microfluidic device bonded to glass, Teflon,

and polyurethane for the study of platelet adhesion and thrombus formation under coronary-like WSS (Valtin et al., 2021). Although capably addressed, the thrombogenicity of vascular prosthetics and antithrombogenic coatings on microfluidic devices (OOCs) has been seldom described. Moreover, these devices have not been used for *in vitro* performance testing and translation of vascular prostheses.

Below is a table presenting selected applications of the microfluidic (OOC) devices for vascular and thrombogenicity studies *in vitro*. Applied wall shear stress and images of the platform set-up(s) have also been included for reference.

**Table 3:** Microfluidic Vascular Thrombosis Models and Applications

	<b>Application</b>	<b>Geometry</b>	<b>Surface and Mode of Thrombogenicity</b>	<b>Reference</b>
1	Arterial Stenosis/Occlusion Study of Shear-Activated tPA-Drug Release ( $\tau_w = 10\text{-}1000$ dyne/cm <sup>2</sup> )		<i>Extrinsic</i> (TF)/Collagen Coating	[18]
2	Arterial Flow Study of Platelet Deposition and Coagulation on collagen/TF coated surfaces ( $\gamma_s = 100\text{s}^{-1}$ )		<i>Extrinsic</i> (TF)/ Collagen-TF coating	[19]
3	Platelet Aggregation Under Physiological Flow Conditions ( $\gamma_s = 500\text{s}^{-1}\text{-}10,000\text{s}^{-1}$ )		<i>Extrinsic</i> (TF)/ Collagen Coating	[20]

<p>4</p>	<p>Endothelial cell proliferation on PDMS with shear-gradient flow (<math>\tau_w = 1-10 \text{ dyne/cm}^2</math>)</p>	<p>(C)</p> 	<p>Endothelialized/ Endothelialization</p>	<p>[21]</p>
<p>5</p>	<p>Hemocompatibility of Cardiovascular Prosthetic Materials: Compliment C5a, platelet adhesion (<math>\tau_w = 12-22 \text{ dyne/cm}^2</math>)</p>		<p><i>Intrinsic:</i> Teflon, Glass, Polyurethane</p>	<p>[22]</p>
<p>6</p>	<p>Thrombosis on Coated Material(s): Pressure/Occlusion (<math>\gamma_s = 1250 \text{ s}^{-1}</math>)</p>		<p><i>Intrinsic:</i> Tethered liquid fluorocarbon (TLP) coated PDMS</p>	<p>[23]</p>

\*HUVEC (human umbilical vein endothelial cell), TF (Tissue Factor), PDMS (polydimethylsiloxane), tPA (tissue plasminogen activator)

[18] Korin, N. in *Science*. 2012 from American Association for Advancement of Science ®; [19] Zhu, S. in *Blood*. 2015 (12) from American Society of Hematology ®; [20] Li, M. in *Lab. Chip*. 2012 (7) from Royal Society of Chemistry ®; [21] Kim, T. in *Biochip. J.* 2018 (4) from Springer ®; [22] Valtin, J. in *Curr. Dir. Biomed. Eng.* 2021 (2) from De Gruyter ®. [23] Leslie, D. in *Nat. Biotech.* 2014 (32) from Springer Nature ®.

## 1.9 Vascular Graft On-a-Chip

### 1.9.1 Rationales

This literature review captures three important themes. Firstly, we have observed the importance of surface coating(s) as a low-risk, low-cost, and effective antithrombogenic strategy for vascular grafts *in vitro*. It is moreover apparent that the development of novel antithrombogenic coatings is an active research topic- and that the testing of these coatings is required for their translation into the clinical space. We have seen that some of these testing methods involve the use of static *in vitro* devices, and that these devices preclude an important determinant of thrombosis (e.g. blood flow and WSS) *in vivo*.



Secondly, through Virchow's Triad, we have learned that blood flow is an important aspect of graft thrombosis *in vivo* and is required for realistic assessment of thrombosis *in vitro*. We then learned that *in vitro* flow platforms exist – but that some of these devices, like the Chantler loop and parallel plate flow chamber- require large volumes of blood, have poor visibility and complex set-ups involving gaskets, loops, and fixed test surfaces. The shear testing range(s) are limited in these devices and may fail to capture (patho)physiological values of wall shear stress present *in vivo* contexts. Our third and final key observation is the role of microfluidics and OOC as a facile, high-throughput, *in vitro* flow platform that realistically captures thrombosis *in vivo*. We have seen, upon review of organ on a chip/microfluidic studies, that the vascular microenvironment has been generated on-chip, and that thrombosis has been realistically modeled under both arterial and venous flow conditions.

Here, the vascular graft on-a-chip arises from the intersection of the above three themes. In this project, I sought to realistically capture thrombosis in an *in vitro* testing device. Moreover, recognizing the poor visibility and low-throughput of conventional *in vitro* platforms as a hindrance for the translation of novel antithrombogenic coatings/materials, an efficient and high-throughput alternative was sought. Microfluidics and OOC present a means of achieving both goals. In this project, a microfluidic vascular graft on a chip device that captures both the flow and surface determinants of thrombosis *in vitro* was developed. Due to the microfluidic properties of the device; high throughput testing with low reagent volume and good visibility is a built-in capability. Considering these advantages, the overarching vision for this project is that the vascular graft on-a-chip device could aid in the development of those coatings/prostheses and help illuminate their translational potential.

This idea will be investigated through a proof-of-concept integrating ePTFE (vascular graft material) and lubricant infused surface (LIS) coatings (novel antithrombogenic coatings) as the subject of thrombogenicity testing.

### 1.8.2 Objectives

Following from the above rationales, the project involves four specific objectives.

#### **First Objective:**

Generate an expanded polytetrafluoroethylene (ePTFE) vascular graft on-a-chip device that exhibits robust binding under flow conditions. At a minimum, the bonded device should tolerate physiological WSS 10-70 dyne/cm<sup>2</sup> but ideally sustain >500 dyne/cm<sup>2</sup> in the event suprphysiological WSS is required. Visibility of the graft surface should be preserved for real-time observation of the test surface(s).

#### **Second Objective:**

Demonstrate that novel antithrombogenic coatings can be incorporated onto the device. The introduction of coatings should not compromise the integrity of the device or alter the channel dimensions. The novel coating(s) of interest is the perfluorinated lubricant infused surface (LIS) and the anti-CD34 lubricant infused surface.

#### **Third Objective:**

Test the thrombogenicity of novel antithrombogenic coatings (LIS) under clinically relevant vascular flow scenario(s) (e.g. arterial wall shear stress). Quantify thrombogenic performance by measuring fibrin(ogen) deposition and thrombin activity. Explore the efficiency of the platform by conducting testing in real-time with coated and uncoated surfaces in parallel.

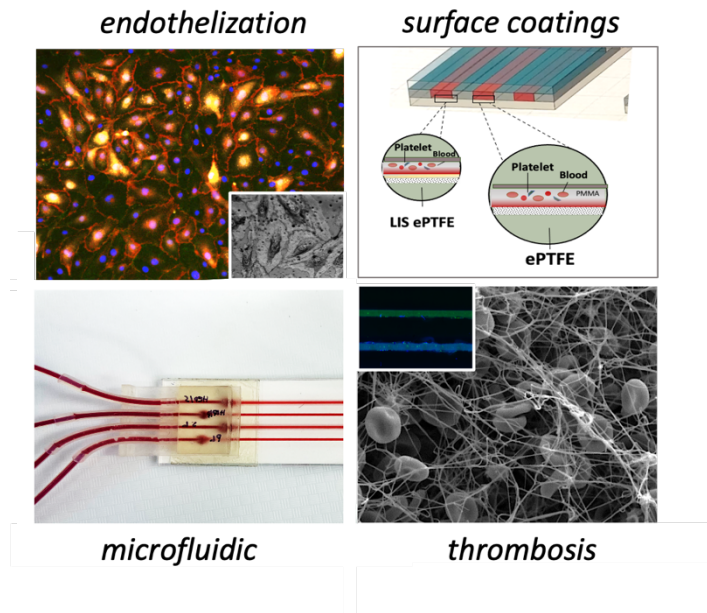
#### **Fourth Objective:**

Introduce CD34 antibody lubricant infused (anti-CD34 LIS) surface and probe endothelization of the surface. Verify the platform is compatible with endothelial cells and repeat the thrombogenicity test with the above measurement parameters.

Chapter 2: A vascular graft on a chip platform for assessing thrombogenicity  
with tuneable flow and surface conditions

Veronica Bot, Amid Shakeri, Jeffrey Weitz, Tohid Didar\*

Prepared for Submission to *Lab on a Chip*



**Visual Abstract**

## **A vascular graft on a chip platform for assessing thrombogenicity with tuneable flow and surface conditions**

Veronica A. Bot<sup>1</sup>, Amid Shakeri<sup>1</sup>, Jeffrey I. Weitz<sup>3</sup>, and Tohid F. Didar<sup>1,2\*</sup>

<sup>1</sup>School of Biomedical Engineering, McMaster University, <sup>2</sup>Department of Mechanical Engineering, McMaster University, <sup>3</sup>Thrombosis and Atherosclerosis Research Institute, McMaster University, Canada

### 2.1 Abstract

Vascular grafts are essential for the management of cardiovascular disease. However, the lifesaving potential of these devices is undermined by thrombosis arising from material and flow interactions on the blood contacting surface. To combat this issue, antithrombogenic coatings have emerged as a promising strategy for modulating blood and graft interaction *in vivo*. Although an important determinant of graft performance, hemodynamics are frequently overlooked in *in vitro* testing of coatings and their translatability remains poorly understood. We address this limitation with a microscale platform that incorporates vascular prosthesis and coatings with tuneable flow and surface conditions *in vitro*. As a proof of concept, we use the platform to test the thrombogenic performance of lubricant infused (LIS) and antibody lubricant infused (anti-CD34 LIS) coated ePTFE vascular grafts in the presence of arterial wall shear stress (WSS) with and without endothelial cells. Our findings suggest ePTFE-LIS is thromboresistant under flow and may have potential for *in vivo* arterial vascular grafting applications. It is moreover apparent that the microscale properties of the device could be advantageous for the testing and translation of novel antithrombogenic coatings and or blood contacting prosthesis in general.

**Key Words:** thrombosis, vascular graft, microfluidics, wall shear stress

### 2.2 Introduction

Cardiovascular disease (CVD) is the leading cause of death and disability worldwide (Roth et al., 2020). Vascular prostheses including stents, grafts, and heart valves play an integral role in overcoming CVD through surgical interventions (Criado et al., 2002; Lumsden et al., 2015; Dargas et al., 2016). Despite widespread use, the failure of vascular prosthesis due to thrombosis is an ongoing problem *in vivo*.

Restenosis of grafts, occlusion, and thromboembolism arising from the material surface can lead to limb-loss and death in affected individuals (Jaffer et al., 2015; Araki et al., 2020; Dolmatch et al., 2007; Jackson et al., 2002; Goodney et al., 2010; Bosiers et al., 2006). The etiology of graft thrombosis *in vivo* is complex and involves both activation of the clotting system and blood flow at the material surface in endothelialized vascular environment(s) (Jaffer et al., 2019; Hathcock., 2006; Hong et al., 2020). The material surface mediates adhesion and activation of plasma proteins, platelets, and the formation of thrombi through the intrinsic “contact” pathway (Hathcock., 2006). This process is modulated by hemodynamics and the presence of wall shear stress (WSS) *in vivo* (Dangas et al., 2016; Hathcock., 2006; Girdhar & Bluestein., 2008). Poorly performing prostheses have prompted efforts to develop antithrombogenic strategies capable of attenuating this process *in vivo*.

Compared to systemic anticoagulant drug treatment(s), surface coatings are a versatile and low risk method of attenuating thrombosis on blood contacting materials (Leslie et al., 2014). Bioinert and bio-active coatings incorporating zwitterions, anticoagulant drugs, and vascular agents have been described (Badv et al., 2020; Qi et al., 2013). Pyrolytic carbon coated heart valves (MHV) and heparin bonded (HePTFE) vascular grafts have moreover been deployed for clinical use (Samson et al., 2016; More., 2000). More recently, a novel class of lubricant infused surface (LIS) coatings have been developed and have rendered ePTFE grafts less thrombogenic in static *in vitro* testing platforms (Badv et al., 2019). Although compelling, emphasis on surface in the development and testing of these coatings neglects the role of blood flow in graft thrombosis *in vivo*. The absence of dynamic testing conditions *in vitro* renders thrombogenic performance unclear and contributes to impaired translation of an otherwise scalable and potentially lifesaving technology for vascular prosthesis (Hong et al., 2020; Braune et al., 2013).

More recently, organ on-a-chip technology has advanced our *in vitro* modeling capability of *in vivo* conditions. Numerous studies have used microfluidics to model human vascular flow and pathophysiology (Ma et al., 2021). Vein on-a-chip, pulmonary artery on-a-chip, and microvascular models of venous and arterial flow have been described (Rajeeva- Pandian et al., 2020; Al-Hilal et al., 2020; Berry et al., 2021). Thrombosis and endothelization have been captured on these devices (Ortseifen et al., 2020; Streets & Huang., 2013). Even though capable of modeling vascular environments and the properties of thrombosis *in vivo*, the use of microfluidics for testing the thrombogenicity of vascular prostheses *in vitro* has been poorly described. Moreover, the small scale, low-cost, controllability of these devices has not been exploited as an advantage for the testing and translation of novel antithrombogenic coatings and blood-contacting materials.

The rationale for a microfluidic vascular graft device is two-fold: (1) generate testing environment(s) that capture the flow and surface determinants of graft thrombosis *in vivo*, and (2) provide high throughput, low cost, scalable platform for testing/translation of vascular prosthesis and coatings *in vitro*. In this work, these rationales are realized with a “vascular graft on-a-chip” device. We first introduce a versatile design for integrating vascular prosthesis and coatings into a chip with endothelialization *in vitro*. As a proof of concept, we generate lubricant infused coating (LIS) and CD34 antibody LIS on ePTFE vascular grafts and test their thrombogenic performance in the presence of blood flow with/without endothelial cells in real time. To extend the range of our analyses, we apply arterial-like wall shear stress to simulate and probe the translatability of LIS ePTFE for *in vivo* grafting scenarios. To explore the flow modeling capability of the platform, we moreover investigate occlusion patterns in flow channels and compare with those predicted by *in vivo* hemodynamics.

## 2.3 Results

### 2.3.1 Principle, Fabrication, and Functionalization of the Vascular Graft On-a-Chip Device

#### 2.3.1.1 Fabrication of the Graft On-a-Chip Device

Novel antithrombogenic coatings are required on a range of prosthetic devices including heart valves, stents, and grafts made of polymeric and elastomeric materials (Pareta et al., 2009; Stasi et al., 2021). We sought to develop a universal fabrication protocol that could incorporate these materials and facilitate their thrombogenic testing with/without coatings in a microfluidic format. Current methods of generating microfluidic devices involve the use of soft lithography, micromachining, wet or dry etching (Fiorini & Chiu., 2005). Although effective for generic substrates like glass or cyclic olefin copolymer (COC), these methods are poorly adapted to accommodate substrates with differing material properties. We addressed this issue with medical grade double-sided pressure sensitive acrylic adhesive (PSA) tape which generates switchable and reversible attachment of planar substrates on two separate surfaces (figure 1b). In Chapter 4- “Supplementary Information and Methods Elaboration”, Subchapter 4.1.1.2, we demonstrate bonded forms of the device containing polyvinyl chloride, polymethylmethacrylate (PMMA), nylon, silicone, polyurethane, and ePTFE attached to inlets. The shear stress tolerance and channel leakage margins of these platforms is moreover provided in figure 1c and Chapter 4- “Supplementary Information and Methods Elaboration”, Subchapter 4.1.1.2.

The platform implemented in our study “vascular graft on-a-chip” is comprised of a layered assembly of ePTFE, polymethyl(methacrylate) (PMMA), 3D printed biocompatible UV-cured resin inlets, and biocompatible pressure sensitive adhesive (PSA) tape (figure 1a and b). Given the nonstick properties of the ePTFE vascular graft surface, binding the microfluidic platform was a challenge. One candidate approach was the use of heat assisted plasma (HAP) as described in (Ohkubo et al., 2018). Although demonstrating strong adhesion with other low-energy surfaces like polydimethylsiloxane (PDMS), this method involves nitrogen plasma and high temperatures which could alter the chemistry and/or porosity of the vascular graft surface(s) (Ohkubo et al., 2018). Moreover, while whole Teflon chips have been used for microfluidic applications, they are made of nonporous perfluoroalkoxy alkane (PFA) or fluorinated ethylene propylene (FEP) polymers which differ from clinical grade ePTFE (Ren et al., 2011). Chemical etching with sodium naphthalene has also been described by (Kim., 2000) but is known to cause defluorination of the graft surface.

Herein PSA offers a second distinct advantage. Unlike HAP and chemical etching, the use of PSA tape does not require alteration of the graft surface and its surface properties are preserved. Even though extensively used in paper-based and point-of-care (POC) microfluidics, the application of PSA to ePTFE for thrombogenicity testing has not been described (Walsh et al., 2017). In the graft-chip device, the PSA served as the mid layer and was dual purposed as flow channel(s). The thickness of the tape served as the height of the microfluidic channel(s) ( $81\mu\text{m}$ ). Channels were prepared by cutting the PSA tape with both  $\text{CO}_2$  laser and die cutter. In combination with the Navier-Stokes wall shear stress formula in (Sonmez et al., 2020) as derived in Chapter 1, Subchapter 1.8.2.3 “Microfluidic Flow Properties”- Equation 10, we generated a facile fabrication method for integrating channels of a specified geometry, arrangement, and wall shear stress (WSS) (figures d and e). Our fabrication method moreover reflects the timing and throughput constraints of rapid prototype microfluidics (Walsh et al., 2017). We believe these fabrication properties could streamline material testing protocols that are conventionally low-throughput and limited to a single flow condition- and moreover contribute to the role of the platform as a translational tool.

#### 2.3.1.2 Shear Tolerance of the Graft On-a-Chip Device

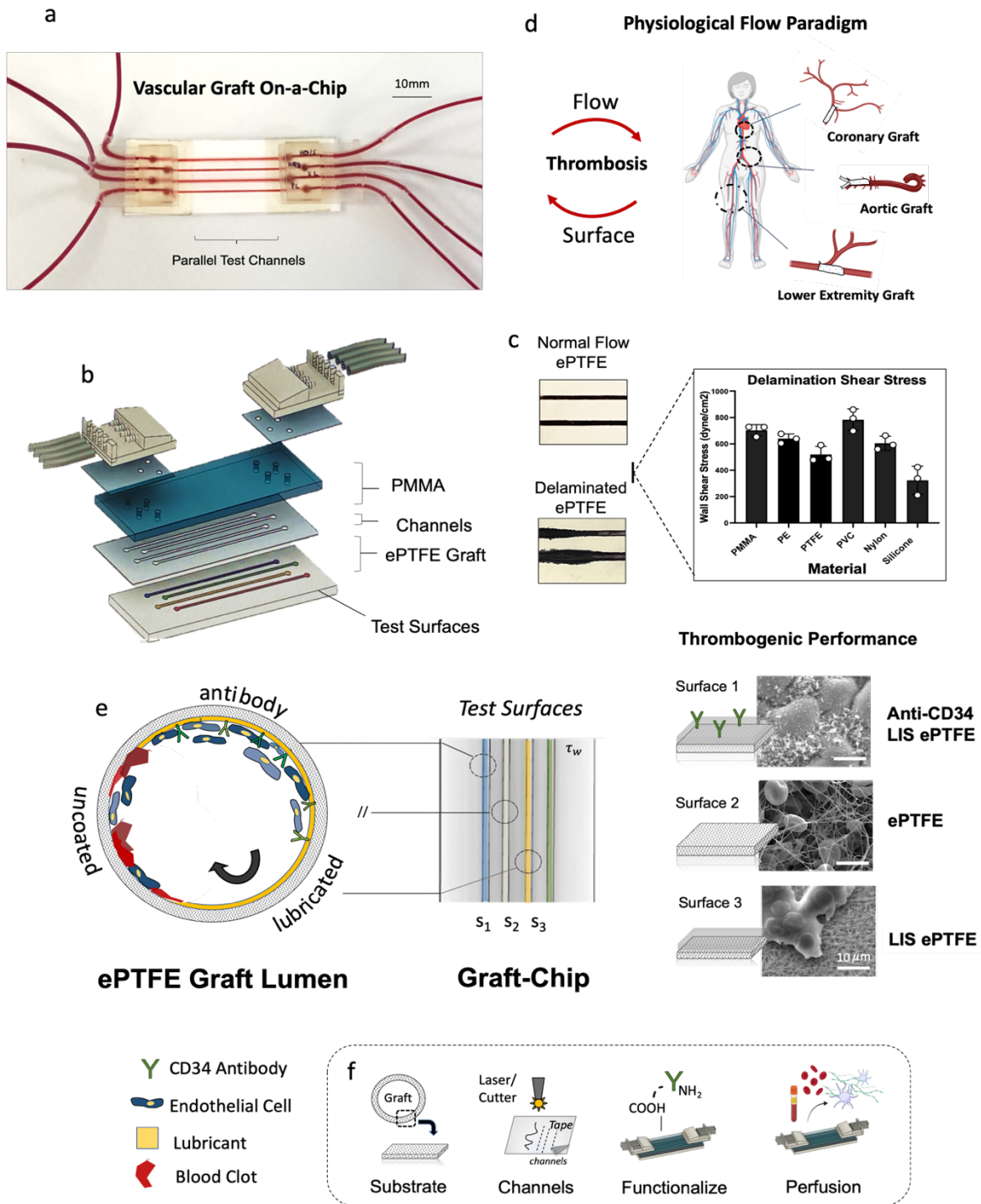
The shear stress tolerance of the bonded ePTFE vascular graft-chip device was investigated by perfusing dyed water through a rectangular channel array at a sequentially increasing flow rate over a 1-hour period (figure 1c). The shear tolerance was taken to be the point when the device delaminated or burst

in the interior of the channel array. We observed a burst WSS of 519 dyne/cm<sup>2</sup> as shown in figure 1b. This WSS exceeds the normal physiological range of 10-70 dyne/cm<sup>2</sup> but may preclude pathological shear stress (upwards of 1000 dyne/cm<sup>2</sup> for arterial stenosis) (Papioannou & Stefandis., 2005). This suggests the vascular graft on-a-chip was firmly assembled and can be implemented with a range of normal physiological vascular wall shear stress. The shear stress tolerance of bonded polyvinyl chloride, PMMA, nylon, silicone, and polyurethane devices were also tested using the same perfusion and delamination protocol(s) (figure 1b). Once again, a shear tolerance of >300 dyne/cm<sup>2</sup> was observed, indicating that robust attachment was achieved. This finding indicates the device is versatile and could be implemented with a range of blood-contacting prosthesis and or vascular flow conditions.

#### 2.3.1.3 Generation of LIS and anti-CD34 LIS ePTFE Surfaces

In our proof-of-concept investigation, we introduced lubricant infused (LIS) and anti-CD34 lubricant infused (anti-CD34 LIS) coatings on ePTFE vascular graft(s) using methods described by (Badv et al., 2019) (figure 1f). The stability and biocompatibility of these coatings has been prior validated by (Badv et al., 2019). Briefly, LIS coated surfaces were generated by infiltrating microfluidic channels with biocompatible perfluorinated lubricant (C<sub>14</sub>F<sub>24</sub>). To minimize the chance of lubricant leaching from the surface, the coated surfaces were inspected and washed the surfaces vigorously with phosphate buffered saline (PBS) prior to perfusion. The likelihood of leaching was moreover reduced by the inbuilt affinity of the porous fluorinated ePTFE surface for the perfluorinated lubricant in the presence of intermolecular force(s) (Badv et al., 2019). Anti-CD34 LIS coated surfaces were generated via CO<sub>2</sub> plasma treatment (carboxyl functionalization), amine-carbodiimide crosslinker chemistry, and subsequent infiltration with perfluorinated lubricant (C<sub>14</sub>F<sub>24</sub>) (Badv et al., 2019). Here the PSA tape was exploited as a mask for the ePTFE such that carboxyl groups were patterned within the channel region. Leveraging the double-sided PSA adhesive, we then bonded the carboxyl terminated ePTFE onto the chip and incubated the surface(s) with anti-CD34 EDC-NHS to immobilize the antibody on the graft surface. The antibody coated surface was then infiltrated with lubricant to generate the anti-CD34 LIS coated surface (the presence of immobilized antibody confirmed with Alexa Fluor anti-CD34 in Chapter 4- “Supplementary Information and Methods Elaboration”, Subchapter 4.2.2). The resulting surfaces possessed distinct functionality as illustrated in figure 1d.





**Figure 12:** Conceptual sketch of the graft on-a-chip platform, fabrication, and functionalization, with (a) graft on-a-chip platform with blood perfusion. (b) expanded diagram of the platform with component

layers, including: PMMA, channels (PSA biocompatible tape sheet), ePTFE, and 3D printed inlets. **(c)** shear tolerance of the graft-chip device when bonded to 6 clinically relevant materials: poly (methyl methacrylate) (PMMA), polyethylene (PE), ePTFE, polyvinyl chloride, nylon, silicone used in catheters, stents, grafts, hemofilters, and heart valves respectively (Pareta et al., 2009; Stasi et al., 2021). Delamination of ePTFE bonded PSA adhesive is illustrated in the left panel with dyed water. **(d)** common grafting sites with corresponding wall shear stresses and recapitulation of *in vivo* grafting conditions *in vitro* on the graft-chip device **(e)** illustration of graft thrombosis, antithrombogenic graft surfaces, and functionalization of those surfaces in the graft on-a-chip device. Uncoated surface exhibiting non-specific adhesion and thrombosis, CD34 antibody LIS exhibiting endothelial proliferation and attenuated thrombosis, LIS showing **(f)** 4-step fabrication protocol requiring: substrate selection, cutting PSA channels, functionalization, and perfusion.

### 2.3.2 Assessing the Thrombogenicity of Lubricant Infused (LIS) and Uncoated ePTFE

#### Vascular Graft Surfaces Without Endothelial Cells

To date, the thrombogenic performance of lubricant infused (LIS) coated ePTFE grafts has only been shown under static conditions *in vitro* (Badv et al., 2019). Its thrombogenic performance has been incompletely assessed and its translatability remains poorly understood. As a proof of concept, we used the platform to test the thrombogenicity of the LIS coated ePTFE vascular graft in the presence of blood flow conditions. To probe its clinical relevance, we moreover test in a failure prone “arterial bypass”-like flow scenario with vascular WSS 15 dyne/cm<sup>2</sup> (Kornet et al., 2000; Sarkar et al., 2006). Here we introduced lubricant-infused (LIS) ePTFE coated graft surfaces in parallel with uncoated ePTFE graft surfaces as shown in figure 2a. This was done to compare LIS ePTFE to standard graft(s) and to explore the scalability/throughput of the microfluidic model for *in vitro* prosthesis testing. The parallel format moreover eliminated batch-to-batch variation in donor blood which could skew thrombogenic testing outcomes (e.g. phenotypic variation in shear-mediated vWF platelet binding) (Dunne et al., 2019).

#### 2.3.2.1 Thrombus Formation

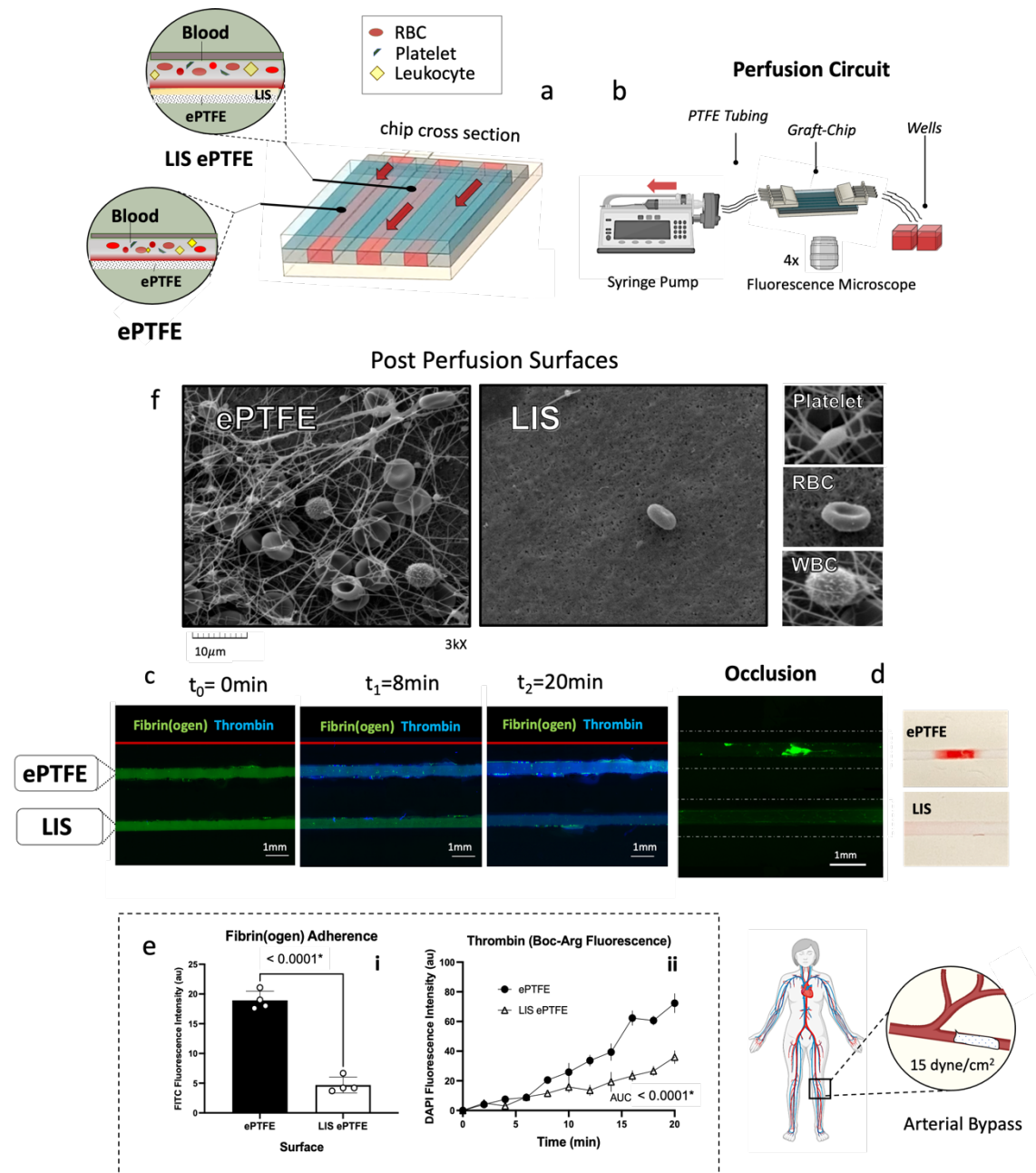
Our experimental perfusion circuit consisted of a syringe pump, fluorescent microscope, and reagent reservoir containing recalcified whole blood and fluorescent markers (figure 2b). During the formation of thrombi *in vivo*, thrombin proteolytically cleaves fibrinogen to form fibrin (Jaffer et al., 2015). Fibrin then polymerizes and enmeshes with platelets, leukocytes, and red blood cells in the formed thrombus (Jaffer et al., 2015). To capture these phenomena in our system, Boc-Val-Pro-Arg-7-AMC was used as a fluorogenic substrate for thrombin (blue), and fluorescein fibrin(*ogen*) (green) was used to monitor

the growth of thrombi under flow. When interacting with thrombin, Boc-Val-Pro-Arg-7-AMC is cleaved and fluorescent 7-amino-4-methylcoumarin (AMC) is released into solution as evidenced by the blue color in figure 2c. Together these markers provided both structural and functional measures of thrombosis which could be monitored in real time. We moreover investigated the mode of surface-thrombus interaction by inspecting the surfaces for adhered platelets (activated and non-activated), leukocytes, fibrin, and red blood cells in post-perfusion SEM (figure 2b).

Figure 2c shows the extent of thrombus formation on coated (LIS) and uncoated ePTFE surfaces over time, with observed occlusion in figure 2d. Here fluorescent images show the status of the channels at 0 min, 8 min, and 20 min during blood perfusion. As shown in figure 2c and e(i), uncoated ePTFE exhibited a marked increase in fluorescent 7-amino-4-methylcoumarin (AMC) fluorescence intensity over all 3 timepoints with a correspondingly high area under curve (AUC- cumulative fluorescence) in figure 2e(ii). This finding was matched by the heightened presence of fluorescein fibrin(*ogen*) on uncoated ePTFE in figure 2d. These findings suggest that lubricant infused surface(s) have improved thrombogenic performance compared to uncoated graft surface(s). During perfusion, we moreover observed that clot occlusion(s) occurred in different parts of the channels and were not localized. This suggests that uniform hemodynamics were present, and thrombosis was not spatially constrained (Hathcock., 2006).

#### 2.3.2.2 Scanning Electron Microscopy of LIS-Coated and Uncoated ePTFE Surfaces

To investigate the mechanism of thromboresistance, we inspected the surfaces with SEM post-perfusion. As shown in figure 2f, LIS coated ePTFE exhibits little to no fibrin adherence and broad repellence of multiple blood species including platelets (activated), leukocytes, fibrin, and red blood cells. This is in contrast with uncoated ePTFE which reveals a fully formed adherent thrombus with activated platelets, fibrin, leukocytes, red blood cells visible in the field of view. Based on these results, it could be inferred that the lubricous properties of the LIS surface attenuate both non-specific adhesion and thrombogenicity under flow. For the first time, these findings may suggest that the properties of LIS coating(s) may be robust enough overcome both the hemodynamic and surface determinants of graft thrombosis present *in vivo*. Although not comprehensive, this finding illuminates the translational potential of LIS ePTFE as a novel prosthesis for arterial grafting applications.



**Figure 13:** Application of graft on-a-chip platform for probing the thrombogenicity of ePTFE and LIS ePTFE graft surfaces under arterial WSS. **(a)** illustration of the device cross section with associated testing surfaces and channel geometry with physiological WSS inspiration (lower extremity bypass). **(b)** perfusion set-up consisting of syringe pump, reservoir, and fluorescent microscope. **(c)** qualitative assessment of thrombogenicity at 3 time points: 0min (left), 8 min (middle), 20min (right). Fluorescent labels include: fibrin(ogen) (AlexaFluor488 in green  $\lambda_{488\text{nm}}$ ), thrombin activity with Boc-Val-Pro-Arg-

AMC (blue  $\lambda_{350\text{nm}}$ ). **(d)** appearance of occluded channel(s) both with and without fluorescence. **(e)** in **(i)** quantification of adherent fibrin(ogen) post-occlusion, after gently washing the channel with HEPES buffer and in **(ii)** Boc-Val fluorescent intensity as a function of time during the course of perfusion. **(f)** SEM images of surfaces post-perfusion with the presence of activated platelet (PLT), red blood cells (RBC), and white blood cells (WBC). Data are shown with Mean $\pm$ SD error bars with significance  $p < 0.05$ , area under the curve (AUC) was tabulated in **(e-ii)**.

### 2.3.3 Assessing the Thrombogenicity of Endothelialized LIS, anti-CD34 LIS ePTFE Graft Surfaces With Endothelial Cells

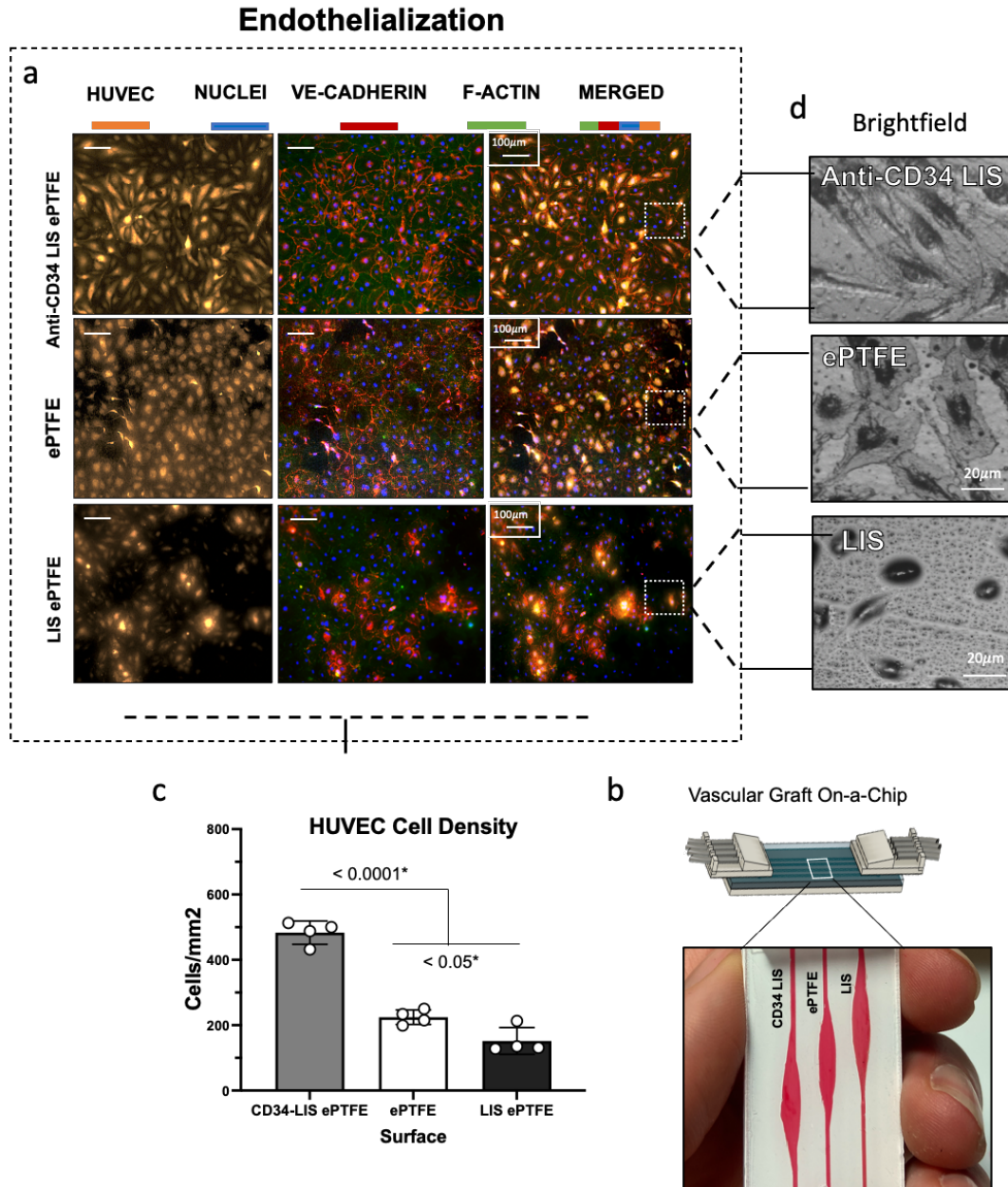
Vascular graft performance not only depends material surface(s) and hemodynamics but also the presence of endothelial cells *in vivo*. Together with blood flow and the graft surface, endothelial cells modulate thrombosis by secreting anticoagulant and antiplatelet agents such as thrombomodulin and prostaglandins (Yau et al., 2015). An absence of endothelial cells hinders prosthesis ability to suppress clot formation on the surface (Sanchez et al., 2018). This is especially true of prosthetic graft anastomoses, which have poor endothelialization and suboptimal hemodynamics *in vivo* (Khruasingkeaw et al., 2016). The anti-CD34 LIS coating is a postulated solution for this problem (Badv et al., 2019). Having both endothelial cell affinity and lubricity, the anti-CD34 LIS coating has shown exceptional thromboresistance *in vitro* static studies (Badv et al., 2019). Building on our previous model, we investigate the translatability of this coating by simulating its thrombogenic performance in an “anastomosis”-like flow context with 5-35 dyne/cm<sup>2</sup> (Khruasingkeaw et al., 2016) WSS with endothelial cells *in vitro* (figure 4a).

#### 2.3.3.1 Endothelialization and Immunofluorescence Staining

We first generated anti-CD34 LIS ePTFE on the graft-chip as described prior and in (Badv et al., 2019). To discern its mode of thromboresistance, we compared the thrombogenic performance of LIS and unmodified ePTFE in parallel (figure 4a). To probe graft endothelialization and generate a physiologic “anastomosis”-like testing environment, we cultured red fluorescent protein expressing human umbilical endothelial cells (RFP-HUVEC) on the vascular graft surface(s) in the device. This was achieved by seeding the surfaces with a RFP HUVEC endothelial growth medium suspension and incubating for 4 days under static conditions. We then labeled the cells using immunofluorescence (IF) to characterize the adherent HUVEC monolayer on LIS, anti-CD34 LIS and uncoated ePTFE surfaces. Figure 3a presents a side-by-side comparison of IF-labeled endothelialized test surfaces before

thrombogenicity testing under flow (sacrificial replicates are shown with IF). We labeled HUVECs with Alexa Fluor 647 (CD-144) VE-cadherin (red), FITC f-actin (green), Hoescht 34442 nuclei (blue), with RFP-HUVEC in orange/TRITC. These labels were chosen to visualize the morphology and confluence of adherent ECs. VE-cadherin is a cell-cell adhesion molecule implicated in EC survival and confluency (Lampugnani., 2010). Concurrently, f-actin has been cited as a key feature of normal EC cell morphology (Lampugnani., 2010). Taken together, the presence of both markers is suggestive of a healthy and functional EC phenotype (Lampugnani., 2010). We moreover quantified EC proliferation on the surfaces after 4 days with cell density measurements (cells/mm<sup>2</sup>) in figure 3c.

In agreement with prior literature, in figure 3a and c the anti-CD34 LIS graft surface exhibited significantly higher cell density and a native-like cell morphology with elongated and interconnected cell junctions (VE-Cadherin) (figure 3a and d). The presence of f-actin in a regularly distributed orientation on the antibody coated surface was also noted and corroborates this finding (figure 3a). Contrastingly, we observed lowered cell density on regular ePTFE, with sparse endothelization and little to no cells present on lubricant infused ePTFE (figure 3a). This finding agrees with the known non-specific repellency properties of ePTFE and LIS. Figure 3d illustrates the graft-chip channels during perfusion with a human hand to scale.



**Figure 14:** (a) Endothelialized channel surfaces prior to thrombogenicity testing with: top row- Anti-CD34 lubricant infused (LIS) ePTFE, middle row- ePTFE, bottom row- lubricant infused (LIS) ePTFE. Immunofluorescence labels include: endothelial cells (RFP HUVEC in orange  $\lambda_{544\text{nm}}$ ), nuclei (Hoescht 33342 in blue  $\lambda_{350\text{nm}}$ ), VE-Cadherin CD-144 (AlexaFluor 647 in red  $\lambda_{647\text{nm}}$ ), and F-actin (AlexaFluor 488 in green  $\lambda_{488\text{nm}}$ ). (b) Distinct graft-chip testing channels and surfaces during blood perfusion with



human hand for size comparison. **(c)** Cell density on the 3 test surfaces. **(d)** Brightfield images of each surface at 20X.

### 2.3.3.2 Thrombus Formation

To probe the clinical translatability of the surfaces, we then tested their thrombogenic performance in the presence of “anastomosis”-like flow context with 5-35 dyne/cm<sup>2</sup>. Here we perfused recalcified whole blood with fluorescein fibrin(*ogen*) (green) and fluorogenic thrombin substrate Boc-Val-Pro-Arg-7-AMC (blue) as described in our previous experiment. The deposition of fibrin(*ogen*) and fluorescence intensity of Boc-Val-Pro-Arg-7-AMC (thrombin activity) were once again observed until occlusion was reached (figure 4c). Figure 4b shows the status of the channels at 0 min, 8 min, and 20 min respectively. Here we observed marked deposition of fibrin(*ogen*) within the uncoated ePTFE test channel culminating in total occlusion of the channel in figure 4c. The uncoated ePTFE surface moreover exhibited heightened accumulation of 7-amino-4-methylcoumarin (AMC) (blue) with a correspondingly high area under curve (AUC) in figure 4d(ii). In figure 4c, thrombi occlusion(s) appeared localized in the tapered region of the flow channel(s). This may suggest shear flow gradients contributed to heightened thrombogenicity as observed *in vivo* and in other *in vitro* thrombosis models (Hathcock., 2006; Jain et al., 2016). We also noticed increased fibrin(*ogen*) deposition in the wide part of the channel, suggesting that reduced flow velocity and increased residence time may have promoted blood interaction(s) and the formation of large thrombi on the graft surface (Hathcock., 2006; Jain et al., 2016).

In contrast to the uncoated ePTFE graft, both lubricant infused (LIS) and anti-CD34 lubricant infused (anti-CD34 LIS) surfaces show reduced fibrin(*ogen*) deposition during perfusion and a lesser cumulative 7-amino-4-methylcoumarin (AMC) (blue) AUC. Although 7-amino-4-methylcoumarin fluorescence of LIS and ePTFE differ by a significant margin, anti-CD34 LIS and ePTFE do not. It appears that LIS and anti-CD34 LIS are equally capable of attenuating fibrin(*ogen*) deposition but not thrombin activity. This may suggest interference from tubing and/or syringes and warrants further investigation.

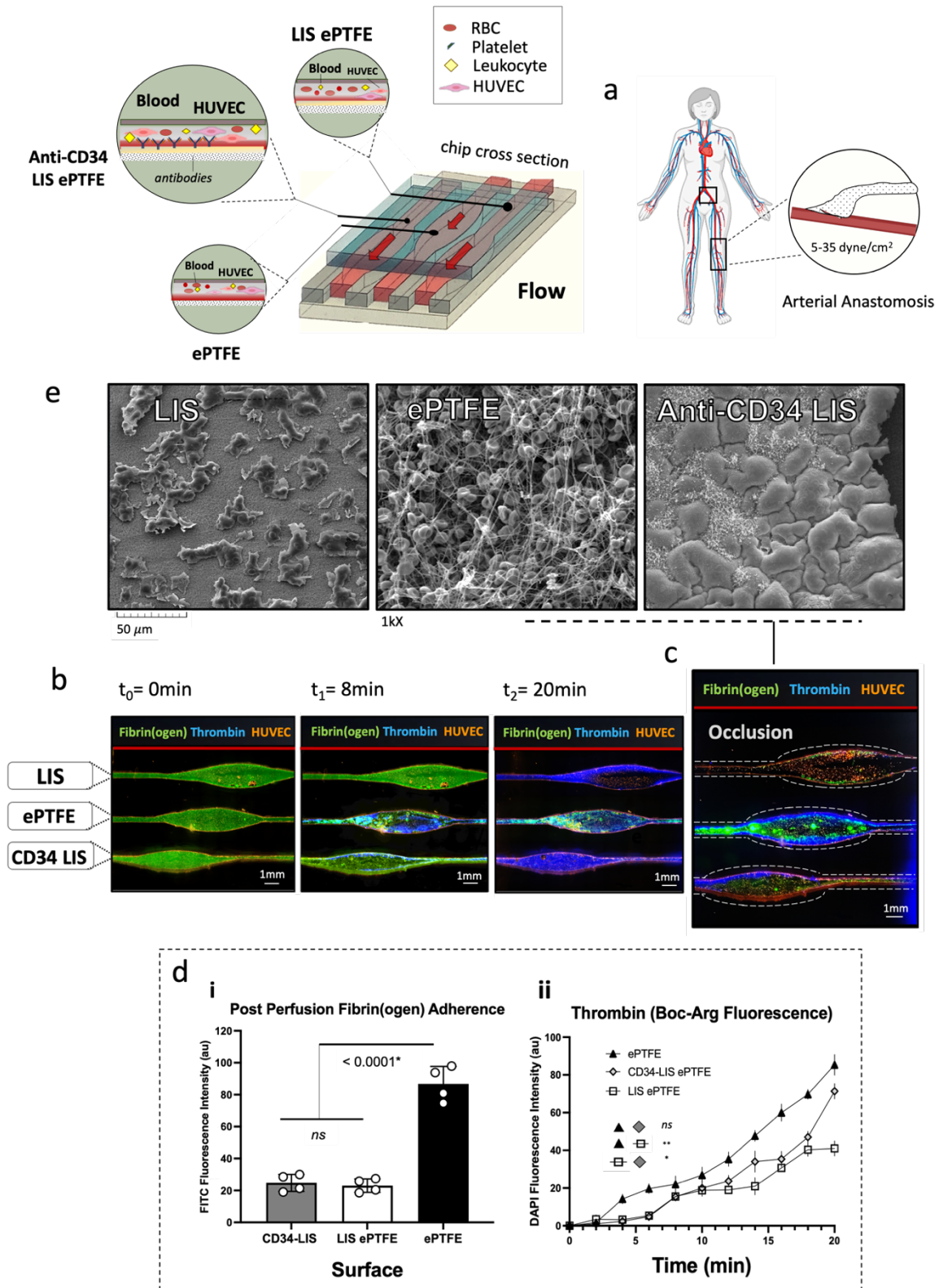
### 2.3.3.3 Scanning Electron Microscopy

To gain insight into the mechanism of thromboresistance of uncoated, LIS and anti-CD34 LIS coated grafts, we then performed SEM to assess the adherence of cells and/or blood species on the surface(s) (figure 4e). In figure 4e uncoated ePTFE exhibits endothelial cells and a dense fibrin network adherent



on the surface. The presence of activated platelets, red blood cells, and leukocytes was also noted. Consistent with the known repellency property of LIS, lubricant-infused surface(s) demonstrated a disrupted endothelial layer, negligible thrombus presence and repellence of multiple blood species. Anti-CD34 lubricant-infused surface(s) show a similarly low thrombus presence, with sparsely adhered fibrin patches. This latter surface condition also appears to have a confluent adhered endothelial monolayer as was described in VE-cadherin and cell density IF results in figures 3 (a) and (c).

Together, SEM and thrombogenicity results suggest that both anti-CD34 LIS and LIS prostheses may overcome the flow and surface determinants of thrombosis present *in vivo*. It is moreover apparent, for the first time, that anti-CD34 LIS could confer an antithrombogenic advantage in the presence of physiological WSS. In agreement with (Badv et al., 2019), anti-CD34 LIS showed extensive EC coverage– further suggesting that thromboresistance may be generated through the dual presence of both EC monolayer and lubricous interface on the graft surface. These findings reveal both LIS and anti-CD34 LIS as promising candidates for vascular prosthesis for *in vivo* grafting scenarios. It is moreover apparent that these coating strategies may attenuate thrombosis in failure-prone grafting scenarios such as arterial bypass and anastomosis which were simulated *in vitro*.



**Figure 15:** Application of graft on-a-chip platform for probing the thrombogenicity of endothelialized ePTFE, LIS ePTFE and Anti-CD34 LIS ePTFE grafts in parallel. **(a)** Illustration of the device cross section with associated testing surfaces and channel geometry, with physiological WSS inspiration (arterial anastomosis) **(b)** Qualitative assessment of thrombogenicity at 3 time points: 0min (left), 8 min (middle), 20min (right). Fluorescent labels include fibrin(ogen) (AlexaFluor488 in green  $\lambda_{488\text{nm}}$ ), thrombin activity with Boc-Val-Pro-Arg-AMC (blue  $\lambda_{350\text{nm}}$ ), endothelial cells (RFP HUVEC in orange  $\lambda_{544\text{nm}}$ ). **(c)** Representative image of channels at occlusion. **(d-i)** quantification of adherent fibrin(ogen) post-occlusion after gently washing the channel with HEPES buffer and **(d-ii)** Boc-Val fluorescent intensity as a function of time during perfusion. **(e)** SEM images of surfaces post perfusion with the presence of red blood cells, fibrin, activated platelets (top-bottom). Data are shown with Mean $\pm$ SD error bars with significance  $p < 0.05$ , area under the curve (AUC) was tabulated in **(d-ii)**.

## 2.4 Discussion

Thrombogenic failure of vascular prosthesis is an ongoing problem in healthcare. This issue has urged the development of testing platforms that can aid translation of novel antithrombogenic coatings and materials at the benchtop. Current methods of *in vitro* thrombogenicity testing involve the use of static, agitating, and or shear-flow systems (Van Oeveren et al., 2012; Braune et al., 2019). Miniaturized parallel plate and microfluidic platforms have also been described (Valtin et al., 2021; Yang et al., 2021), but fail to incorporate vascular prosthesis, coatings, and endothelial cells in a singular device. These platforms moreover fail to exploit the control and versatility of microscale perfusion as an advantage for the testing and translation of blood-contacting prosthesis and coatings *in vitro*. We addressed these limitations with a vascular graft on a chip platform that integrates tunable flow and surface conditions with microfluidics and parallelized testing *in vitro*. Our approach enables thrombogenicity testing with up to 10-fold reduction in blood volume compared to conventional flow testing models (Van Oeveren et al., 2012).

We report a fabrication method that achieves robust integration of vascular prostheses on-chip using acrylic medical grade pressure sensitive adhesive (PSA). In contrast to standard microfluidic fabrication protocols, we find PSA capable of reversible and switchable attachment of distinct substrates on-chip (Chapter 4- “Supplementary Information and Methods Elaboration”, Subchapter 4.1.1.2). We demonstrate the utility of this approach by generating platform(s) containing six clinically relevant vascular prosthetic materials including polyurethane, PVC, polyethylene, PMMA, nylon and ePTFE, as used in catheters, heart valves, stents, and grafts respectively (Pareta et al., 2009; Stasi et al., 2021). We report robust attachment with delamination shear stress (WSS) of  $>300$  dyne/cm<sup>2</sup> (e.g. supraphysiological). We moreover show that PSA channels facilitate precise and controlled surface

functionalization, wherein plasma treatment can be coupled with antibodies and or lubricant in a defined spatial pattern. This versatile fabrication approach enables incorporation of distinct testing substrates, coatings, and wall shear stress in a parallel array of channels.

As a proof of concept, we used the platform to test the thrombogenic performance of lubricant infused (LIS) and anti-CD34 lubricant infused (anti-CD34 LIS) coated ePTFE vascular grafts surfaces on-chip. Leveraging the small scale and visibility of the platform, we carried out thrombogenicity testing in real-time with fluorescence microscopy and fluorogenic markers. In the presence of blood flow and clinically inspired wall shear stress, LIS ePTFE surfaces exhibited reduced fibrin(*ogen*) deposition and cumulative 7-amino-4-methylcoumarin (AMC) thrombin activity compared to uncoated controls. We moreover discovered that these surfaces repel of a broad range of blood species including platelets (activated and nonactivated), leukocytes, and red blood cells in post-perfusion SEM. These findings align with the known properties of LIS coated ePTFE (Badv et al., 2019; Imani et al., 2019) and suggest its antithrombogenic properties are retained in the presence of blood flow. It is moreover apparent that LIS ePTFE could be a promising novel antithrombogenic strategy for *in vivo* arterial grafting applications.

Our investigation also revealed physiological-like occlusion patterns in the flow channels. In the straight channel with arterial flow, thrombi occlusion(s) occurred randomly and did not appear constrained to a particular region of the channel. In contrast, the tapered channel almost always occluded in narrow regions with increased fibrin(*ogen*) deposition observed in the wide regions. It is possible that increased WSS and heightened flow velocity contributed to heightened platelet activation and as observed in (Rajeeva-Pandian et al., 2020) and (Jain et al., 2016). Contrastingly, lowered WSS and flow velocity may have prolonged surface interactions and increased fibrin(*ogen*) deposition in the wide region as described in figure 4c and (Hathcock., 2006). Our *in vitro* occlusion observations appear to agree with the known properties of shear stress, flow velocity (hemodynamic effects) and thrombosis *in vivo* (Hathcock., 2006; Girdhar & Bluestein., 2008; Jain et al., 2016). This suggests that the vascular graft on-a-chip may capture the hemodynamic determinants of thrombosis present *in vivo*. This property of the device could be used to better understand the impact of prosthesis geometry on thrombosis as has been achieved for the optimization of prosthetic heart valves and leaflets (Dangas et al., 2016, Girdhar & Bluestein., 2008).

Future studies should investigate the flow properties of the vascular graft on-a-chip device and its use for other performance tests. The adhesion of blood cells (e.g. platelets, leukocytes, red blood cells) and

proteins (e.g. von Willebrand Factor, factor XII) could be investigated on graft surfaces using direct (visual) or indirect (pressure or eluent assay) methods. Endothelial proliferation, capture, and injury could be studied under flow to better understand intimal hyperplasia and vascular remodeling on vascular prostheses (Freeman et al., 2018). A graft-tissue injury model with TNF- $\alpha$  could moreover be explored with smooth muscle cell (SMC) and EC co-culture. These investigations could be extended to a range of blood contacting materials and or devices requiring specific WSS per endpoint application. Since vascular graft failure is a long-term phenomenon, future studies involving prolonged perfusion periods could be applied. This could be achieved with a peristaltic perfusion and/or selected anticoagulant(s) such as low dose heparin (0.25-1U/mL) (Leslie et al., 2014). Additionally, given the unexpected marginal improvement of the antithrombogenicity of EC anti-CD34 LIS ePTFE surfaces, it could be of interest to rule out the possibility of in HUVEC (venous origin) versus arterial ECs causing thrombogenic detriment. To better elucidate the role of ECs on coated surfaces, a prolonged perfusion period in the presence of arterial-derived ECs may be preferred.

## 2.5 Conclusion

Well-performing vascular prostheses are essential for the success of CVD intervention(s). Here we developed a graft on-a-chip device that enables thrombogenic testing of vascular prosthesis and coatings with and without endothelial cells under vascular flow conditions *in vitro*. Using the device, we have shown that LIS and anti-CD34 LIS coated ePTFE grafts are thromboresistant under vascular WSS and that their surface properties are retained in the presence of blood flow. This finding reinforces the known properties of LIS and suggests that their clinical translatability could be promising. We moreover investigated occlusion patterns in the channels and found similarity with the known behavior of thrombosis *in vivo*. Our work reveals that a vascular graft on-a-chip device could be effective for testing the thrombogenicity of novel vascular prosthesis and coatings and moreover contribute to their translation into the clinical space.

## 2.6 Materials and Methods

### 2.6.1 Materials

Perfluoroperhydrophenanthrene lubricant (PFPP), N-(3-dimethylaminopropyl)-N'-ethylcarbodiimide (EDC), 0.1M MES buffer, N-hydroxysuccinimide (NHS), 2-(N-morpholino)ethanesulfonic acid (MES),

ePTFE tubing was purchased from Cole Parmer (Oakville, Canada). Poly-L-Lysine Poly(ethylene glycol) (PLL-g-PEG) was obtained from Nanosoft Polymers (Salem, United States). Alexa Fluor-488-conjugated mouse anti-human CD34 antibody, trypsin–ethylenediaminetetraacetate (0.25%), SuperBlock Buffer, Alexa Fluor 647- conjugated mouse anti-human CD144 (VE-cadherin) antibody, Hoechst 33342 nucleic acid stain, and methanol-free formaldehyde were purchased from Thermo Fisher Scientific (Massachusetts, United States). Phalloidin F-actin (ab235137) was obtained from Abcam (Toronto, ON). Red fluorescent protein expressing human umbilical endothelial cells (RFP-HUVEC) were generously donated by Dr. P. Ravi Selvaganapathy’s lab at McMaster University. The cell media kit (EGM-2 BulletKit) and trypsin neutralizing agent were purchased from Lonza (Basel, Switzerland). Biocompatible 3D printing resin was obtained as a raw material for inlet fabrication from Form Labs (N.B. resin composition was patented and has not been disclosed; Massachusetts, United States). The thrombin-directed fluorescent substrate, Boc-Val-Arg-Arg-AMC, was purchased from Thermo Fisher Scientific (Massachusetts, United States). ePTFE vascular grafts were provided by Gore (Toronto, ON). Polymethylmethacrylate (PMMA), nylon, polyethylene (PE), polyvinylchloride (PVC), silicone, and polyurethane (PU) were obtained from online distributors. 1M Calcium Chloride solution (PH 7), FITC fibrin(ogen), and (4-(2-hydroxyethyl)-1-piperazineethanesulfonic acid) HEPES buffer (PH 7) were generously donated by the Thrombosis and Atherosclerosis Research Institute at McMaster University (Hamilton, ON). Human whole blood was provided by blood samples collected from healthy donors. A signed written consent was collected from donors and all procedures were approved by the McMaster University Research Ethics Board.

### 2.6.2 Chip Fabrication

The ePTFE graft-on-a-chip was fabricated using a stepwise layered assembly protocol. Firstly, 1.36mm thick expanded polytetrafluoroethylene (ePTFE) (GORE ®), 81µm thick biocompatible double-sided adhesive (AR Care AR90445-Q), and 800µm thick polymethylmethacrylate (PMMA) were obtained as planar sheets and processed for assembly. Double sided adhesive AR90445-Q contained a medical grade (AS-110) acrylic, pressure sensitive adhesive which was found non cytotoxic by third party testing (AR Adhesives, USA). All planar substrates were cut to 25 x 75 mm dimension using a carbon dioxide (50W,  $\lambda=10600\text{nm}$ ) laser, with PMMA also containing rounded inlet holes of diameter 2.5mm. Laser cut sketches were drawn using Corel Draw 10.1.2. Chip dimension was chosen to best accommodate real-time imaging on the microscope stage (but could be further miniaturized). Channels were sketched and

subsequently cut using a craft cutter (Cricut®) and internal software. All laser and craft-cut layers were then sonicated in ethanol for 5 minutes post-fabrication to remove debris and adherent particulates. Channels were inspected under 10X brightfield to inspect for roughness or anomalies in the channel geometry. Nonuniform channels were discarded. Inlets were 3D resin printed using internal software. 3D printed inlets were arranged in rows (spaced 2mm, hole diameter 0.68mm) to enable real time comparison of a parallelized array of microfluidic channels. Inlets were designed using AutoDesk Fusion 360. Once the ePTFE, PEG-blocked PMMA, adhesive and inlet layers were produced, they were applied in a sandwich configuration and manually pressed for 30 seconds to facilitate strong binding. The resultant chip was of dimension 25mm ( $w$ ) x 75mm ( $l$ ) x 2.24mm ( $h$ ) and was fitted to the microscope stage.

### 2.6.3 Blocking Polymethylmethacrylate (PMMA) with PLL-g-PEG Copolymer

PMMA was blocked with PLL-g-PEG to suppress non-specific adhesion on the non-ePTFE blood contacting surface. Briefly, PMMA was masked with adhesive channels and treated with high pressure oxygen plasma for 5 minutes (Plasma Etch PE-100 Benchtop Plasma Etching System, Carson City, Nevada). The induced hydroxyl groups were used to covalently attach PLL-g-PEG to the PMMA surface. After plasma treatment, the exposed channel regions were then passivated with a 12  $\mu$ L droplet of 0.2 $\mu$ g/mL PLL-g-PEG in 1X phosphate buffered saline (PBS, Sigma Alderich) solution for 45 minutes at room temperature (20°C). After PEG passivation, the exposed PMMA segments were rinsed with PBS, unmasked and sandwiched between ePTFE and inlet units. Quality control measures were taken on randomly selected replicates to ensure effective coating. The replicates were gently washed with PBS and a brief sliding angle test was performed to gauge surface repellency. A decrease of 10-15 $\pm$ 5 degrees was considered indicative of successful passivation.

### 2.6.4 Shear Tolerance and Perfusion Tests

Shear tolerance tests were carried out on planar ePTFE, PVC, silicone, nylon, polyethylene, and PMMA materials. Shear tolerance tests were performed by adding dye to deionized (DI) water and perfusing at an incrementally increasing flow rate. The flow rate was stepped from 100  $\mu$ L/min to 2500  $\mu$ L/min (35-880 dyne/cm<sup>2</sup>) with each step corresponding to a 200  $\mu$ L/min increment with a corresponding 2-minute duration at each step. The shear tolerance of each substrate was taken to be the point when visible delamination occurred in the interior part of the channel array. The solution tests were carried out at a

low shear (5 dyne/cm<sup>2</sup>) flow condition for a sustained period (30 minutes). Channel leakage was measured using handheld calipers. Channel width for shear tolerance and solution tests was 700µm. Shear tolerance and perfusion tests were carried out at room temperature (20°C).

### 2.6.5 Channel Geometry and Wall Shear Stress

Steady-state laminar flow Navier-Stokes equation was employed, with non-slip boundary assumption. A wall shear stress formula for microfluidic channels was employed as described in [36]. A derivation of WSS is provided in 1.8.2.3- “Microfluidic Flow Properties” (Equation 10). Parameter table and channel dimensions/sketches are provided in Chapter 4- “Supplementary Information and Methods Elaboration”, Subchapter 4.5.

### 2.6.6 Perfusion

Devices were attached using ePTFE tubing (ID 3/32”) and silicone conduit segments (Tygon, Saint-Gobain, Courbevoie, France). A multichannel syringe pump was attached to the tubing and four 3mL syringes were loaded into the pumping rack (New Era Pump Systems, Farmingdale, New York, USA). Each channel was connected to an independent syringe to mitigate unwanted pressure flux that would otherwise occur with a forked or merged flowline. Blood was diluted in a 1:1 ratio with HEPES buffer and pulled through the device (to improve visibility and suppress bubble formation). 100 µg/ml of FITC fibrin(ogen) (final concentration) and 125 µg/ml of Boc-Val-Pro-Arg-AMC (final concentration) were added to the blood-HEPES solution. This solution was then mixed with pipette and withdrawn from 2mL reservoir chambers opposite the graft-chip device, and the device was mounted on a microscope stage to enable real-time observation of thrombogenicity. The circuit was filled with blood-HEPES solution prior to adding 15mM (final concentration) of 1M CaCl<sub>2</sub> solution into the reservoir via 10uL aliquots over a 1-minute period. A flow rate of 45µL/min was used for experiment 1, and a flow rate of 100 uL/min was used in experiment 2. The typical timeframe to observe occlusion was 20 minutes ± 7 minutes. Once occlusion occurred, the channels were gently washed with HEPES buffer to visualize adherent fibrin(ogen) in the channels. We did not encounter the need to reversibly pump flow and thus, we sustained unidirectional flow for the duration of perfusion. Perfusion was conducted at room temperature (20°C).



### 2.6.7 Surface Coating Procedures

For lubricant infused surface (LIS), ePTFE surfaces were cleaned with ethanol and air dried using in line air system for 2 minutes. The ePTFE was then sealed into the device as prior described. Perfluoroperhydrophenanthrene lubricant was infused in the channels and incubated for 20 minutes per protocols described by (Badv et al., 2019). Surfaces were randomly sampled and sliding angles were tested to verify alteration of the surface occurred. Following incubation, the channels were gently rinsed with 2 cycles of HEPES buffer and rested until perfusion was initiated. For CD34-LIS surfaces, ePTFE surfaces were cleaned as prior described and placed in the biosafety cabinet (BSC) to dry. ePTFE surfaces were then placed under CO<sub>2</sub> plasma for 5 minutes, and EDC-NHS solution was prepared concurrently. 28mg of EDC and 16.8mg of NHS were weighed in a wax sheet and suspended in 700 $\mu$ L of MES buffer (PH 5.5) via pipette. 7 $\mu$ L of anti CD34 solution (5 $\mu$ g/mL) was then added to the mixture and added to the plasma treated channel surfaces. Surfaces were incubated for 3h and gently rinsed with PBS to remove non-attached antibodies. After incubation and rinsing, the surfaces were infiltrated with PFPP lubricant as described prior and 80 $\mu$ L HUVEC cell-EGM2 media solution was added to the surfaces for static cell seeding (2x10<sup>5</sup> cells/mL). Coating procedures were conducted at room temperature (20°C).

### 2.6.8 HUVEC Cell Culture

RFP HUVEC cells were cultured in cell culture dishes using EGM-2 media for a period of 4 days, or, until 80% confluence was attained via inspection with brightfield and or fluorescence microscopy (passage # 8 cells were used). Following trypsinization and suspension of the cultured cells, a HUVEC-EGM-2 solution was generated (seeding concentration 2x10<sup>5</sup> cells/mL) and 80  $\mu$ L aliquots were added to the test surfaces. Surfaces were left to seed for a period of 3h. After seeding, the surfaces were gently rinsed and filled with EGM-2 and left to reach confluence for a period of 4 days in an incubator at 37 °C and 5% CO<sub>2</sub>. Cell media was changed every day for the first 2 days and then every other day thereafter. After removing the surfaces from the incubator, surfaces were rinsed with prewarmed cell media (3x) to remove the non-adhered cells. Moreover, surfaces were once again visually inspected with upright fluorescent microscope to ensure that 80% confluence had been attained prior to initiating perfusion. Replicates were randomly selected to be sacrificed and fixed for cell density (cells/mm<sup>2</sup>) and confluence inspection via VE-Cadherin staining.

### 2.6.9 VE-Cadherin, F-Actin, and Nuclear Staining

After taking out the samples from the incubator, surface replicates were washed with prewarmed cell media (3x) in order to remove the non-adhered cells, then fixed with 4% methanol free formaldehyde. Following fixing, surfaces were then rinsed with PBS 2 times, permeabilized with 0.1% Triton X-100 (incubated for 10 minutes at room temperature), rinsed with PBS 2 times, and blocked with Superblock reagent for 1 hour. Following fixing, permeabilization and blocking, the cells were incubated with Hoescht 33342 for 15 minutes and washed with PBS. Hoescht labelling enabled easier cell density measurement(s) and enabled refined exploration into cell confluence observations. For VE-Cadherin labelling, surfaces were incubated overnight with 3  $\mu\text{g}/\text{mL}$  of primary mouse anti-human CD144 antibody in blocking buffer, rinsed 2x with PBS and subsequently incubated with 1:500 (v/v) of goat anti-mouse AlexaFluor 647 for 45 minutes. The surfaces were then rinsed 2x with PBS buffer and cut from the platform by delaminating the tape layer. F-actin labelling was carried out by adding 20  $\mu\text{g}/\text{ml}$  of FITC phalloidin F-actin for a period of 30 minutes. The surface segments (3mm x 3mm) were then mounted using Diamond Anti-Fade reagent. Sufficient mounting reagent was added so that the entire surface(s) were submerged and would attach to glass mounting slide.

### 2.6.9 Scanning Electron Microscopy

SEM was performed on ePTFE samples in order to investigate blood-graft interaction and clot formation on control and modified surfaces. Samples were fixed in 2% glutaraldehyde (2% v/v in 0.1 M sodium cacodylate buffer) overnight. The samples were rinsed twice in buffer solution, postfixed in 1% osmium tetroxide in 0.1 M sodium cacodylate buffer for 1 h, and then dehydrated through a graded ethanol series. While the samples were immersed in 100% ethanol, they were transferred to the chamber of a Leica EM CPD300 critical point dryer (Leica Mikrosysteme GmbH, Wien, Austria). The dried samples were mounted onto SEM stubs with a double-sided carbon tape. The samples on stubs were then placed in the chamber of a Polaron model E5100 sputter coater (Polaron Equipment Ltd., Watford, Hertfordshire) and approximately 4 nm of gold was deposited onto the samples. Samples were then removed from the sputter coater and SEM imaging (JSM-7000 F) was performed at 3kX and 1kX magnification.

## 2.7 Statistical Analysis

Data are presented as means  $\pm$  standard deviation (SD) in all the figures. Data were statistically analyzed by unpaired, 2-tailed t-test. P values less than 0.05 were considered significant. Replicates of 4 were used unless otherwise stated. For Boc-Val-AMC (thrombin) graphs, area under the curve (AUC) was tabulated and compared using unpaired 2-tailed t-test. All graphing and statistical analyses were performed on Graph Pad Prism. Cell counting was performed using Image J. Fibrin(*ogen*) FITC and Boc-Val-AMC (thrombin) fluorescence intensity were quantified on ImageJ using a sum of ROIs of fixed area and number of frames.

## 2.8 Acknowledgements

Thank you to the Canadian Center of Electron Microscopy for your invaluable advice on preparing samples for SEM. Thank you to the Thrombosis and Atherosclerosis Research Institute for your generous donation of fluorescein fibrin(*ogen*) and your expertise on thrombosis.

## 2.9 Disclosures

There are no conflicts of interest to disclose. This project did not receive funding

## Chapter 3: Closing Remarks and Future Directions

### 3.1 Findings

In this study, we present a vascular graft on-a-chip platform that incorporates tuneable surface and flow conditions. We used the device to test the thrombogenic performance of two novel antithrombogenic coatings: perfluorinated lubricant infused surface coating (LIS) and CD34 antibody lubricant infused surface coating (anti-CD34 LIS) under vascular-like flow conditions with and without endothelial cells. Through the use of pressure sensitive adhesive (PSA) double-sided tape bonding, the device exhibited robust attachment to ePTFE and 5 other clinically relevant substrates including PMMA, polyethylene, nylon, silicone, PVC. The shear tolerance of the device exceeded 300 dyne/cm<sup>2</sup>, indicating that it could be used to test a range of (patho)physiological wall shear stress conditions required for *in vitro* simulation of vascular flow conditions. We moreover demonstrated that the embedded ePTFE vascular graft surfaces were functionalizable and that distinct coatings could be introduced in a parallel array of channels. Upon testing the thrombogenic performance of the surfaces, we showed that significant differences in fibrin(*ogen*) deposition, thrombin activity, and surface adhesion could be ascertained on the device. It was moreover apparent that endothelial cells could be introduced onto the device and that anti-CD34 LIS capably generate thromboresistant endothelialized surfaces. These findings suggest that lubricant infused coatings can attenuate thrombosis in the presence of flow and may hold translational potential for *in vivo* ePTFE grafting applications.

### 3.2 Contribution to the Field

This project makes three significant contributions to existing literature.

1. We have expanded our existing knowledge of coated ePTFE perfluorinated lubricant infused surfaces (LIS) and shown that they are thromboresistant under flow. This finding illuminates their translational potential and may help guide their development towards clinical application(s).
2. We performed a novel extension of microfluidic organ on-a-chip technology to capture the flow and surface determinants of thrombosis *in vitro*. Compared to existing *in vitro* testing platforms, the vascular graft on-a-chip shows improved versatility, visibility, high-

throughput thrombogenicity testing with tuneable flow and surface conditions. Moreover, to our knowledge, for the first time, we demonstrated integration of endothelial cells into a microfluidic testing platform for vascular prosthesis testing application(s).

3. The modularity and scale of the device may streamline conventional materials testing protocols that are cumbersome and costly. This could aid the translation of novel vascular grafts/prostheses with or without coatings and enable swifter delivery of life-saving vascular technologies for CVD sufferers.

### 3.3 Future Directions and Closing Remarks

The vascular graft on-a-chip has shown to be a versatile and robust *in vitro* device for testing the thrombogenicity of vascular prostheses. It is plausible that the platform could be integrated with other blood contacting prosthetic devices such as hemofilters (e.g. PMMA), heart valves (e.g. nylon, carbon), catheters (e.g. polyethylene), or stents (e.g. PVC) (Stasi et al., 2021; Pareta et al., 2009). Of course, the autofluorescence of these substrates should be addressed when considering their implementation in the system with real-time fluorescence detection. Novel coatings could moreover be tested on these substrates, including but not limited to those already described in sub-chapter 1.4. To facilitate translation, other physiologically relevant wall shear stress conditions could be applied per the targeted clinical application of the vascular prostheses (e.g. arterial bypass, coronary stent flow conditions). Data pertaining to shear flow conditions is available in clinical literature and can be generated on-chip using wall shear stress formulation Equation 10 or through computational simulation with COMSOL/Ansys. It is also possible that biological species could be interchanged in these studies, and that different aspects of the blood-material interaction could be probed under flow. For example, the adsorption of fluorescently labeled proteins could be explored, or the adhesion of platelets could be assessed separately, or concurrently in the same channel.

To my knowledge, endothelial cell proliferation on vascular prostheses has not yet been studied in a microfluidic system. It could be of interest to introduce cells into the platform once again and monitor proliferation on different surfaces in the presence of flow. This *ex vivo* simulation of endothelial integration could be informative for developing strategies to enhance reendothelialization following graft implantation *in vivo*. The graft model could moreover glean insight into intimal hyperplasia if TNF- $\alpha$  is introduced as an inflammatory agent (Zimmerman et al., 2002). Co-culture with smooth

muscle cells could be achieved using methods described by Wei et al. With the modularity of the platform, it is possible to deconvolute *in vivo* blood and material interaction(s) and carry out targeted optimization (e.g. parallel test channels with distinct flow, surface or biological species).

Although promising, this study does have limitations. Firstly, it is not known how “physiological” the flow profile in the channel is, particularly considering the presence of rectangular versus rounded cross-sectional flow geometry. It is possible that there are secondary flows in the channel or that shear-induced hemolysis of red blood cells may occur (Van Oeveren et al., 2012). This possibility should be explored using a computer simulation program such as COMSOL/Ansys, where the impacts of the channel geometry could be better visualized. In addition, blood could be assayed for hemolysis using protocols described by Van Oeveren et al. Given these uncertainties, “clinical translatability” as an experimental aim could be questionable. During the fabrication process, it was noted that the device was incapable of bonding material surfaces exhibiting macroscale roughness or fabric-like texture (e.g. knitted Dacron). It has thus been assumed that the device is solely suitable for bonding planar substrates or those with microscale texture. Leakage was not an observed issue; this was likely due to the fact most blood-contacting vascular prosthetic materials repel blood and do not promote leaching outside of perfusion channels. To potentiate further work with endothelial cells (and exploit the OOC paradigm), the cytotoxicity of the platform could also be more comprehensively addressed using cell viability assays such as calorimetric MTT or fluorescent live/dead staining. Moreover, since human umbilical vein endothelial cells (HUVECs) originate from veins and not arteries, it is possible that the antithrombogenic effect of the cells is reduced in thrombogenic testing scenarios. In future studies, it could be of interest to incorporate arterial endothelial cells (of bovine or human origin) to more comprehensively address the antithrombogenic potential of EC coatings on vascular prosthetic devices.

### 3.4 Challenges

This project introduced several challenges that required distinct clusters of knowledge to overcome. The non-sticking properties of ePTFE made fabrication challenging. There was limited literature on bonding ePTFE into microfluidic formats and thus- an innovative solution was required. To overcome this issue, microfluidic fabrication, surface energy, different adhesives, bonding methods, and types of microfluidic devices were studied (literature in Lab on a Chip, Microsystems and Nanoengineering, Biomicrofluidics, among others). This module of the project also allowed me to learn about microfluidic flow properties; I experimented with COMSOL Multiphysics® velocity field mapping/shear stress

mapping/ the Non-Newtonian Carreau-Yasuda model, laminar flow mixing, peristaltic and steady pumping to further develop expertise in this area.

Grasping the importance of flow for thrombogenicity testing required a comprehensive understanding of thrombosis. This knowledge contributed to proper selection of applied wall shear stress and fluorescent detection markers. To develop this knowledge, I studied literature in journals such as: Journal of Thrombosis and Haemostasis, Blood, Journal of Vascular Surgery, among others. I moreover learned the role of vascular grafts in clinical contexts to further refine the focus and aim of this project. With an understanding of these themes, I was able to envision the project as a translational tool in addition to a means of testing the lubricant infused surface coatings. It was through this process that I developed expertise about cardiovascular disease, the coagulation cascade, material induced thrombosis, hemodynamics, and the clinical role(s) of vascular prosthetics. I also developed an understanding of SEM clot morphology and implemented this knowledge to discern the type of adhesion that occurred on test surfaces.

Functionalizing the surfaces required knowledge of surface properties and coating protocols. This knowledge was acquired through literature review of journals including Advanced Functional Interfaces, Small, among others. I moreover developed laboratory skills in plasma treatment, EDC-NHS antibody immobilization, sliding angle, and fluorescent microscopy. In latter modules of the project, I worked with endothelial cells and learned how to perform BSL2 cell culture and implement endothelialized interfaces *in vitro*. This latter experiment required knowledge of immunofluorescent staining which was acquired from lab mates and various literature articles. I moreover had the opportunity to collaborate on a related project, “Transparent and Highly Flexible Hierarchically Structured Polydimethylsiloxane Surfaces Suppress Bacterial Attachment and Thrombosis under Static and Dynamic Conditions” now published in Small- where I helped develop an *in vitro* perfusion protocol for testing the thrombogenicity and bacterial adhesion of on nanostructured polydimethylsiloxane surfaces.

Finally, to develop an understanding of the impact of the device in existing literature, I reviewed current *in vitro* materials testing platforms and assessed their advantages/disadvantages. This knowledge cluster involved journals such as Biomaterials and Materials Advances. This process enabled me to develop novel properties of the vascular graft on-a-chip device (e.g. integration of endothelial cells) and apply

relevant testing methods. I moreover learned different methods of preparing and implementing whole blood into a perfusion system.

## Chapter 4: Supplementary Information and Methods Elaboration

### 4.1 Chip Fabrication

#### 4.1.1 Development of the Platform

##### 4.1.1.1 Polydimethylsiloxane (PDMS) and ePTFE

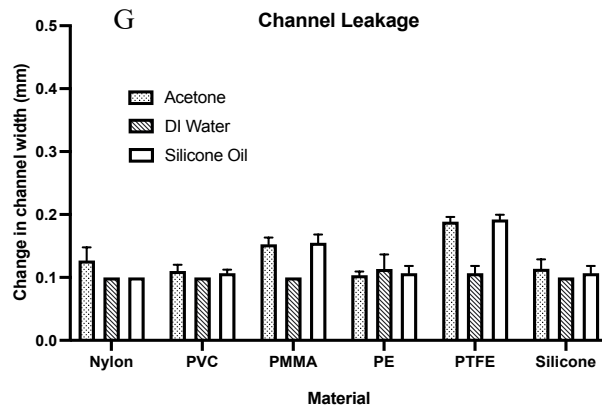
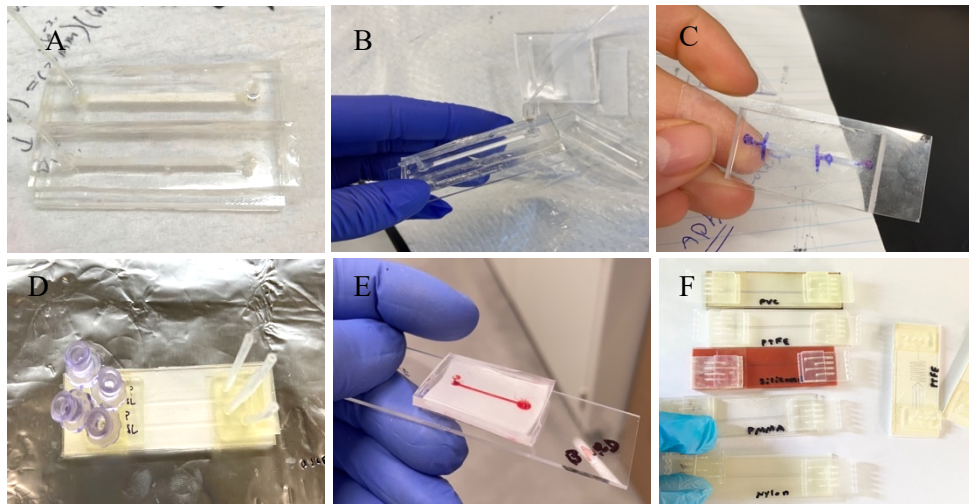
Prior to adopting pressure sensitive adhesive (PSA), several approaches to bonding ePTFE in a microfluidic format were explored. The first approach was integrating ePTFE through conventional microfluidic fabrication protocols using polydimethylsiloxane (PDMS) casting. Direct encasement of the substrate with (wet) PDMS was considered but required a complex and time-consuming procedure. Moreover, this approach did not achieve secure bonding and made surface functionalization challenging. A second method involving pre-cured PDMS and ePTFE insertion was attempted but yielded no improvement. Oxygen plasma treatment, physical compression with clips, and epoxy/silicone glue were explored as potential methods of bonding the device. Several configurations of PDMS and ePTFE substrate were tested and performed similarly. The PDMS approach was abandoned after several weeks of intensive development effort. Obtaining smooth negative molds for casting also proved difficult without the use of resin printer (printing resolution of standard Dremel® 3D printers was too low and resulted in non-bondable PDMS interfaces). Basic perfusion experiments were performed but prematurely failed due to separation of the device and/or the formation of air bubbles. Based on these findings, PDMS was not pursued as a vessel or bonding medium.

##### 4.1.1.2 Pressure sensitive adhesive (PSA), Polymethylmethacrylate (PMMA) and ePTFE

Following from the prior investigation, alternative bonding media and/or vessels for ePTFE were sought. The use of engraving to preform channels on the ePTFE substrate was briefly explored and attempted with high-power CO<sub>2</sub> laser but yielded imprecise channel width(s) and sintering of the surface (e.g. undesired modification of the test interface). Gasket-like clamp approaches were attempted per methods described in existing parallel plate *in vitro* flow models. To simplify the fabrication protocol,



the device was then reimagined in a stacked planar arrangement involving a spacer adhesive bonded to both ePTFE and a transparent overlayer. Polymethylmethacrylate (PMMA) was selected for the overlayer due to its biocompatibility, inertness, and ease of manipulation for surface blocking and laser cutting. The use of medical-grade microfluidic spacer tape was opted and applied to the device. Due to the absence of soft lithography and a flexible puncturable chip material, an alternative method of generating inlets was required. The use of plasma bonded PDMS “blocks” on PMMA was explored but found non-robust under flow conditions. The use of 3D resin printed inlets bonded by PSA spacer tape was pursued. The inlets were designed in Fusion 360 and subsequently printed with a UV-curable 3D printing resin supplied by Form Labs®. Resin printed inlets were configured parallel to the direction of flow to reduce flow disturbances in the channel, as shown in figure 16(F).



**Figure 16: Microfluidic Chip Design-** (A-C) early iterations of the platform involving PDMS casting, embedding of the ePTFE graft. Inlet integration was at an undesired 90-degree angle and the device performed poorly. (D-F) Later iterations of the platform involving pressure sensitive adhesive spacer tape was the bonding agent. Device exhibited robust attachment to ePTFE, PVC, PMMA, nylon, silicone, polyethylene. 3D printed inlets were produced in a parallel configuration and attached using spacer tape. (G) Inspecting channel leakage on various clinically relevant substrates after sustained flow (30 minutes) under low shear stress conditions (5 dyne/cm<sup>2</sup>).

Channel leakage on the bonded device(s) was briefly investigated by perfusing dyed water for a sustained period (30 mins) under low shear stress conditions (5 dyne/cm<sup>2</sup>) in a rectangular array of channels (700µm width) in Figure 16(G). Mean leakage for all substrates was <0.2mm, constituting a total margin of 13.8% of the total channel width. As a secondary investigation, three distinct fluids were perfused to test the resilience of the platform for future investigations involving other fluids with varying properties (based on kinematic viscosity,  $\nu$ , acetone, water, and silicone oil). Leakage margins were measured with a hand-held caliper.

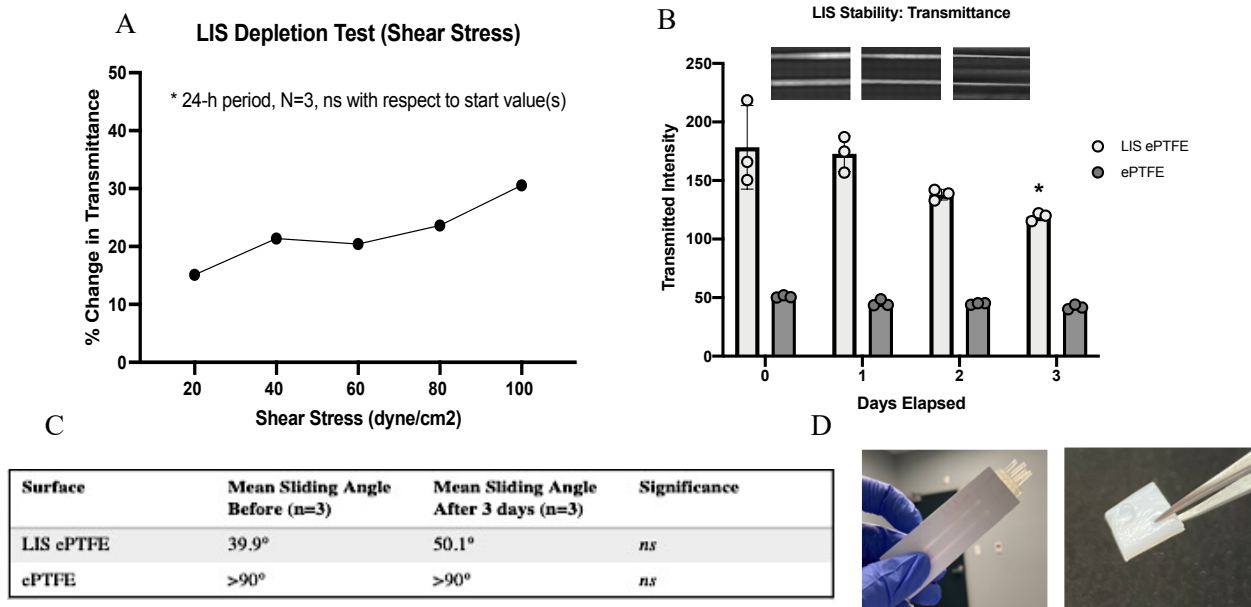
## 4.2 Coating Protocols

### 4.2.1 Stability of Lubricant Infused Surface (LIS) Under Shear Flow Conditions

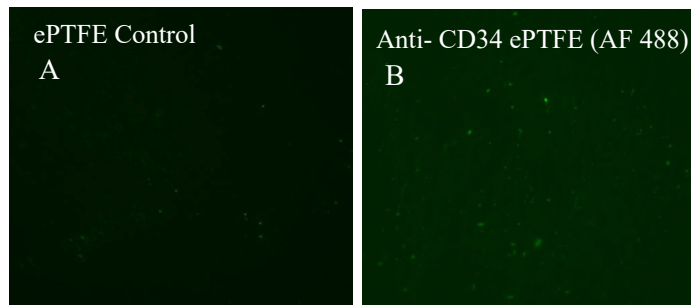
Once chip fabrication established, it was of interest to explore integrating coatings on the device. Lubricant infused surfaces (LIS) were generated through direct infiltration of perfluoroperhydrophenanthrene (PFPP) onto into the microfluidic channels. To verify saturation of the surface, optical transmittance was measured and sliding angle was investigated. Moreover, in anticipation of perfusion studies, the stability of the lubricant was investigated under wall shear stresses of 20-100 dyne/cm<sup>2</sup> for both short (24 hours) and long (72 hours) durations. LIS exhibited increasing depletion as a function of time, with a significant change in transmittance found after 72 hours of perfusion. Sliding angle moreover increased after sustained perfusion. These findings suggest that lubricant infused ePTFE may not retain its lubricous surface property under sustained flow periods. It is moreover apparent that the depletion of the coating was accelerated under high shear stress conditions. These observations raise concerns about the *in vivo* application(s) of the LIS coating(s) and may indicate more robust functionalization is required.

#### 4.2.2 Verifying the Presence of anti-CD34 On Anti-CD34 LIS Surfaces

AlexaFluor 488 conjugated CD34 antibodies were applied in the generation of anti-CD34 LIS surfaces. To verify immobilization on the surface, coated ePTFE was vigorously washed with PBS for three cycles and subsequently inspected with fluorescence microscopy. The presence of fluorescence was suggestive of attached CD34 antibody. Characterization of both LIS and anti-CD34 LIS on ePTFE was prior described by Badv in (Badv et al., 2019).



**Figure 17: Surface Functionalization and Coating Stability-** (A-D) To verify the presence lubricant on LIS coated ePTFE surfaces, optical transmittance and sliding angle were measured. Increased transmittance and lowered sliding angle were suggestive of lubricant infiltration on the surface. Stability was tested under a physiological range of wall shear stresses and changes in transmittance were quantified.

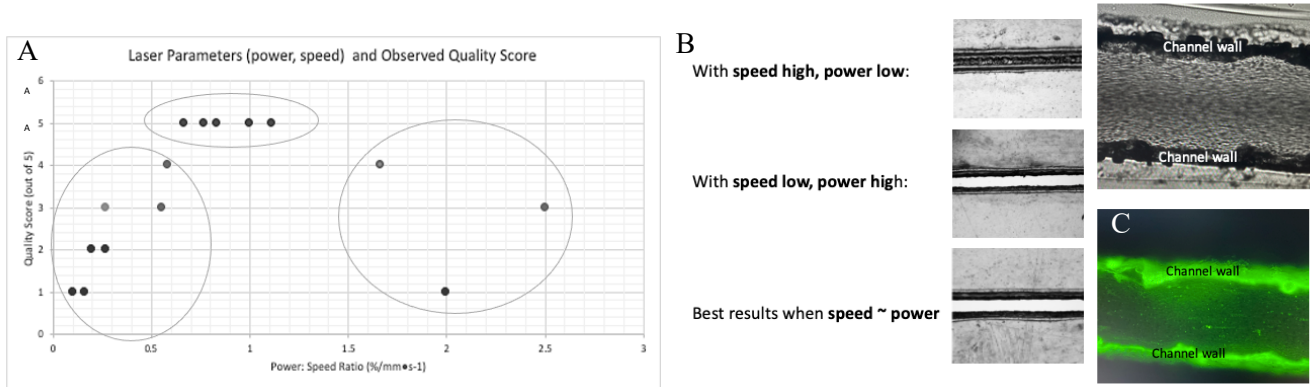


**Figure 18: Immobilization of Anti-CD34 on ePTFE-** Verifying the presence anti-CD34 AlexaFluor 488 conjugated primary antibody on EDC-NHS and CO<sub>2</sub> plasma treated ePTFE substrates for testing the CD34-LIS ePTFE surface condition. (A) ePTFE control, and (B) anti-CD34 ePTFE. Images were taken prior to lubricating the surface, immediately following incubation with EDC-NHS anti-CD34 solution and gently washing with PBS. FITC 4x fluorescence microscopy was used.

### 4.3 Channel Fabrication

#### 4.3.1 Optimization of Laser Settings

Laser cutting the perfusion channels and PMMA inlet openings was difficult and required process refinement. The use of 60-watt CO<sub>2</sub> laser was opted but variations in the quality of the cut were evident. To reduce the roughness of cut edges, the power and speed settings of the laser were optimized. The cleanest cut (quality factor 5) was obtained with an approximate 1:1 ratio of laser power and speed. The quality of the cut was further enhanced through application of 2.6 PSI compressed air with 17mm focal lens. Quality factor ratings were based on prior described standards in laser processing/resolution.



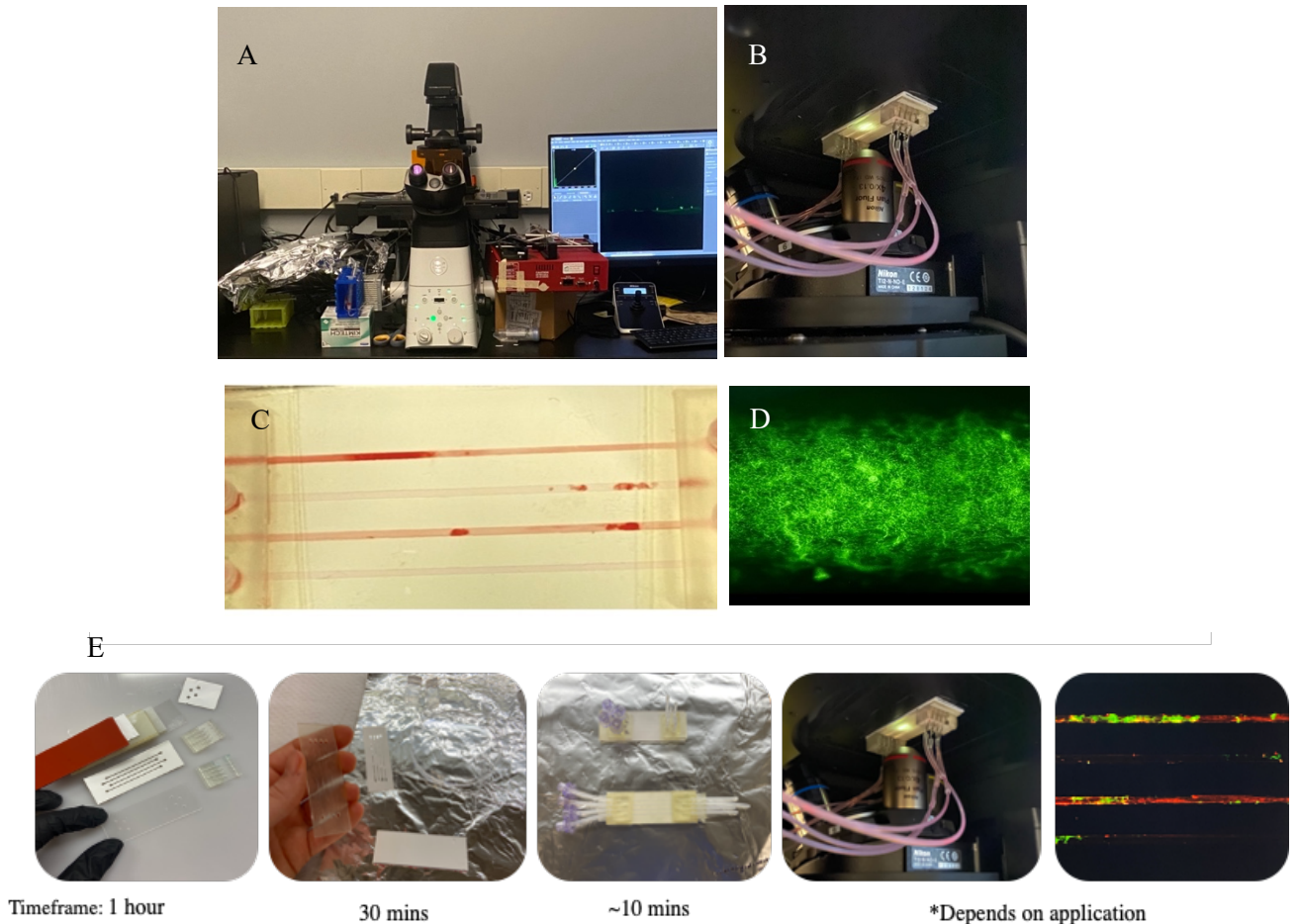
**Figure 19: Channel Fabrication-** (A) Quality of laser cut as function of power and speed ratio, with (B) Representative images of cut performance with varying power/speed parameters. (C) Illustration of channel edges under 20x magnification.

### 4.4 Perfusion and Clot Formation

#### 4.4.1 Experimental Set-Up

The perfusion set-up involved syringe pump (far right), reservoir (far left), and fluorescence microscope (middle). The chip platform was inverted to accommodate the microscope configuration and the chip

was sized to fit the stage. A representative image of clot formation in the perfusion channels. Fluorescent image of a formed clot in the channel exhibiting a highly branched fibrin(*ogen*) network.

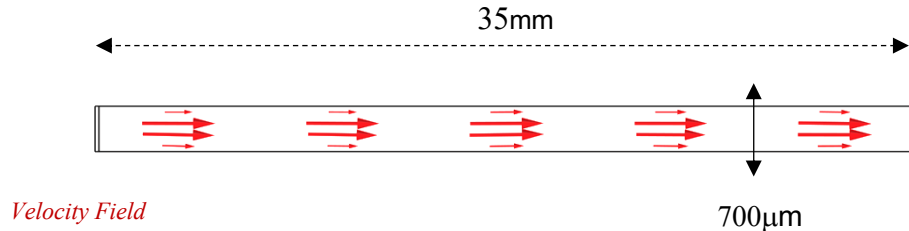


**Figure 20: Perfusion Set-Up and Channel Occlusion-** (A-B) perfusion set up with chip placement on the microscope stage. (D-C) Representative image of clot formation in the perfusion channel(s) with 20X fluorescent image of fluorescein fibrin(*ogen*). (E) A facile fabrication protocol was developed as shown with time estimates in the bottom panel: preparing PMMA, PSA channels, bonding, functionalization, and perfusion.

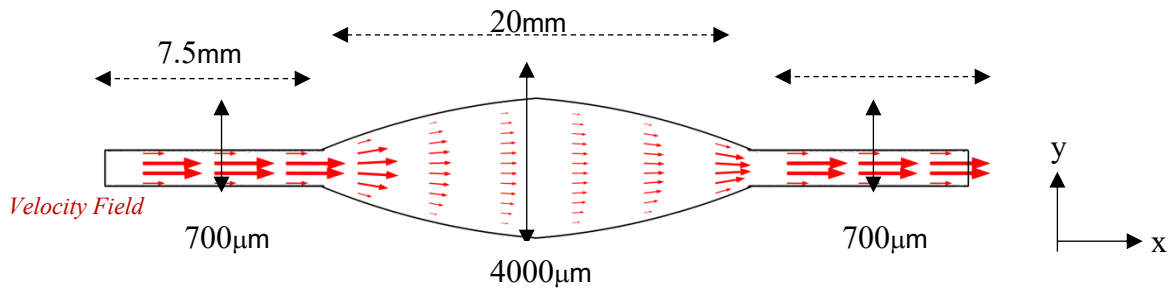
To reduce bubble formation in the perfusion circuit, low-friction PTFE tubing was used. This tubing was moreover selected to generate a homogenous blood contacting interface. In combination with the ePTFE substrate, the flow path consisted entirely of fluorinated surfaces.

#### 4.5 Channel Dimensions and Flow Parameters

Channel 1: Rectangular Geometry with Velocity Field Mapping (COMSOL)



Channel 2: Tapered Geometry with Velocity Field Mapping (COMSOL)



**Figure 4.5: Channel Dimensions-** straight rectangular channel and tapered flow channel.

**Table 4:** Channel Parameters and Flow Calculations

Parameter	Symbol	Value	Reference
Dynamic Viscosity	$\mu$	$1.5 \times 10^{-3} \text{ Pa s}$	[52]
Density	$\rho$	$1060 \text{ kg/m}^3$	[53]
Volumetric Flow Rate	$Q$	$42 \mu\text{L/min}$ - $100 \mu\text{L/min}$	-
Channel Dimensions	$w, h$	$700 \mu\text{m}$ - $4000 \mu\text{m}$ , $81 \mu\text{m}$	-
Wall Shear Stress	$\tau_w$	$15 \text{ dyne/cm}^2$ - $5\text{-}35 \text{ dyne/cm}^2$	Eq.10
Reynold's Number	Re	51-290	Eq.1
Aspect Ratio	$\alpha$	0.12 – 0.02	Eq.10
Entrance Length	$L_e$	0.3mm – 2.2mm	[54]

**N.B.** blood plasma was selected as a model for the perfusion medium ( $\mu$ ) due to the dilution of blood with HEPES buffer. [52] Késmárky, G. in *Clin Hemo and Microcirculation*, 39 (1-4), 243-246, 2008 from IOS Press ®; [53] Benim, A. in *Appl Mathematical Modelling* 35(7), 3175-3188, 2011 from Elsevier ® ; [54] Ferreira, G. in *Fluids* 6(7), 240, 2021 from MDPI ®.

## Appendix

### A.1 Fluorescent Protein Labeling Protocol

**NOTE:** This procedure may be scaled maintaining the same molar ratios of reagents. Also, it is important to consider that the number and surface position of amines will vary among proteins and so will the reactivity of the dyes.

1. Dissolve 10mg of protein in 1mL of 0.1 M sodium bicarbonate buffer.

The protein concentration should be between 5-20 mg/mL. Concentrations lower than 2mg/mL will decrease the efficiency of the reaction. Proteins should be free of any amine containing substances (eg: TRIS, glycine, ammonium ions, BSA). If present, dialyze the protein in 20 mM PBS. Low concentrations of azide will not interfere with the conjugation reaction.

2. Dissolve the amine-reaction probe in DMSO at 10 mg/mL.

Dissolve 10 mg of dye in 1mL of DMSO. Briefly vortex or pipette up and down to mix the dye solution. Dissolve the dye immediately before starting the reaction as reactive compounds are not stable in solution.

3. Slowly add 100  $\mu$ L of the reactive dye solution (volume corresponds to 1 mg of amine-reactive dye)

Usually 1/3 to 1/4 of the reactive dye will conjugate to the protein. This ratio is higher with isothiocyanates (ITC)

4. Incubate the reaction for 1 hour at room temperature with continuous stirring

**NOTE:** Cover the reaction tube with aluminum foil to prevent bleaching of the fluorophore.

5. Equilibrate the PD-10 (GE Healthcare) with 1X PBS (filtered with 0.2 $\mu$ m filter) and collect 20-30 fractions in plastic tubes.

**NOTE:** using the Beer-Lambert Law, the approximate number of dye molecules per protein can be calculated.

1. Measure the absorbance of the protein-dye conjugate at 280 nm and the maximum wavelength for the dye ( $A_{\max}$ )



Dilute the protein-dye fractions to 1/100 dilution and then measure the absorbance using the UV-Vis spectrophotometer. For FITC:  $A_{\max}=494\text{nm}$ ;  $EM=518$ ,  $\epsilon=68,000$ ,  $CF_{280}=0.30$

$$[Protein](M) = \frac{(A_{280} - (A_{\max}(dyeCF)))}{Protein\ extinction\ coefficient\ (\epsilon)(M^{-1}cm^{-1})} \times dilution\ factor\ (DF)$$

The degree of labeling (DOL) of the protein-dye yields moles of dye to moles of protein ratio:

$$DOL = \frac{A_{\max} \times Dilution\ factor\ (DF)}{Dye\ \epsilon\ (M^{-1}cm^{-1}) \times [protein](M)}$$

**Table A.1 Fluorophores, Absorbance, Emission, Extinction Parameters**

**Table 1. Spectral properties of Thermo Scientific DyLight Fluorescent Dyes.**

Emission	DyLight Dye	Ex/Em*	$\epsilon^\dagger$	Spectrally Similar Dyes
Blue	350	353/432	15,000	AMCA, Alexa Fluor 350 Dye
Blue	405	400/420	30,000	Alexa Fluor 405 and Cascade Blue® Dyes
Green	488	493/518	70,000	Alexa Fluor 488, fluorescein and FITC Dyes
Yellow	550	556/576	80,000	Alexa Fluor 546, Alexa Fluor 555, Cy®3 and TRITC Dyes
Red	594	593/618	80,000	Alexa Fluor 594 and Texas Red® Dyes
Red	633	638/658	170,000	Alexa Fluor 633 Dye
Red	650	652/677	250,000	Alexa Fluor 647 and Cy5 Dyes
Near-IR	680	692/712	140,000	Alexa Fluor 680 and Cy5.5 Dyes
Near-IR	755	754/776	220,000	Alexa Fluor 750 and Cy7 Dyes
Near-IR	800	777/790	270,000	IRDye® 800 Dye

\*Excitation and emission maxima in nanometers ( $\pm 4\text{nm}$ )

† Molar extinction coefficient ( $M^{-1} cm^{-1}$ )

## References

- Agrawal, G., Negi, Y. S., Pradhan, S., Dash, M., & Samal, S. K. (2017). Wettability and contact angle of polymeric biomaterials. In M. C. Tanzi & S. Farè (Eds.), *Characterization of Polymeric Biomaterials* (57–81). doi:10.1016/B978-0-08-100737-2.00003-0
- Araki, M., Hikita, H., Sudo, Y., Hishikari, K., & Takahashi, A. (2020). Restenosis of a Polytetrafluoroethylene-Covered Stent Visualized by Coronary Angioscopy and Optical Coherence Tomography: A Case Report. *The International journal of angiology : official publication of the International College of Angiology, Inc*, 29(1), 58–62. <https://doi.org/10.1055/s-0039-1685510>
- Akduman, C., & Kumbasar, E. P. (2017). Electrospun polyurethane nanofibers. *Aspects of Polyurethanes*. <https://doi.org/10.5772/intechopen.69937>
- Al-Hilal, T. A., Keshavarz, A., Kadry, H., Lahooti, B., Al-Obaida, A., Ding, Z., ... Ahsan, F. (2020). Pulmonary-arterial-hypertension (PAH)-on-a-chip: fabrication, validation and application. *Lab Chip*, 20, 3334–3345. doi:10.1039/D0LC00605J
- Arikan, T., Mammadov, E., Emek, E., Bozkurt, B., Inan Gurcan, N., Yazici, P., ... Tokat, Y. (2019). Utility of Polyethylene Terephthalate (Dacron) Vascular Grafts for Venous Outflow Reconstruction in Living-Donor Liver Transplantations. *Transplantation Proceedings*, 51(7), 2442–2445. doi:10.1016/j.transproceed.2019.02.040
- Assadian, A., Senekowitsch, C., Assadian, O., Eidher, U., Hagmüller, G. W., & Knöbl, P. (2005). Antithrombotic Strategies in Vascular Surgery: Evidence and Practice. *European Journal of Vascular and Endovascular Surgery*, 29(5), 516–521. doi:10.1016/j.ejvs.2005.01.021
- Assender, H., Bliznyuk, V., & Porfyraakis, K. (2002). How surface topography relates to materials' properties. *Science (New York, N.Y.)*, 297(5583), 973–976. <https://doi.org/10.1126/science.1074955>
- Badv, M., Bayat, F., Weitz, J. I., & Didar, T. F. (2020). Single and multi-functional coating strategies for enhancing the biocompatibility and tissue integration of blood-contacting medical implants. *Biomaterials*, 258, 120291. <https://doi.org/10.1016/j.biomaterials.2020.120291>
- Badv, M., Alonso-Cantu, C., Shakeri, A., Hosseinidoust, Z., Weitz, J. I., & Didar, T. F. (2019). Biofunctional lubricant-infused vascular grafts functionalized with silanized bio-inks suppress thrombin generation and promote endothelialization. *ACS Biomaterials Science & Engineering*, 5(12), 6485–6496. <https://doi.org/10.1021/acsbomaterials.9b01062>
- Baek, I., Bai, C. Z., Hwang, J., Park, J., Park, J. S., & Kim, D. J. (2012). Suppression of neointimal hyperplasia by sirolimus-eluting expanded polytetrafluoroethylene (ePTFE) haemodialysis grafts in comparison with paclitaxel-coated grafts. *Nephrology, dialysis, transplantation: official publication*

- of the European Dialysis and Transplant Association - European Renal Association, 27(5), 1997–2004. <https://doi.org/10.1093/ndt/gfr545>
- Bauer, J. W., Xu, L. C., Vogler, E. A., & Siedlecki, C. A. (2017). Surface dependent contact activation of factor XII and blood plasma coagulation induced by mixed thiol surfaces. *Biointerphases*, 12(2), 02D410. <https://doi.org/10.1116/1.4983634>
- Bayraktar, T., & Pidugu, S. B. (2006). Characterization of liquid flows in microfluidic systems. *International Journal of Heat and Mass Transfer*, 49(5-6), 815–824. <https://doi.org/10.1016/j.ijheatmasstransfer.2005.11.007>
- Benim, A. C., Nahavandi, A., Assmann, A., Schubert, D., Feindt, P., & Suh, S. H. (2011). Simulation of blood flow in human aorta with emphasis on outlet boundary conditions. *Applied Mathematical Modelling*, 35(7), 3175–3188. <https://doi.org/10.1016/j.apm.2010.12.022>
- Bergheanu, S. C., Bodde, M. C., & Jukema, J. W. (2017). Pathophysiology and treatment of atherosclerosis : Current view and future perspective on lipoprotein modification treatment. *Netherlands heart journal: monthly journal of the Netherlands Society of Cardiology and the Netherlands Heart Foundation*, 25(4), 231–242. <https://doi.org/10.1007/s12471-017-0959-2>
- Berry, J., Peaudecerf, F. J., Masters, N. A., Neeves, K. B., Goldstein, R. E., & Harper, M. T. (2021). An “occlusive thrombosis-on-a-chip” microfluidic device for investigating the effect of anti-thrombotic drugs. *Lab Chip*, 21, 4104–4117. doi:10.1039/D1LC00347J
- Bittl J. A. (1996). Advances in coronary angioplasty. *The New England journal of medicine*, 335(17), 1290–1302. <https://doi.org/10.1056/NEJM199610243351707>
- Bosiers, M., Deloose, K., Verbist, J., Schroë, H., Lauwers, G., Lansink, W., & Peeters, P. (2006). Heparin-bonded expanded polytetrafluoroethylene vascular graft for femoropopliteal and femorocrural bypass grafting: 1-year results. *Journal of vascular surgery*, 43(2), 313–319. <https://doi.org/10.1016/j.jvs.2005.10.037>
- Brash, J. L., Horbett, T. A., Latour, R. A., & Tengvall, P. (2019). The blood compatibility challenge. Part 2: Protein adsorption phenomena governing blood reactivity. *Acta biomaterialia*, 94, 11–24. <https://doi.org/10.1016/j.actbio.2019.06.022>
- Braune, S., Latour, R., Reinthaler, M., Landmesser, U., Lendlein, A., & Jung, F. (10 2019). In Vitro Thrombogenicity Testing of Biomaterials. *Advanced Healthcare Materials*, 8. doi:10.1002/adhm.201900527
- Braune, S., Grunze, M., Straub, A., & Jung, F. (2013). Are there sufficient standards for the in vitro hemocompatibility testing of biomaterials? *Biointerphases*, 8(1), 33. <https://doi.org/10.1186/1559-4106-8-33>

- Brockman, K.S. (2015). Hemocompatibility of Degradable Polar Hydrophobic Ionic Polyurethane for Blood Contacting Applications.
- Bush, H. L. (1989). Mechanisms of graft failure. *Journal of Vascular Surgery*, 9(2), 392–394.  
[https://doi.org/10.1016/0741-5214\(89\)90073-6](https://doi.org/10.1016/0741-5214(89)90073-6)
- Callow, A., Kambic, H.E., Kantrowitz, A., & Sung, P. (1986). Vascular Graft Update: Safety and Performance. *ASTM*, 312-360. doi: 10.1520/STP898-EB
- Camiade, C., Maher, A., Ricco, J.-B., Roumy, J., Febrer, G., Marchand, C., & Neau, J.-P. (2003). Carotid bypass with polytetrafluoroethylene grafts: a study of 110 consecutive patients. *Journal of Vascular Surgery*, 38(5), 1031–1037. doi:10.1016/S0741-5214(03)00708-0
- Carrabba, M., & Madeddu, P. (2018). Current Strategies for the Manufacture of Small Size Tissue Engineering Vascular Grafts. *Frontiers in bioengineering and biotechnology*, 6, 41.  
<https://doi.org/10.3389/fbioe.2018.00041>
- Castner D. G. (2017). Biomedical surface analysis: Evolution and future directions (Review). *Biointerphases*, 12(2), 02C301. <https://doi.org/10.1116/1.4982169>
- Chester, J. F. (2008). The causes of synthetic vascular graft failure. *Annals of the College of Surgeons Hong Kong*, 6(4), 97–101. <https://doi.org/10.1046/j.1442-2034.2002.00149.x>
- Cihova, M., Müller, E., Chandorkar, Y., Thorwarth, K., Fortunato, G., Maniura-Weber, K., ... Rottmar, M. (2022). Palladium-Based Metallic Glass with High Thrombogenic Resistance for Blood-Contacting Medical Devices. *Advanced Functional Materials*, 32(4), 2108256.  
doi:10.1002/adfm.202108256
- Chiu, J. J., & Chien, S. (2011). Effects of disturbed flow on vascular endothelium: pathophysiological basis and clinical perspectives. *Physiological reviews*, 91(1), 327–387.  
<https://doi.org/10.1152/physrev.00047.2009>
- Chong, D. S. T., Turner, L.-A., Gadegaard, N., Seifalian, A. M., Dalby, M. J., & Hamilton, G. (2015). Nanotopography and Plasma Treatment: Redesigning the Surface for Vascular Graft Endothelialisation. *European Journal of Vascular and Endovascular Surgery*, 49(3), 335–343.  
doi:10.1016/j.ejvs.2014.12.008
- Clauder, F., Zitzmann, F. D., Friebe, S., Mayr, S. G., Robitzki, A. A., & Beck-Sickinger, A. G. (2020). Multifunctional coatings combining bioactive peptides and affinity-based cytokine delivery for enhanced integration of degradable vascular grafts. *Biomater. Sci.*, 8, 1734–1747.  
doi:10.1039/C9BM01801H

- Colace, T. V., Tormoen, G. W., McCarty, O. J. T., & Diamond, S. L. (2013). Microfluidics and Coagulation Biology. *Annual Review of Biomedical Engineering*, 15(1), 283–303. doi:10.1146/annurev-bioeng-071812-152406
- Convery, N., & Gadegaard, N. (2019). 30 years of Microfluidics. *Micro and Nano Engineering*, 2, 76–91. <https://doi.org/10.1016/j.mne.2019.01.003>
- Costa, P. F., Albers, H. J., Linssen, J., Middelkamp, H., van der Hout, L., Passier, R., van den Berg, A., Malda, J., & van der Meer, A. D. (2017). Mimicking arterial thrombosis in a 3D-printed microfluidic in vitro vascular model based on computed tomography angiography data. *Lab Chip*, 17(16), 2785–2792. <https://doi.org/10.1039/c7lc00202e>
- Criado, F. J., Lingelbach, J. M., Ledesma, D. F., & Lucas, P. R. (2002). Carotid artery stenting in a vascular surgery practice. *Journal of Vascular Surgery*, 35(3), 430–434. doi:10.1067/mva.2002.121209
- Crombez, M., Chevallier, P., -Gaudreault, R. C., Petitclerc, E., Mantovani, D., & Laroche, G. (2005). Improving arterial prosthesis neo-endothelialization: Application of a proactive VEGF construct onto PTFE surfaces. *Biomaterials*, 26(35), 7402–7409. doi:10.1016/j.biomaterials.2005.05.051
- Cutlip, D., Abbott J. D. (2022). Drug-eluting intracoronary stents: Stent types, UptoDate. Retrieved from <https://www.uptodate.com/contents/drug-eluting-intracoronary-stents-stent-types#:~:text=Current%2Dgeneration%20DES%20include%20everolimus,similar%20safety%20and%20efficacy%20profile>.
- Dangas, G. D., Weitz, J. I., Giustino, G., Makkar, R., & Mehran, R. (2016). Prosthetic heart valve thrombosis. *Journal of the American College of Cardiology*, 68(24), 2670–2689. <https://doi.org/10.1016/j.jacc.2016.09.958>
- Davies, M. & Woolf, N. (1993). Atherosclerosis: what is it and why does it occur?. *British heart journal*, 69(1 Suppl), S3–S11. [https://doi.org/10.1136/hrt.69.1\\_suppl.s3](https://doi.org/10.1136/hrt.69.1_suppl.s3)
- Dolmatch, B., Dong, Y. H., & Heeter, Z. (2007). Evaluation of three polytetrafluoroethylene stent-grafts in a model of neointimal hyperplasia. *Journal of vascular and interventional radiology : JVIR*, 18(4), 527–534. <https://doi.org/10.1016/j.jvir.2007.02.011>
- Duffy, D. C., McDonald, J. C., Schueller, O. J., & Whitesides, G. M. (1998). Rapid prototyping of microfluidic systems in poly(dimethylsiloxane). *Analytical Chemistry*, 70(23), 4974–4984. <https://doi.org/10.1021/ac980656z>
- Dunne, E., Qi, Q. M., Shaqfeh, E. S., O’Sullivan, J. M., Schoen, I., Ricco, A. J., O’Donnell, J. S., & Kenny, D. (2019). Blood group alters platelet binding kinetics to von Willebrand factor and

- consequently platelet function. *Blood*, 133(12), 1371–1377. <https://doi.org/10.1182/blood-2018-06-855528>
- Duvnjak, S., Andersen, P. E., Larsen, K. E., & Roeder, O. (2014). Endovascular repair of postoperative vascular graft related complications after aorto-iliac surgery. *International angiology : a journal of the International Union of Angiology*, 33(4), 386–391.
- Esmon, C. T., Vigano-D'Angelo, S., D'Angelo, A., & Comp, P. C. (1987). Anticoagulation proteins C and S. *Advances in experimental medicine and biology*, 214, 47–54. [https://doi.org/10.1007/978-1-4757-5985-3\\_4](https://doi.org/10.1007/978-1-4757-5985-3_4)
- Fang, Y., Wu, D., & Birukov, K. G. (2019). Mechanosensing and Mechanoregulation of Endothelial Cell Functions. *Comprehensive Physiology*, 9(2), 873–904. <https://doi.org/10.1002/cphy.c180020>
- Ferreira, G., Sucena, A., Ferrás, L. L., Pinho, F. T., & Afonso, A. M. (2021). Hydrodynamic entrance length for laminar flow in microchannels with rectangular cross section. *Fluids*, 6(7), 240. <https://doi.org/10.3390/fluids6070240>
- Fiorini, G. S., & Chiu, D. T. (2005). Disposable microfluidic devices: Fabrication, function, and application. *BioTechniques*, 38(3), 429–446. <https://doi.org/10.2144/05383rv02>
- Freeman, J., Chen, A., Weinberg, R. J., Okada, T., Chen, C., & Lin, P. H. (2018). Sustained thromboresistant bioactivity with reduced intimal hyperplasia of heparin-bonded polytetrafluoroethylene Propaten graft in a chronic canine femoral artery bypass model. *Annals of Vascular Surgery*, 49, 295–303. <https://doi.org/10.1016/j.avsg.2017.09.017>
- Freudenberger RS, Hellkamp AS, Halperin JL, et al. (2007) Risk of thromboembolism in heart failure: an analysis from the Sudden Cardiac Death in Heart Failure Trial (SCD-HeFT). *Circulation*, 115: 2637–41.
- Galley, H., & Webster, N. R. (08 2004). Physiology of the endothelium. *British journal of anaesthesia*, 93, 105–113. doi:10.1093/bja/ae163
- Gale, B., Jafek, A., Lambert, C., Goenner, B., Moghimifam, H., Nze, U., & Kamarapu, S. (2018). A review of current methods in microfluidic device fabrication and future commercialization prospects. *Inventions*, 3(3), 60. <https://doi.org/10.3390/inventions3030060>
- Gambir, R., & Weerasekera., A. (2017). Antithrombotics in vascular surgery: Current practice guidelines. *Indian Journal of Vascular & Endovascular Surgery*. 4(2), 85-91.
- Gbyli, R., Mercaldi, A., Sundaram, H. S., & Amoako, K. (2017). Achieving Total Local Anticoagulation on Blood Contacting Devices. *Advanced Materials Interfaces*, 5, 1700954. doi:10.1002/admi.201700954

- Girdhar, G., & Bluestein, D. (2008). Biological effects of dynamic shear stress in cardiovascular pathologies and devices. *Expert Review of Medical Devices*, 5(2), 167–181. <https://doi.org/10.1586/17434440.5.2.167>
- Gomes De Almeida, V. (2013). *New Methods for Hemodynamic Evaluation: A multi-parametric approach* (dissertation).
- Goodney, P. P., Nolan, B. W., Schanzer, A., Eldrup-Jorgensen, J., Bertges, D. J., Stanley, A. C., Stone, D. H., Walsh, D. B., Powell, R. J., Likosky, D. S., Cronenwett, J. L., & Vascular Study Group of Northern New England (2010). Factors associated with amputation or graft occlusion one year after lower extremity bypass in northern New England. *Annals of vascular surgery*, 24(1), 57–68. <https://doi.org/10.1016/j.avsg.2009.06.015>
- Gourlay, T., & Black, R. A. (Eds.) (2010). *Biomaterials and Devices for the Circulatory System*. Woodhead Publishing in Materials. ISBN-13: 978-1845694647
- Gupta, P., Chaudhuri, G., Guru, J., Agarwala, M., Ghosh, D., Nandi, S., & Mandal, B. (2021). Functionalized Silk Vascular Grafts with Decellularized Human Wharton's Jelly Improves Remodeling via Immunomodulation in Rabbit Jugular Vein. *Advanced Healthcare Materials*, 10. doi:10.1002/adhm.202100750
- Han, Q., Shea, S. M., Arleo, T., Qian, J. Y., & Ku, D. N. (2021). Thrombogenicity of biomaterials depends on hemodynamic shear rate. *Artificial Organs*. <https://doi.org/10.1111/aor.14093>
- Hathcock J. J. (2006). Flow effects on coagulation and thrombosis. *Arteriosclerosis, thrombosis, and vascular biology*, 26(8), 1729–1737. <https://doi.org/10.1161/01.ATV.0000229658.76797.30>
- Herbertson, L. H., Deutsch, S., & Manning, K. B. (2011). Near valve flows and potential blood damage during closure of a bileaflet mechanical heart valve. *Journal of biomechanical engineering*, 133(9), 094507. <https://doi.org/10.1115/1.4005167>
- Hlady, V., V., & Buijs, J. (1996). Protein adsorption on solid surfaces. *Current opinion in biotechnology*, 7(1), 72–77. [https://doi.org/10.1016/s0958-1669\(96\)80098-x](https://doi.org/10.1016/s0958-1669(96)80098-x)
- Hong, J. K., Gao, L., Singh, J., Goh, T., Ruhoff, A. M., Neto, C., & Waterhouse, A. (2020). Evaluating medical device and material thrombosis under flow: Current and emerging technologies. *Biomaterials Science*, 8(21), 5824–5845. <https://doi.org/10.1039/d0bm01284j>
- Hoffman A. S., Ratner, B. D., Schoen, F. J., & Lemons, J. E. (Eds.). (2013). *An Introduction to Materials in Medicine* (Third Edition). ISBN: 978-0080877808

- Holme, P. A., Ørvim, U., Hamers, M. J. A. G., Solum, N. O., Brosstad, F. R., Barstad, R. M., & Sakariassen, K. S. (1997). Shear-Induced Platelet Activation and Platelet Microparticle Formation at Blood Flow Conditions as in Arteries With a Severe Stenosis. *Arteriosclerosis, Thrombosis, and Vascular Biology*, 17(4), 646–653. doi:10.1161/01.ATV.17.4.646
- Housholder G. T. (1991). The role of the endothelium in in vivo anticoagulation. *Journal of oral and maxillofacial surgery: official journal of the American Association of Oral and Maxillofacial Surgeons*, 49(5), 507–511. [https://doi.org/10.1016/0278-2391\(91\)90177-n](https://doi.org/10.1016/0278-2391(91)90177-n)
- Hoshian, S., Kankuri, E., Ras, R. H., Franssila, S., & Jokinen, V. (2017). Water and blood repellent flexible tubes. *Scientific Reports*, 7(1). <https://doi.org/10.1038/s41598-017-16369-3>
- Hassan, M. I., Saxena, A., & Ahmad, F. (2012). Structure and function of von Willebrand factor. *Blood Coagulation & Fibrinolysis*, 23(1), 11–22. <https://doi.org/10.1097/mbc.0b013e32834cb35d>
- Hyltegren, K., Hulander, M., Andersson, M., & Skepö, M. (2020). Adsorption of Fibrinogen on Silica Surfaces—The Effect of Attached Nanoparticles. *Biomolecules*, 10, 413. doi:10.3390/biom10030413
- Imani, S. M., Badv, M., Shakeri, A., Yousefi, H., Yip, D., Fine, C., & Didar, T. F. (2019). Micropatterned biofunctional lubricant-infused surfaces promote selective localized cell adhesion and patterning. *Lab on a Chip*, 19(19), 3228–3237. <https://doi.org/10.1039/c9lc00608g>
- Jackson, M. R., Johnson, W. C., Williford, W. O., Valentine, R. J., & Clagett, G. P. (2002). The effect of anticoagulation therapy and graft selection on the ischemic consequences of femoropopliteal bypass graft occlusion: results from a multicenter randomized clinical trial. *Journal of vascular surgery*, 35(2), 292–298. <https://doi.org/10.1067/mva.2002.120383>
- Jain, A., van der Meer, A. D., Papa, A. L., Barrile, R., Lai, A., Schlechter, B. L., Otieno, M. A., Loudon, C. S., Hamilton, G. A., Michelson, A. D., Frelinger, A. L., 3rd, & Ingber, D. E. (2016). Assessment of whole blood thrombosis in a microfluidic device lined by fixed human endothelium. *Biomedical microdevices*, 18(4), 73. <https://doi.org/10.1007/s10544-016-0095-6>
- Jaffer, I. H., Fredenburgh, J. C., Hirsh, J., & Weitz, J. I. (2015). Medical device-induced thrombosis: what causes it and how can we prevent it?. *Journal of thrombosis and haemostasis : JTH*, 13 Suppl 1, S72–S81. <https://doi.org/10.1111/jth.12961>
- Jaffer, I., & Weitz, J. (2019). The blood compatibility challenge. Part 1: Blood-contacting medical devices: The scope of the problem. *Acta Biomaterialia*, 94, 2-10.
- Jain, A. (2020). Abstract 151: Vein-on-chip: Microengineered Modeling of Venous Valves, Thrombosis and Therapeutics. *Arteriosclerosis, Thrombosis, and Vascular Biology*, 40A151–A151. doi:10.1161/atvb.40.suppl\_1.151



- Jain, A., Graveline, A., Waterhouse, A., Vernet, A., Flaumenhaft, R., & Ingber, D. E. (2016). A shear gradient-activated microfluidic device for automated monitoring of whole blood haemostasis and platelet function. *Nature communications*, 7, 10176. <https://doi.org/10.1038/ncomms10176>
- Jamiolkowski, M. A., Pedersen, D. D., Wu, W.-T., Antaki, J. F., & Wagner, W. R. (2016). Visualization and analysis of biomaterial-centered thrombus formation within a defined crevice under flow. *Biomaterials*, 96, 72–83. doi:10.1016/j.biomaterials.2016.04.022
- Jamiolkowski, M. A., Snyder, T. A., Perkins, I. L., Malinauskas, R. A., & Lu, Q. (2021). Preclinical Device Thrombogenicity Assessments: Key Messages From the 2018 FDA, Industry, and Academia Forum. *ASAIO journal (American Society for Artificial Internal Organs: 1992)*, 67(2), 214–219. <https://doi.org/10.1097/MAT.0000000000001226>
- Jamiolkowski, M., Woolley, J., Kameneva, M., Antaki, J., & Wagner, W. (2015). Real Time Visualization and Characterization of Platelet Deposition under Flow onto Clinically-Relevant Opaque Surfaces. *Journal of Biomedical Materials Research Part A*, 103. doi:10.1002/jbm.a.35202
- Jordan, S. W., & Chaikof, E. L. (2007). Novel thromboresistant materials. *Journal of Vascular Surgery*, 45(6, Supplement), A104–A115. doi:10.1016/j.jvs.2007.02.048
- Kakisis, J. D., Antonopoulos, C., Mantas, G., Alexiou, E., Katseni, K., Sfyroeras, G., Moulakakis, K., & Geroulakos, G. (2017). Safety and efficacy of polyurethane vascular grafts for early hemodialysis access. *Journal of vascular surgery*, 66(6), 1792–1797. <https://doi.org/10.1016/j.jvs.2017.06.083>
- Kaneko, T., & Aranki, S. F. (2013). Anticoagulation for prosthetic valves. *Thrombosis*, 2013, 346752. <https://doi.org/10.1155/2013/346752>
- Katritsis, D., Kaiktsis, L., Chaniotis, A., Pantos, J., Efstathopoulos, E. P., & Marmarelis, V. (2007). Wall shear stress: Theoretical considerations and methods of measurement. *Progress in Cardiovascular Diseases*, 49(5), 307–329. <https://doi.org/10.1016/j.pcad.2006.11.001>
- Kauffman, D. (2020). Cardiovascular Disease Burden, Deaths are Rising Around the World. *The Journal of the American College of Cardiology*. <https://www.acc.org/about-acc/press-releases/2020/12/09/18/30/cvd-burden-and-deaths-rising-around-the-world>
- Khoffi, F., Mathieu, D., Dieval, F., Chakfé, N., & Durand, B. (2014). Compliance properties of collagen-coated polyethylene terephthalate vascular prostheses. *Journal of applied biomaterials & functional materials*, 12(3), 163–171. <https://doi.org/10.5301/jabfm.5000189>
- Kim, S. (2000). Surface modification of poly(tetrafluoroethylene) film by chemical etching, plasma, and ion beam treatments. *Journal of Applied Polymer Science*, 77, 1913–1920. doi:10.1002/1097-4628(20000829)77:9

- Kinlay S. (2016). Management of Critical Limb Ischemia. *Circulation. Cardiovascular interventions*, 9(2), e001946. <https://doi.org/10.1161/CIRCINTERVENTIONS.115.001946>
- Klement, P., Du, Y. J., Berry, L., Andrew, M., & Chan, A. K. (2002). Blood-compatible biomaterials by surface coating with a novel antithrombin-heparin covalent complex. *Biomaterials*, 23(2), 527–535. [https://doi.org/10.1016/s0142-9612\(01\)00135-1](https://doi.org/10.1016/s0142-9612(01)00135-1)
- Klinken, P. (2002). Red blood cells. *The International Journal of Biochemistry & Cell Biology*, 34(12), 1513–1518. doi:10.1016/S1357-2725(02)00087-0
- Khan, S., Jarad, N. A., Ladouceur, L., Rachwalski, K., Bot, V., Shakeri, A., Maclachlan, R., Sakib, S., Weitz, J. I., Brown, E. D., Soleymani, L., & Didar, T. F. (2022). Transparent and highly flexible hierarchically structured polydimethylsiloxane surfaces suppress bacterial attachment and thrombosis under static and dynamic conditions. *Small*, 2108112. <https://doi.org/10.1002/smll.202108112>
- Khruasingkeaw, S., Khunatorn, Y., Rerkasem, K., & Srisuwan, T. (2016). Wall Shear Stress Distribution in Graft Anastomosis Using Computational Fluid Dynamics. *International Journal of Pharma Medicine and Biological Sciences*, 5(1). <https://doi.org/10.18178/ijpmbs.5.1.71-75>
- Kokozidou, M., Katsargyris, A., Verhoeven, E. L. G., & Schulze-Tanzil, G. (2019). Vascular access animal models used in research. *Annals of Anatomy - Anatomischer Anzeiger*, 225, 65–75. <https://doi.org/10.1016/j.aanat.2019.06.002>
- Kornet, L., Hoeks, A. P. G., Lambregts, J., Reneman, R. S. (2000). Mean Wall Shear Stress in the Femoral Arterial Bifurcation Is Low and Independent of Age at Rest. *J Vasc Res.* 37:112-122. doi: 10.1159/000025722
- Krüger-Genge, A., Blocki, A., Franke, R. P., & Jung, F. (2019). Vascular Endothelial Cell Biology: An Update. *International journal of molecular sciences*, 20(18), 4411. <https://doi.org/10.3390/ijms20184411>
- Kuchinka, J., Willems, C., Telyshev, D. V., & Groth, T. (2021). Control of blood coagulation by hemocompatible material surfaces—a review. *Bioengineering*, 8(12), 215. <https://doi.org/10.3390/bioengineering8120215>
- Kyziol, K., & Thakur, V (Eds). (2017). *Handbook of Composites from Renewable Materials*. Scrivener Publishing LLC. ISBN: 978-1119224365
- Késmárky, G., Kenyeres, P., Rábai, M., & Tóth, K. (2008). Plasma viscosity: A forgotten variable. *Clinical Hemorheology and Microcirculation*, 39(1–4), 243–246. <https://doi.org/10.3233/ch-2008-1088>

- Kim, T. H., Lee, J. M., Ahrberg, C. D., & Chung, B. G. (2018). Development of the microfluidic device to regulate shear stress gradients. *BioChip Journal*, 12(4), 294–303.  
<https://doi.org/10.1007/s13206-018-2407-9>
- Korin, N., Kanapathipillai, M., Matthews, B. D., Crescente, M., Brill, A., Mammoto, T., Ghosh, K., Jurek, S., Bencherif, S. A., Bhatta, D., Coskun, A. U., Feldman, C. L., Wagner, D. D., & Ingber, D. E. (2012). Shear-activated nanotherapeutics for drug targeting to obstructed blood vessels. *Science*, 337(6095), 738–742. <https://doi.org/10.1126/science.1217815>
- Krüger-Genge, A., Blocki, A., Franke, R. P., & Jung, F. (2019). Vascular Endothelial Cell Biology: An Update. *International journal of molecular sciences*, 20(18), 4411.  
<https://doi.org/10.3390/ijms20184411>
- Lampugnani, M. G. (04 2010). Endothelial adherens junctions and the actin cytoskeleton: an “infinity net”? *Journal of biology*, 9, 16. doi:10.1186/jbiol232
- Li, M., Ku, D. N., & Forest, C. R. (2012). Microfluidic system for simultaneous optical measurement of platelet aggregation at multiple shear rates in whole blood. *Lab on a Chip*, 12(7), 1355.  
<https://doi.org/10.1039/c2lc21145a>
- Lumsden, A. B., Morrissey, N. J., Staffa, R., Lindner, J., Janousek, L., Treska, V., ... Cayne, N. (2015). Randomized controlled trial comparing the safety and efficacy between the FUSION BIOLINE heparin-coated vascular graft and the standard expanded polytetrafluoroethylene graft for femoropopliteal bypass. *Journal of Vascular Surgery*, 61(3), 703-712.e1.  
doi:10.1016/j.jvs.2014.10.008
- Labarrere, C. A., Dabiri, A. E., & Kassab, G. S. (2020). Thrombogenic and Inflammatory Reactions to Biomaterials in Medical Devices. *Frontiers in bioengineering and biotechnology*, 8, 123.  
<https://doi.org/10.3389/fbioe.2020.00123>
- Latour, R. (2008). Biomaterials: Protein–Surface Interactions. *Encycl Biomater Biomed Eng*, 1.  
doi:10.1201/b18990-27
- Lau, H., & Cheng, S. W. (2000). Long-term outcome of aortofemoral bypass for aortoiliac occlusive disease. *Annals of the Academy of Medicine, Singapore*, 29(4), 434–438.
- Lau, S., Liu, Y., Maier, A., Braune, S., Gossen, M., Neffe, A. T., & Lendlein, A. (2021). Establishment of an in vitro thrombogenicity test system with cyclic olefin copolymer substrate for Endothelial Layer Formation. *MRS Communications*. <https://doi.org/10.1557/s43579-021-00072-6>
- Law K. Y. (2014). Definitions for Hydrophilicity, Hydrophobicity, and Superhydrophobicity: Getting the Basics Right. *The journal of physical chemistry letters*, 5(4), 686–688.  
<https://doi.org/10.1021/jz402762h>

- Leeman, M., Choi, J., Hansson, S., Storm, M. U., & Nilsson, L. (2018). Proteins and antibodies in serum, plasma, and whole blood-size characterization using asymmetrical flow field-flow fractionation (AF4). *Analytical and bioanalytical chemistry*, 410(20), 4867–4873. <https://doi.org/10.1007/s00216-018-1127-2>
- Leslie, D. C., Waterhouse, A., Berthet, J. B., Valentin, T. M., Watters, A. L., Jain, A., Kim, P., Hatton, B. D., Nedder, A., Donovan, K., Super, E. H., Howell, C., Johnson, C. P., Vu, T. L., Bolgen, D. E., Rifai, S., Hansen, A. R., Aizenberg, M., Super, M., Aizenberg, J., ... Ingber, D. E. (2014). A bioinspired omniphobic surface coating on medical devices prevents thrombosis and biofouling. *Nature biotechnology*, 32(11), 1134–1140. <https://doi.org/10.1038/nbt.3020>
- Lowe, G. (2010). How do antithrombotics work? *The British Journal of Cardiology*. 17(Suppl 1):S3-S4
- Luna, D. J., R. Pandian, N. K., Mathur, T., Bui, J., Gadangi, P., Kostousov, V. V., Hui, S.-K. R., Teruya, J., & Jain, A. (2020). Tortuosity-powered microfluidic device for assessment of thrombosis and antithrombotic therapy in whole blood. *Scientific Reports*, 10(1), 5742. <https://doi.org/10.1038/s41598-020-62768-4>
- Ma, Q., Ma, H., Xu, F., Wang, X., & Sun, W. (2021). Microfluidics in cardiovascular disease research: state of the art and future outlook. *Microsystems & nanoengineering*, 7, 19. <https://doi.org/10.1038/s41378-021-00245-2>
- Mallis, P., Kostakis, A., Stavropoulos-Giokas, C., & Michalopoulos, E. (2020). Future perspectives in small-diameter vascular graft engineering. *Bioengineering*, 7(4), 160. <https://doi.org/10.3390/bioengineering7040160>
- Manivasagam, V. K., Sabino, R. M., Kantam, P., & Popat, K. C. (2021). Surface modification strategies to improve titanium hemocompatibility: a comprehensive review. *Materials advances*, 2(18), 5824–5842. <https://doi.org/10.1039/d1ma00367d>
- Mapari, S., Mestry, S., & Mhaske, S. T. (2021). Developments in pressure-sensitive adhesives: A review. *Polymer Bulletin*, 78(7), 4075–4108. <https://doi.org/10.1007/s00289-020-03305-1>
- Mathias, C. J., & Welch, M. J. (1984). Radiolabeling of platelets. *Seminars in Nuclear Medicine*, 14(2), 118–127. doi:10.1016/S0001-2998(84)80025-2
- Ma, Q., Ma, H., Xu, F., Wang, X., & Sun, W. (2021). Microfluidics in cardiovascular disease research: State of the Art and Future Outlook. *Microsystems & Nanoengineering*, 7(1). <https://doi.org/10.1038/s41378-021-00245-2>

- McCollum, C., Kenchington, G., Alexander, C., Franks, P. J., & Greenhalgh, R. M. (1991). PTFE or HUV for femoro-popliteal bypass: A multi-centre trial. *European Journal of Vascular Surgery*, 5(4), 435–443. doi:10.1016/S0950-821X(05)80177-X
- Merten, M., Chow, T., Hellums, J. D., & Thiagarajan, P. (2000). A new role for P-selectin in shear-induced platelet aggregation. *Circulation*, 102(17), 2045–2050. <https://doi.org/10.1161/01.cir.102.17.2045>
- Mitra, S., Wang, Z., Paul, S., Stein, L. H., & Salemi, A. (2022). Recent developments in blood-compatible superhydrophobic surfaces. *Polymers*, 14(6), 1075. <https://doi.org/10.3390/polym14061075>
- More, R. B. (2000). Pyrolytic carbons and the design of mechanical heart valve prostheses. *Materials: Book of Abstracts*. <https://doi.org/10.1115/imece2000-2672>
- Nalezinková, M. (2020). In vitro hemocompatibility testing of medical devices. *Thrombosis Research*, 195, 146–150. <https://doi.org/10.1016/j.thromres.2020.07.027>
- Nie, S., Qin, H., Cheng, C., Zhao, W., Sun, S., Su, B., Zhao, C., & Gu, Z. (2014). Blood activation and compatibility on single-molecular-layer biointerfaces. *J. Mater. Chem. B*, 2(30), 4911–4921. <https://doi.org/10.1039/c4tb00555d>
- Nielsen, J. B., Hanson, R. L., Almughamsi, H. M., Pang, C., Fish, T. R., & Woolley, A. T. (2019). Microfluidics: Innovations in materials and their fabrication and functionalization. *Analytical Chemistry*, 92(1), 150–168. <https://doi.org/10.1021/acs.analchem.9b04986>
- Nath, N. N., Pocivavsek, L., Pugar, J. A., Gao, Y., Salem, K., Pitre, N., McEnaney, R., Velankar, S., & Tzeng, E. (2020). Dynamic luminal topography: A potential strategy to prevent vascular graft thrombosis. *Frontiers in Bioengineering and Biotechnology*, 8, 573400. <https://doi.org/10.3389/fbioe.2020.573400>
- Nechipurenko, D. Y., Receveur, N., Yakimenko, A. O., Shepelyuk, T. O., Yakusheva, A. A., Kerimov, R. R., Obydenny, S. I., Eckly, A., Léon, C., Gachet, C., Grishchuk, E. L., Ataulakhanov, F. I., Mangin, P. H., & Panteleev, M. A. (2019). Clot Contraction Drives the Translocation of Procoagulant Platelets to Thrombus Surface. *Arteriosclerosis, thrombosis, and vascular biology*, 39(1), 37–47. <https://doi.org/10.1161/ATVBAHA.118.311390>
- Nygaard, H., Paulsen, P. K., Hasenkam, J. M., Pedersen, E. M., & Røvsing, P. E. (1994). Turbulent stresses downstream of three mechanical aortic valve prostheses in human beings. *The Journal of Thoracic and Cardiovascular Surgery*, 107(2), 438–446. doi:10.1016/S0022-5223(94)70088-5

- Ogawa, S., Richardson, J., Sakai, T., Ide, M., & Tanaka, K. (2012). High mortality associated with intracardiac and intrapulmonary thromboses after cardiopulmonary bypass. *Journal of anesthesia*, 26, 9–19. doi:10.1007/s00540-011-1253-x
- Ohkubo, Y., Endo, K., & Yamamura, K. (2018). Adhesive-free adhesion between heat-assisted plasma-treated fluoropolymers (PTFE, PFA) and plasma-jet-treated polydimethylsiloxane (PDMS) and its application. *Scientific Reports*, 8.
- Okoshi, T., Soldani, G., Goddard, M., & Galletti, P. M. (1993). Very small-diameter polyurethane vascular prostheses with rapid endothelialization for coronary artery bypass grafting. *The Journal of thoracic and cardiovascular surgery*, 105(5), 791–795.
- Ortseifen, V., Viefhues, M., Wobbe, L., & Grünberger, A. (2020). Microfluidics for Biotechnology: Bridging Gaps to Foster Microfluidic Applications. *Frontiers in Bioengineering and Biotechnology*, 8, 1324
- Palta, S., Saroa, R., & Palta, A. (2014). Overview of the coagulation system. *Indian journal of anaesthesia*, 58(5), 515–523. <https://doi.org/10.4103/0019-5049.144643>
- Pareta, R. A., Reising, A. B., Miller, T., Storey, D., & Webster, T. J. (2009). Increased endothelial cell adhesion on plasma modified nanostructured polymeric and metallic surfaces for vascular stent applications. *Biotechnology and Bioengineering*, 103(3), 459–471. <https://doi.org/10.1002/bit.22276>
- Pantelev, M. A., Korin, N., Reesink, K. D., Bark, D. L., Cosemans, J. M. E. M., Gardiner, E. E., & Mangin, P. H. (2021). Wall shear rates in human and mouse arteries: Standardization of hemodynamics for in vitro blood flow assays: Communication from the ISTH SSC subcommittee on biorheology. *Journal of Thrombosis and Haemostasis*, 19(2), 588–595. doi:10.1111/jth.15174
- Papaoannou, T. G., & Stefanadis, C. (2005). Vascular wall shear stress: basic principles and methods. *Hellenic journal of cardiology : HJC, Hellenike kardiologike epitheorese*, 46(1), 9–15.
- Pareta, R., Reising, A., Miller, T., Storey, D., & Webster, T. (2009). Increased Endothelial Cell Adhesion on Plasma Modified Nanostructured Polymeric and Metallic Surfaces for Vascular Stent Applications. *Biotechnology and bioengineering*, 103, 459–471. doi:10.1002/bit.22276
- Paszковиak, J. J., & Dardik, A. (2003). Arterial wall shear stress: Observations from the bench to the bedside. *Journal of Vascular and Endovascular Surgery*, 37(1), 47–57. <https://doi.org/10.1177/153857440303700107>
- Pineda, D. M., Dougherty, M. J., Wismer, M. C., Carroll, C., Tyagi, S., Troutman, D. A., & Calligaro, K. D. (2017). Bovine carotid artery xenografts for hemodialysis access. *Journal of vascular surgery*, 65(6), 1729–1734. <https://doi.org/10.1016/j.jvs.2016.12.109>

- Pocivavsek, L., Ye, S. H., Pugar, J., Tzeng, E., Cerda, E., Velankar, S., & Wagner, W. R. (2019). Active wrinkles to drive self-cleaning: A strategy for anti-thrombotic surfaces for vascular grafts. *Biomaterials*, 192, 226–234. <https://doi.org/10.1016/j.biomaterials.2018.11.005>
- Qiu, X., Lee, B. L.-P., Ning, X., Murthy, N., Dong, N., & Li, S. (2017). End-point immobilization of heparin on plasma-treated surface of electrospun polycarbonate-urethane vascular graft. *Acta Biomaterialia*, 51, 138–147. <https://doi.org/10.1016/j.actbio.2017.01.012>
- Qi, P., Maitz, M. F., & Huang, N. (2013). Surface modification of cardiovascular materials and implants. *Surface and Coatings Technology*, 233, 80–90. doi:10.1016/j.surfcoat.2013.02.008
- Rajeeva-Pandian, N. K., Walther, B. K., Suresh, R., Cooke, J. P., & Jain, A. (2020). Microengineered human vein-chip recreates venous valve architecture and its contribution to thrombosis. *Small*, 16(49), 2003401. <https://doi.org/10.1002/sml.202003401>
- Rana, A., Westein, E., Niego, B., & Hagemeyer, C. E. (2019). Shear-Dependent Platelet Aggregation: Mechanisms and Therapeutic Opportunities. *Frontiers in Cardiovascular Medicine*, 6. doi:10.3389/fcvm.2019.00141
- Ren, K., Dai, W., Zhou, J., Su, J., & Wu, H. (2011). Whole-Teflon microfluidic chips. *Proceedings of the National Academy of Sciences of the United States of America*, 108(20), 8162–8166.
- Resmi, K. R., Varghese, N., & Krishnan, L. K. (2004). Procedure for quantification of platelet adhesion to biomaterials by radiosciintigraphy. *Thrombosis research*, 114(2), 121–128. <https://doi.org/10.1016/j.thromres.2004.05.014>
- Rhodes, N., Shortland, A., Rattray, A., & Williams, D. (1999). Platelet reactions to modified surfaces under dynamic conditions. *Journal of materials science. Materials in medicine*, 9, 767–772. doi:10.1023/A:1008971406590
- Roth, G. A., Mensah, G. A., Johnson, C. O., Addolorato, G., Ammirati, E., Baddour, L. M., ... Fuster, V. (2020). Global Burden of Cardiovascular Diseases and Risk Factors, 1990–2019: Update From the GBD 2019 Study. *Journal of the American College of Cardiology*, 76(25), 2982–3021. doi:10.1016/j.jacc.2020.11.010
- Samson, R. H., Morales, R., Showalter, D. P., Lepore, M. R., Jr, & Nair, D. G. (2016). Heparin-bonded expanded polytetrafluoroethylene femoropopliteal bypass grafts outperform expanded polytetrafluoroethylene grafts without heparin in a long-term comparison. *Journal of vascular surgery*, 64(3), 638–647.
- Sanchez, P., Brey, E., & Briceno, J. (2018). Endothelialization mechanisms in vascular grafts. *Tissue Engineering and Regenerative Medicine*, 12(11), 2164–2178. <https://doi.org/https://doi.org/10.1002/term.2747>

- Sandoo, A., van Zanten, J. J., Metsios, G. S., Carroll, D., & Kitas, G. D. (2010). The endothelium and its role in regulating vascular tone. *The open cardiovascular medicine journal*, 4, 302–312. <https://doi.org/10.2174/1874192401004010302>
- Sankar, P., & Varacallo, M. (2021). *Physiology, Blood Plasma*. In StatPearls. StatPearls Publishing.
- Sarode, D. N., & Roy, S. (2019). In Vitro models for thrombogenicity testing of blood-recirculating medical devices. *Expert review of medical devices*, 16(7), 603–616. <https://doi.org/10.1080/17434440.2019.1627199>
- Sarkar, S., Salacinski, H., Hamilton, G., & Seifalian, A (2006). The Mechanical Properties of Infrainguinal Vascular Bypass Grafts: Their Role in Influencing Patency. *European Journal of Vascular and Endovascular Surgery*, 31(6), 627-636
- Sask, K. (2012). *Antithrombogenic Biomaterials: Surface Modification with an Antithrombin-Heparin Covalent Complex* (dissertation).
- Schmidt, D., Waldeck, H., & Kao, J. (2009). Protein Adsorption to Biomaterials. In D. A. Puleo & R. Bizios (Eds.), *Biological Interactions on Materials Surfaces: Understanding and Controlling Protein, Cell, and Tissue Responses* (1–18). doi:10.1007/978-0-387-98161-1\_1
- Secomb T. (2016). Hemodynamics. *Comprehensive Physiology*, 6(2), 975–1003. <https://doi.org/10.1002/cphy.c150038>
- Sen, A., Hassanpour-Tamrin, S., & Sanati-Nezhad, A. (2021). A simple and low-cost approach for irreversible bonding of polymethylmethacrylate and polydimethylsiloxane at room temperature for high-pressure hybrid microfluidics. *Scientific Reports*, 11(1). <https://doi.org/10.1038/s41598-021-83011-8>
- Sena, C., Carrilho, F., & Seça, R. (2018). Endothelial Dysfunction in Type 2 Diabetes: Targeting Inflammation. doi:10.5772/intechopen.76994
- Shankarraman, V., Davis-Gorman, G., Copeland, J. G., Caplan, M. R., & McDonagh, P. F. (2012). Standardized methods to quantify thrombogenicity of blood-contacting materials via thromboelastography. *Journal of Biomedical Materials Research Part B: Applied Biomaterials*, 100B(1), 230–238. doi:10.1002/jbm.b.31942
- Shimada, K., Kobayashi, M., Kimura, S., Nishinaga, M., Takeuchi, K., & Ozawa, T. (1991). Anticoagulant heparin-like glycosaminoglycans on endothelial cell surface. *Japanese circulation journal*, 55(10), 1016–1021. <https://doi.org/10.1253/jcj.55.1016>



- Shim, K., Anderson, P., Tuley, E., Wiswall, E., & Sadler, E. (2008). Platelet-VWF complexes are preferred substrates of ADAMTS13 under fluid shear stress. *Blood*, 111(2).  
<https://doi.org/https://doi.org/10.1182/blood-2007-05-093021>
- Sinn, S., Scheuermann, T., Deichelbohrer, S., Ziemer, G., & Wendel, H. P. (2011). A novel in vitro model for preclinical testing of the hemocompatibility of intravascular stents according to ISO 10993-4. *Journal of Materials Science: Materials in Medicine*, 22(6), 1521–1528.  
<https://doi.org/10.1007/s10856-011-4335-2>
- Sivkova, R., Táborská, J., Reparaz, A., de los Santos Pereira, A., Kotelnikov, I., Proks, V., Kučka, J., Svoboda, J., Riedel, T., & Pop-Georgievski, O. (2020). Surface design of antifouling vascular constructs bearing biofunctional peptides for tissue regeneration applications. *International Journal of Molecular Sciences*, 21(18), 6800. <https://doi.org/10.3390/ijms21186800>
- Sukavaneshvar, S. (2017). Device thrombosis and pre-clinical blood flow models for assessing antithrombogenic efficacy of drug-device combinations. *Advanced Drug Delivery Reviews*, 112, 24–34. <https://doi.org/10.1016/j.addr.2016.07.009>
- Smith, R. S., Zhang, Z., Bouchard, M., Li, J., Lapp, H. S., Brotske, G. R., Lucchino, D. L., Weaver, D., Roth, L. A., Coury, A., Biggerstaff, J., Sukavaneshvar, S., Langer, R., & Loose, C. (2012). Vascular catheters with a nonleaching poly-sulfobetaine surface modification reduce thrombus formation and microbial attachment. *Science translational medicine*, 4(153), 153ra132.  
<https://doi.org/10.1126/scitranslmed.3004120>
- Smolderen, K. G., Bell, A., Lei, Y., Cohen, E. A., Steg, P. G., Bhatt, D. L., Mahoney, E. M., & REACH registry investigators (2010). One-year costs associated with cardiovascular disease in Canada: Insights from the Reduction of Atherothrombosis for Continued Health (REACH) registry. *The Canadian journal of cardiology*, 26(8), 297–305. [https://doi.org/10.1016/s0828-282x\(10\)70437-2](https://doi.org/10.1016/s0828-282x(10)70437-2)
- Sochi, T. (2013). Non-Newtonian Rheology in Blood Circulation. *Arxiv*.  
<https://doi.org/10.48550/arxiv.1306.2067>
- Sonmez, U. M., Cheng, Y.-W., Watkins, S. C., Roman, B. L., & Davidson, L. A. (2020). Endothelial cell polarization and orientation to flow in a novel microfluidic multimodal shear stress generator. *Lab on a Chip*, 20(23), 4373–4390. <https://doi.org/10.1039/d0lc00738b>
- Stasi, A., Franzin, R., Divella, C., Sallustio, F., Curci, C., Picerno, A., Pontrelli, P., Staffieri, F., Lacitignola, L., Crovace, A., Cantaluppi, V., Medica, D., Ronco, C., de Cal, M., Lorenzin, A., Zanella, M., Pertosa, G. B., Stallone, G., Gesualdo, L., & Castellano, G. (2021). PMMA-based continuous hemofiltration modulated complement activation and renal dysfunction in LPS-induced acute kidney injury. *Frontiers in Immunology*, 12. <https://doi.org/10.3389/fimmu.2021.605212>

- Streets, A. M., & Huang, Y. (2013). Chip in a lab: Microfluidics for next generation life science research. *Biomicrofluidics*, 7(1), 11302. <https://doi.org/10.1063/1.4789751>
- Strohbach, A., & Busch, R. (2021). Predicting the in vivo performance of cardiovascular biomaterials: Current approaches in vitro evaluation of blood-biomaterial interactions. *International Journal of Molecular Sciences*, 22(21), 11390. <https://doi.org/10.3390/ijms222111390>
- Takami, Y., Tajima, K., Kato, W., Fujii, K., Hibino, M., Munakata, H., Uchida, K., & Sakai, Y. (2012). Long-term size follow-up of knitted Dacron grafts used in the ascending aorta. *Interactive CardioVascular and Thoracic Surgery*, 14(5), 529–531. <https://doi.org/10.1093/icvts/ivr086>
- Topaz, O., Azadani, A. N., & Dvir, D. (2018). Chapter 28 - Experimental Designs for In Vitro Assessment of Valve Thrombosis. *Cardiovascular Thrombus* (bll 405–420). doi:10.1016/B978-0-12-812615-8.00028-4
- Trachsel, L., Romio, M., Ramakrishna, S., & Benetti, E. (08 2020). Fabrication of Biopassive Surfaces Using Poly(2-alkyl-2-oxazoline)s: Recent Progresses and Applications. *Advanced Materials Interfaces*, 7, 2000943. doi:10.1002/admi.202000943
- Traub, O., & Berk, B. C. (1998). Laminar Shear Stress. *Arteriosclerosis, Thrombosis, and Vascular Biology*, 18(5), 677–685. doi:10.1161/01.ATV.18.5.677
- Tucker, W. D., Arora, Y., & Mahajan, K. (2021). Anatomy, Blood Vessels. In *StatPearls*. StatPearls Publishing.
- Vahidkhah, K., Javani, S., Abbasi, M., Azadani, P. N., Tandar, A., Dvir, D., & Azadani, A. N. (2017). Blood Stasis on Transcatheter Valve Leaflets and Implications for Valve-in-Valve Leaflet Thrombosis. *The Annals of thoracic surgery*, 104(3), 751–759. <https://doi.org/10.1016/j.athoracsur.2017.02.052>
- Valtin, J., Behrens, S., Maitz, M. F., Schmieder, F., Sonntag, F., & Werner, C. (2021). A modular in vitro flow model to analyse blood-surface interactions under physiological conditions. *Current Directions in Biomedical Engineering*, 7(2), 171–174. <https://doi.org/10.1515/cdbme-2021-2044>
- Van Oeveren, W., Tielliu, I.F., & de Hart, J. (2012). Comparison of modified chandler, roller pump, and ball valve recirculation models for in vitro testing in high blood flow conditions: application in testing of different materials for vascular applications. *International journal of biomaterials*, 2012, 673163.
- Villegas, M. (2018). Merging omniphobic lubricant-infused coatings with different microfluidic modalities to enhance device fabrication and functionality (thesis).

- Walsh, D. I., 3rd, Kong, D. S., Murthy, S. K., & Carr, P. A. (2017). Enabling Microfluidics: from Clean Rooms to Makerspaces. *Trends in biotechnology*, 35(5), 383–392. <https://doi.org/10.1016/j.tibtech.2017.01.001>
- Weisel J. W. (2007). Structure of fibrin: impact on clot stability. *Journal of thrombosis and haemostasis : JTH*, 5 Suppl 1, 116–124. <https://doi.org/10.1111/j.1538-7836.2007.02504.x>
- Westerhof, N., Stergiopulos, N., Noble, M. I. M., & Westerhof, B. E. (2019). *Snapshots of hemodynamics an aid for clinical research and graduate education*. Springer International Publishing.
- Williams, D., Leuthardt, E. C., Genin, G. M., & Zayed, M. (2021). Tailoring of arteriovenous graft-to-vein anastomosis angle to attenuate pathological flow fields. *Scientific reports*, 11(1), 12153. <https://doi.org/10.1038/s41598-021-90813-3>
- Wu, Y., Zhou, Z., & Meyerhoff, M. E. (2007). In vitro platelet adhesion on polymeric surfaces with varying fluxes of continuous nitric oxide release. *Journal of biomedical materials research. Part A*, 81(4), 956–963. <https://doi.org/10.1002/jbm.a.31105>
- Yan, W., Ramakrishna, S. N., Romio, M., & Benetti, E. M. (2019). Bioinert and Lubricious Surfaces by Macromolecular Design. *Langmuir : the ACS journal of surfaces and colloids*, 35(42), 13521–13535. <https://doi.org/10.1021/acs.langmuir.9b02316>
- Yang, T., De La Franier, B., & Thompson, M. (2021). Anti-Thrombogenicity Study of a Covalently-Attached Monolayer on Stent-Grade Stainless Steel. *Materials (Basel, Switzerland)*, 14(9), 2342. <https://doi.org/10.3390/ma14092342>
- Yau, J. W., Stafford, A. R., Liao, P., Fredenburgh, J. C., Roberts, R., Brash, J. L., & Weitz, J. I. (2012). Corn trypsin inhibitor coating attenuates the prothrombotic properties of catheters in vitro and in vivo. *Acta Biomaterialia*, 8(11), 4092–4100. <https://doi.org/10.1016/j.actbio.2012.07.019>
- Yau, J. W., Teoh, H., & Verma, S. (2015). Endothelial cell control of thrombosis. *BMC cardiovascular disorders*, 15, 130. <https://doi.org/10.1186/s12872-015-0124-z>
- Yin, W., Shanmugavelayudam, S. K., & Rubenstein, D. A. (2011). The effect of physiologically relevant dynamic shear stress on platelet and Endothelial Cell Activation. *Thrombosis Research*, 127(3), 235–241. <https://doi.org/10.1016/j.thromres.2010.11.021>
- Yu, L. (2018). Universal Polymer Coatings with Tailorable Bioinert and Biospecific Function. [doi:10.17169/refubium-17829](https://doi.org/10.17169/refubium-17829)

- Weber, M., Steinle, H., Golombek, S., Hann, L., Schlensak, C., Wendel, H. P., & Avci-Adali, M. (2018). Blood-contacting biomaterials: In vitro evaluation of the hemocompatibility. *Frontiers in Bioengineering and Biotechnology*, 6. <https://doi.org/10.3389/fbioe.2018.00099>
- Wei, Y. C., Chen, F., Zhang, T., Chen, D. Y., Jia, X., Wang, J. B., Guo, W., & Chen, J. (2014). Vascular smooth muscle cell culture in microfluidic devices. *Biomicrofluidics*, 8(4), 046504. <https://doi.org/10.1063/1.4893914>
- Xu, S., Xu, Z., Kim, O. V., Litvinov, R. I., Weisel, J. W., & Alber, M. (2017). Model predictions of deformation, embolization and permeability of partially obstructive blood clots under variable shear flow. *Journal of The Royal Society Interface*, 14(136), 20170441. <https://doi.org/10.1098/rsif.2017.0441>
- Zhou, J., Kulasinghe, A., Bogseth, A., O'Byrne, K., Punyadeera, C., & Papautsky, I. (2019). Isolation of circulating tumor cells in non-small-cell-lung-cancer patients using a multi-flow microfluidic channel. *Microsystems & Nanoengineering*, 5(1). <https://doi.org/10.1038/s41378-019-0045-6>
- Zhu, T., Gu, H., Ma, W., Zhang, Q., Du, J., Chen, S., ... Zhang, W. (2021). A fabric reinforced small diameter tubular graft for rabbits' carotid artery defect. *Composites Part B: Engineering*, 225, 109274. doi:10.1016/j.compositesb.2021.109274
- Zhu, S., Travers, R. J., Morrissey, J. H., & Diamond, S. L. (2015). FXIa and platelet polyphosphate as therapeutic targets during human blood clotting on collagen/tissue factor surfaces under flow. *Blood*, 126(12), 1494–1502. <https://doi.org/10.1182/blood-2015-04-641472>
- Zimmerman, M. A., Selzman, C. H., Reznikov, L. L., Miller, S. A., Raeburn, C. D., Emmick, J., Meng, X., & Harken, A. H. (2002). Lack of TNF- $\alpha$  attenuates intimal hyperplasia after mouse carotid artery injury. *American Journal of Physiology-Regulatory, Integrative and Comparative Physiology*, 283(2). <https://doi.org/10.1152/ajpregu.00033.2002>